DISSERTATION

CHARACTERIZING THE LUNG-BRAIN AXIS INFLAMMATORY RESPONSE TO AGRICULTURE DUST AND UTILIZING ASPIRIN-TRIGGERED RESOLVIN D1 AS A NOVEL THERAPEUTIC

Submitted by

Alissa Nicole Threatt

Department of Environmental and Radiological Health Sciences

In partial fulfillment of the requirements

For the Degree of Doctor of Philosophy

Colorado State University

Fort Collins, Colorado

Summer 2025

Doctoral Committee:

Advisor: Julie Moreno

Alex Constan
Tara Nordgren
Joshua Schaeffer
Alan Schenkel

Copyright of Alissa Nicole Threatt 2025

All Rights Reserved

ABSTRACT

CHARACTERIZING THE LUNG-BRAIN AXIS INFLAMMATORY RESPONSE TO AGRICULTURE DUST AND UTILIZING ASPIRIN TRIGGERED RESOLVIN D1 AS A NOVEL THERAPEUTIC

Occupational exposure to agriculture dust is strongly linked to the development of chronic pulmonary diseases such as asthma and chronic obstructive pulmonary disease (COPD). The organic dust inhaled in agricultural settings, known as organic dust exposure (ODE), contains high concentrations of immunogenic compounds that lead to immune-mediated chronic lung disease. These pulmonary inflammatory responses to agriculture dust exposure have been extensively characterized, however there is emerging evidence that agriculture dust exposure increases workers' risk for the development of dementia and other neurological disorders. Occupational agriculture dust exposure has been strongly linked to an increased risk of developing dementia and COPD patients experience high rates of memory loss, confusion, depression, and anxiety symptoms. Given this new evidence, we aimed to characterize the neuroinflammatory response to agriculture dust *in vitro* in cultured microglia and *in vivo* in mouse models of repetitive agriculture dust exposure. We also evaluated the behavioral outcomes in mice exposed to agriculture dust to link the exposure with reported patient outcomes.

There are additional risk factors that have been identified in patients with ODE, one of which is the production of the cytokine interleukin-22 (IL-22), which has been shown to have various functions in pulmonary disease. Some models have demonstrated that IL-22 is elevated

in certain disease states and may contribute to susceptibility to secondary exposures, while other models have shown that IL-22 knock-out mouse models experience more severe disease states. We aimed to understand the link between IL-22 and neurological inflammation in an ODE mouse model.

Both COPD and dementia are progressive and fatal diseases with limited effective therapies. The development of novel therapeutics to treat these diseases is urgently needed to address these patients' needs. Omega-3 fatty acid metabolites, such as Aspirin-Triggered Resolvin D1 (AT-RvD1) have shown efficacy in reducing inflammation in models of ODE and other inflammatory exposures. We aimed to evaluate the efficacy of AT-RvD1 as a novel therapeutic for the reduction of pulmonary and neurological inflammation elicited by agriculture dust exposure. We aimed to accomplish this through *in vitro* alveolar macrophage culture and an *in vivo* repetitive ODE, AT-RvD1 treatment mouse model. We also aimed to determine the role of IL-22 in agriculture dust-induced pulmonary and neurological inflammation utilizing an IL-22 knock-out mouse model of repetitive ODE and AT-RvD1 treatment.

Through our investigations, we observed that ODE in macrophages and microglia produce a strong immune response characterized by the secretion of the pro-inflammatory cytokine tumor necrosis factor alpha (TNF-α) and that co-treatment with AT-RvD1 significantly reduces its production. In our *in vivo* mouse models, we determined that exposure to agriculture dust produced increased numbers of microglia and astrocytes, confirming our hypothesis that agriculture dust exposure leads to neuroinflammation. We also found that AT-RvD1 treatment in these animals reduced the number of microglia and astrocytes. Additionally, we found that knock-out of IL-22 produced increased inflammation compared to wildtype controls and that AT-RvD1 treatment significantly reduced this inflammation. Our behavioral assessment of mice

exposed to agriculture dust revealed limited changes in anxiety and memory, warranting further investigation into the effects of ODE on animal behavior.

Overall, our investigations revealed that exposure to agricultural dust leads to neurological inflammation in the form of microglia an astrocyte proliferation and pro-inflammatory cytokine production, that IL-22 plays an important role in the regulation of these inflammatory processes, and that AT-RvD1 may be an effective novel therapeutic for agricultural dust exposure-induced inflammatory diseases.

ACKNOWLEDGEMENTS

This work would not have been possible without the support of many individuals. I would first like to thank my advisors, Dr. Tara Nordgren and Dr. Julie Moreno for not only assisting with the science of this project but also being an important part of my emotional support system throughout this project. I greatly appreciated their gentle mentoring style and feel that this project would not have turned out as well as it did without them. I would also like to thank my committee, some of who have been with me since my Masters. I would like to thank Dr. Alan Schenkel and Dr. Joshua Schaeffer for agreeing to be part of my doctoral committee and for helping me with troubleshooting during this project. I would also like to thank Dr. Alex Constan for agreeing to serve on my committee as well and for being a helpful connection to industry. I appreciate the support of my committee and this work would not have been possible without their guidance.

I would also like to thank Dr. Olivia Arnold for her advice and for being a good friend throughout my time here in the Toxicology Program. Additionally, there have been many individuals in the Environmental and Radiological Health Sciences Department and in the broader CSU community who have been integral to my success. Many other Graduate and Undergraduate students were integral to the success of this work: members Nordgren Laboratory, Logan Dean, Melea Barahona, Emmanuel Oyewole, Kaylee Jones, Casey McDermott, Maelis Wahl, Morgan Pauly, Zach Brier, Rose Reiter, Megan McKay, Ash Ibarra, Nathan Klepper, and Jade White, and members of the Montrose Laboratory, Jacob Smoot, and members of the Moreno Laboratory, Sean Boland, Payton Shirley, and Abdulatif Alsulami.

These individuals helped with the animals and/or cell studies presented in this dissertation, and this work would not have been possible without them.

I would also like to thank my family for their support throughout this journey, my parents Kristin and Doug Threatt, my sister and brother-in-law, Riley and Drake Benton, and my brothers Sampson Brozek and Ethan Lagro. I would also like to thank my partner, Brendan Kelley, for always being there for me during this journey.

This work is more than the culmination of one person's labor; it is a collaboration of all the people who cared about me along the way.

TABLE OF CONTENTS

ABSTRACT ii
ACKNOWLEDGEMENTS v
LIST OF FIGURES x
CHAPTER 1: BACKGROUND 1
1.1 Introduction 1
1.2 Agriculture Dust-Induced Chronic Pulmonary Diseases 4
1.2.1 Allergies 7
1.2.2 Asthma 9
1.2.3 Chronic Obstructive Pulmonary Disease 10
1.2.4 Organic Dust Toxic Syndrome 13
1.2.5 Neurological Disease and Agriculture Dust 14
1.3 The Pulmonary and Neurological Response to Organic Dusts 16
1.3.1 Signaling Molecules in the Pulmonary and Neurological Immune Response 16
1.3.2 Immune Cells in the Pulmonary and Neurological Response to Organic Dusts 18
1.3.3 IL-22 In the Pulmonary and Neurological Immune Response to Organic Dust 19
1.4 Lipids in the Pulmonary and Neurological Inflammatory Response 20
1.4.1 Omega-6 Fatty Acids in Inflammation 22
1.4.2 Omega-3 Fatty Acids in Inflammation 23
1.4.3 Specialized Pro-Resolving Mediators 23
1.4.4 Resolvin D1 and Aspirin-Triggered Resolvin D1 25
1.5 Justification and Specific Aims 28
CHAPTER 2: OPTIMIZING ASPIRIN-TRIGGERED RESOLVIN D1 FOR *IN VIVO* APPLICATIONS 30
2.1 Introduction 30
2.2 Materials and Methods 31
2.2.1 Hog Dust Extract Preparation 31
2.2.2 Mouse Alveolar Macrophage Culture and Co-Exposure Model 31
2.2.3 Mouse Microglia Culture Maintenance 32
2.2.4 Mitochondrial Function (MTT) Assay 33
2.2.5 Lactate Dehydrogenase (LDH) Assay 34
2.2.6 DE and AT-RvD1 Microglia Co-Exposure Model 35
2.2.7 Supernatant Fractions and Cell Lysate Collection 36
2.2.8 Enzyme-Linked Immunosorbent Assays 37

2.2.9 *In Vivo* Repetitive Organic Dust Extract Exposure Model 37
2.3.10 Animal Sacrifice Sample Collection 39
2.3.11 Bronchoalveolar Lavage Cellular Infiltrate Analysis 40
2.3.12 Lung Pathology 41
2.3.13 Immunohistochemistry 42
2.3.14 Statistical Analysis 43
2.3 Results: 43
2.3.1 Effects of AT-RvD1 on cytokine production in DE-exposed alveolar macrophages 43
2.3.2 Effects of DE exposure and AT-RvD1 treatment in cultured microglia 51
2.3.3 Effects of various AT-RvD1 dosages on BALF cellular infiltrates 53
2.3.4 Effects of various AT-RvD1 dosages on lung pathology 55
2.3.5 Effects of DE and AT-RvD1 on neuroinflammatory markers 57
2.4 Discussion 60
CHAPTER 3: ASPIRIN-TRIGGERED RESOLVIN D1 MODULATES PULMONARY AND NEUROLOGICAL INFLAMMATION IN AN IL-22 KNOCK-OUT ORGANIC DUST EXPOSURE MOUSE MODEL 63
3.1 Introduction 63
3.2 Materials and Methods 66
3.2.1 Dust Extract Preparation 66
3.2.2 Animal Husbandry and Care 66
3.2.3 *In Vivo* Repetitive DE Exposure and AT-RvD1 Treatment Model 67
3.2.4 Animal Sacrifice and Sample Collection 69
3.2.5 Cellular Infiltrate Analysis 70
3.2.6 Cytokine Quantification 70
3.2.7 Lung Histopathology 71
3.2.8 Immunofluorescence 72
3.2.9 RNAscope 73
3.2.10 Statistical Analysis 74
3.3 Results 75
3.3.1 IL-22 KO alters lung immune cell trafficking and weekly AT-RvD1 administration reduces cellular infiltration in IL-22 KO mice following repetitive organic dust exposure 75
3.3.2 Impacts of AT-RvD1 on lung inflammatory mediator production in WT and IL-22 KO mice during recovery following repetitive DE exposure 82
3.3.3 Agriculture dust exposure is associated with gliosis and AT-RvD1 administration reduces neuroinflammation 86
3.3.4 AT-RvD1 treatment alters brain transcript expression in animals exposed to DE 90
3.4 Discussion 93

CHAPTER 4: CHARACTERIZATION OF THE LUNG-BRAIN IMMUNE RESPONSE TO AGRICULTURE DUST IN A SUB-CHRONIC MOUSE MODEL 102
4.1 Introduction 102
4.2 Methods 103
4.2.1 Dust Extract Preparation 103
4.2.2 Animal Husbandry and Care 104
4.2.3 *In Vivo* 8-Week Repetitive DE Exposure Model 104
4.2.2 Behavioral Assays 105
4.2.3 Open Field Test 106
4.2.4 Novel Object Recognition Test 106
4.2.5 Animal Sacrifice and Sample Collection 107
4.2.4 Lung Histopathology 107
4.2.5 Immunofluorescence 108
4.2.6 Statistical Analysis 110
4.3 Results 110
4.3.1 Dust exposure does not alter novel object recognition behavioral outcomes 110
4.3.2 Dust exposure alters open field behavioral outcomes in in a sex-specific manner 112
4.3.3 Sub-chronic dust exposure leads to limited lung pathology 115
4.3.4 Sub-chronic dust exposure is associated with gliosis in animals exposed to DE i.n. 117
4.4 Discussion 119
CHAPTER 5: DISCUSSION AND FUTURE DIRECTIONS 122
5.1 Discussion 122
5.2 Limitations 127
5.3 Future Directions 128
5.4 Conclusions 130
REFERENCES 132

LIST OF FIGURES

Figure 1. Agriculture and Food Industry Contribution to US Gross Domestic Product[222] 4
Figure 2. Agriculture and Food Industry Employment Statistics[222] 5
Figure 3. Inflammation-Resolution Relationship Mediated by SPMs[189] 22
Figure 4. Resolution of Inflammation vs Nonrevolving Inflammatory Response[189] 25
Figure 5. Metabolic pathway for formation of RvD1 and AT-RvD1[208] 27
Figure 6. Experimental Plate Set-Up for Cultured Macrophages 32
Figure 7. Experimental set-up for MTT assay 34
Figure 8. Experimental set-up for LDH assay 35
Figure 9. Experimental plate set-up for co-exposed cultured microglia. 36
Figure 10. AT-RvD1 dosing strategy in WT and IL-22 KO mice. 39
Figure 11. Effects of DE exposure and AT-RvD1 treatment on IL-6 induction in alveolar macrophages over 24 hours. 44
Figure 12. Effects of DE exposure and AT-RvD1 treatment on TNF-α induction in alveolar macrophages over 24 hours. 45
Figure 13. Effects of DE exposure and AT-RvD1 treatment on IL-10 induction in alveolar macrophages over 24 hours. 46
Figure 14. Effects of DE exposure and AT-RvD1 treatment on IL-22 induction in alveolar macrophages over 24 hours. 48
Figure 15. Effects of DE exposure and AT-RvD1 treatment on IL-6, TNF-α, IL-10, and IL-22 in alveolar macrophages over 24 hours. 50
Figure 16. Effects of dust exposure on cultured microglia. 53
Figure 17. BALF Cellular infiltrate profiles in mice exposed to DE and treated with various doses of AT-RvD1. 55
Figure 18. Effects of DE exposure and AT-RvD1 treatment on iBALT and peribronchiolar and perivascular inflammation in WT mice. 56
Figure 19. Microglia counts in mice exposed to DE and treated with 250ng AT-RvD1. 58
Figure 20. Astrocyte counts in mice exposed to DE and treated with 250 ng AT-RvD1 59
Figure 21. AT-RvD1 dosing strategies in WT and IL-22 KO mice. 68
Figure 22. Impacts of DE and AT-RvD1 on BALF immune cellular infiltrates in WT and IL-22 KO animals. 77
Figure 23. AT-RvD1 administration once weekly does not improve lung pathology. 78
Figure 24. AT-RvD1 treatment daily reduces iBALT in animals exposed to DE. 81
Figure 25. Effects of repetitive dust exposure and RvD1 treatment on bronchoalveolar lavage fluid (BALF) and lung tissue homogenate cytokines. 84
Figure 26. AT-RvD1 treatment reduces cxcl10 mRNA expression in WT animals exposed to DE. 86
Figure 27. Gliosis is associated with agriculture dust exposure. 90
Figure 28. IL-22 knock-out alters brain mRNA transcripts in the presence of AT-RvD1 and DE. 93
Figure 29. 8-Week Repetitive DE Exposure Model Timeline. 105
Figure 30. Dust exposure does not alter novel object recognition testing 111

Figure 31. Animals exposed to DE have mild changes in average speed during open field testing. 112
Figure 32. Animals exposed to DE have limited changes in time spent mobile during open field testing. 113
Figure 33. Animals exposed to DE exhibit limited changes in time spent immobile during open field testing. 114
Figure 34. Sub-chronic dust exposure is associated with limited lung pathology. 116
Figure 35. Sub-chronic dust exposure is associated with gliosis. 118

CHAPTER 1: BACKGROUND

1.1 Introduction

Agricultural workers report higher incidence of respiratory diseases such as allergies, asthma, chronic obstructive pulmonary disease (COPD), and organic dust toxic syndrome (ODTS)[7,48,60,136,220,249]. There are currently limited treatments for these diseases, which have undesirable immunological side effects, so development of improved pharmacological interventions is of increasing concern in public health[59,110,111,202,203]. Effective treatments exist for many asthma sufferers, but often with immunological side effects[23,116]. COPD patients in particular have limited options for symptom management, no course to slow the progression of the disease, and most inevitably die as a result of the disease[29,211]. Populations living around agriculture facilities are also at increased risk of these diseases[7]. Up to 40% of agriculture workers do not comply with personal protective equipment (PPE) requirements, including but not limited to dust masks, face shields, and/or respirators, citing discomfort and difficulty completing job requirements as reasons for non-compliance [90]. This further necessitates the development of pharmacological interventions for the resulting chronic inflammatory diseases. Inflammation is a desirable process. Many people would be surprised by that statement when medical professionals often prescribe anti-inflammatory drugs. The inflammatory response is beneficial to protect the body from foreign material and pathogens, and restriction of this process would allow for opportunistic infections[73]. Current treatments for many chronic inflammatory diseases focus on reducing inflammation, often resulting in blockage of resolution of the inflammatory response, as both responses are dependent on each other, and the inflammatory

signals are critical to transitioning to a resolution response and restoring tissue homeostasis after injury[61,134].

The goal in the development of new treatments for chronic inflammatory diseases is to regulate the inflammatory response so that it does not become harmful while allowing for the resolution and repair processes to progress unhindered. The inflammatory response is initiated by the release of exosomes and other damage associated molecular patterns (DAMPs) from injured epithelial cells[107]. It is then progressed and primarily coordinated by tissue-resident macrophages that produce pro-inflammatory cytokines such as interlukin-6 (IL-6) and tumor necrosis factor-α (TNF-α) to influence and recruit other immune cells to clear the inflammatory trigger[74,88,144,152,220,238]. Once the trigger has been eliminated, anti-inflammatory and pro-resolution cytokines are produced, such as interleukin-10 (IL-10) and interleukin-22 (IL-22) by macrophages and lymphocytes[51,144].

IL-22 is a member of the IL-10 superfamily, a family of anti-inflammatory cytokines that are up-regulated in inflammation and assist in the resolution response and tissue repair after inflammation[144,231]. We have previously shown that increasing the production of IL-22 may play a role in shifting the immune response from pro-inflammatory to pro-resolution and could be an effective treatment to reduce the chronic inflammation that causes the progression of these diseases and increase epithelial repair and barrier integrity after organic dust exposure[152,220]. Omega-3 (ω-3) fatty acids are metabolized to specialized pro-resolving mediators (SPMs) during the inflammatory response and function to transition inflammation towards resolution and repair processes[102,139,183]. The docosahexaenoic acid (DHA) derivative Resolvin D1 (RvD1), and its epimer aspirin-triggered resolvin D1 (AT-RvD1), in particular has previously demonstrated anti-inflammatory and pro-resolution properties in many murine models of acute lung injury, sepsis,

and chronic organic dust exposure[48,54,99,220]. We have also previously shown that AT-RvD1 assists in the production of IL-22 and modulates the pulmonary immune response to organic dust via studies showing that IL-22 knock-out mice experience more severe disease and that IL-22 is produced by macrophages in response to agriculture dust exposure [220].

1.2 Agriculture Dust-Induced Chronic Pulmonary Diseases

Agriculture workers who directly work on farms account for approximately $164.7 billion, or 0.7% of the United States' (US) Gross Domestic Product (GDP) as shown in (Figures 1 and 2). This provides 2.6 million jobs, or 1.3% of the US workforce[222].

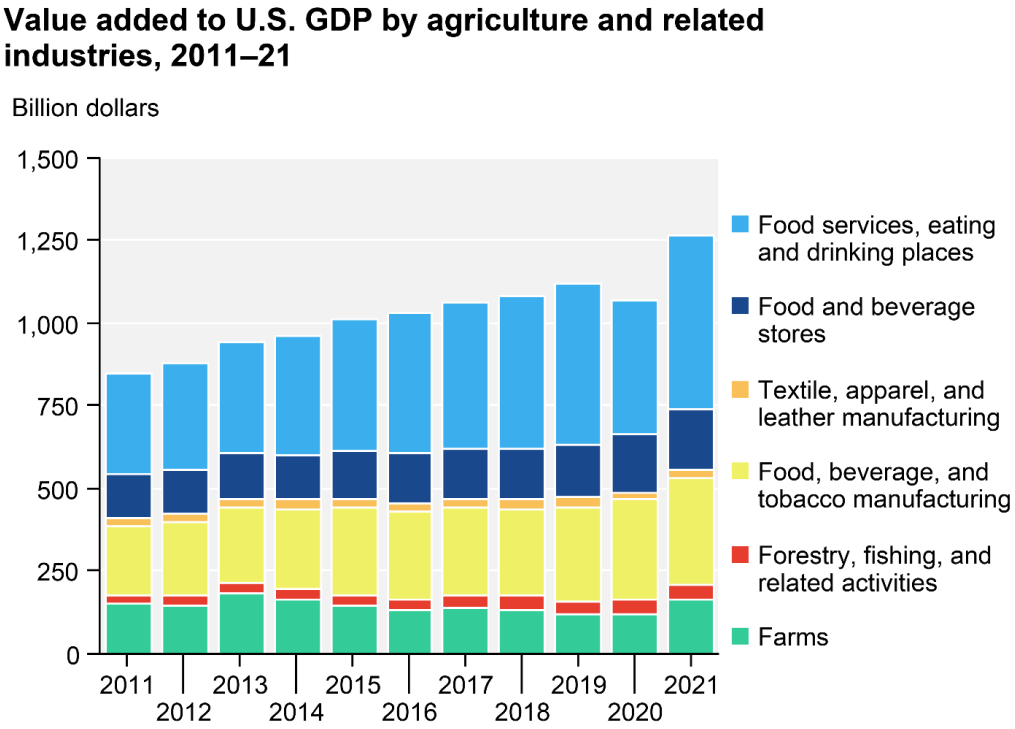


Figure 1. Agriculture and Food Industry Contribution to US Gross Domestic Product[222]

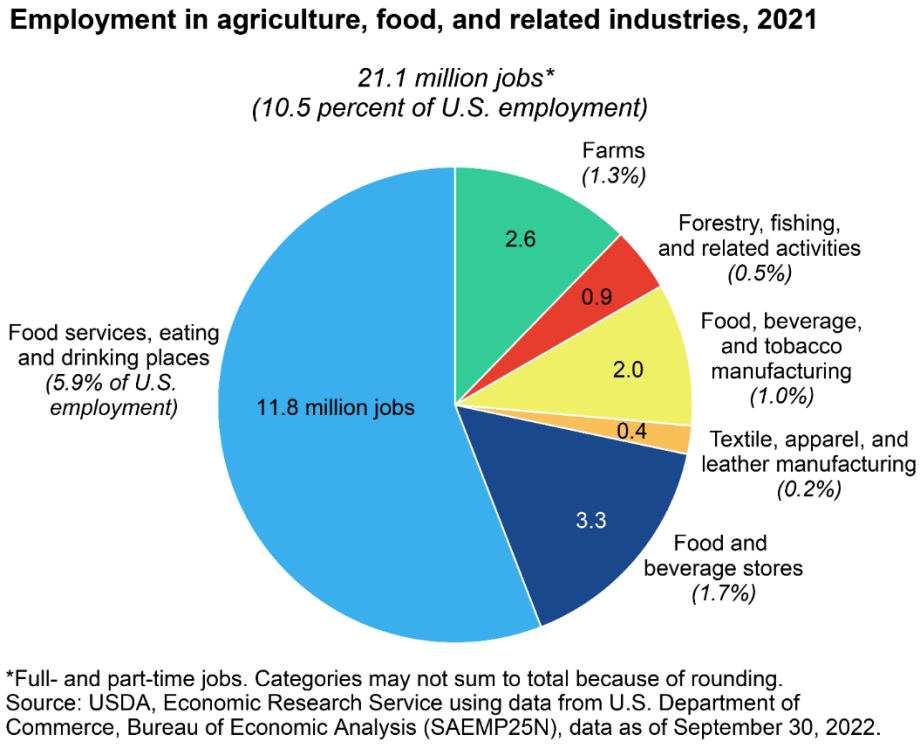


Figure 2. Agriculture and Food Industry Employment Statistics[222]

Agricultural workers are at elevated risk for chronic pulmonary diseases such as allergies, asthma, and COPD due to high exposure to organic dusts[138,176]. Agriculture dusts contain a wide variety of bacteria, fungi, and viruses, as well as endotoxins and lipopolysaccharides (LPS) that can contribute to the immune response[22].

26-53% of COPD cases in patients who have never smoked are attributed to occupational exposures, including dusts, with organic dusts significantly increasing the risk for chronic pulmonary diseases[210]. In addition, chronic lower respiratory tract diseases such as COPD are the 6th leading cause of death in the US[33]. Respiratory diseases associated with agricultural

occupations pose a significant burden to the healthcare system and development of treatments is essential to relieve that burden[232].

Risk for organic dust-induced respiratory diseases can be reduced in workers by using personal protective equipment (PPE) designed to limit respiratory injury including but not limited to, disposable dust masks, respirators with cartridges or canisters, and face shields [6,14,210]. In a publication by Kearney et al., out of 129 workers surveyed, 46% reported never using dust masks, 15% reported using masks more than half of the time, and only 40% reported consistent use. For face shields, 69% of workers reported no use, 9% reported use over half of the time, and 23% reported consistent use. Cartridge respirator users reported no use in 69% of workers, use more than half the time in 11% of workers, and consistent use in 19% of workers. Canister respirator users reported no use in 77% of workers, 6% reported use more than half time, 17% reported consistent use. Workers reported the highest influence for wearing PPE was desire to avoid injury and warning stickers on equipment[90].

Despite this, a large population of workers do not comply with PPE requirements and receive the full potential dose of organic dusts, causing significant risk for respiratory diseases. 48% reported ease of using PPE had some influence over compliance while 36% reported strong influence. 34% reported cost of PPE as having some influence with 22% reporting strong influence. 37% reported the time required to put on PPE as having some influence and 20% reported it having strong influence. 16% reported personal appearance having some influence and 15% reported it having strong influence[90]. Time and effort required to don PPE combined

with the cost makes workers less likely to use equipment intended to prevent respiratory and other diseases, leading to their inevitable development.

As compliance with PPE requirements is variable, therapeutics are needed to combat inevitable disease development. Therefore, a comprehensive approach of campaigns for increasing PPE use in workers and the development of pharmacological therapies for organic dust-induced chronic respiratory diseases is required to reduce the number of patients who progress to severe respiratory disease due to their occupations.

1.2.1 Allergies

Organic dusts inhaled during agricultural work and can cause inflammatory responses in workers[22]. General allergies are caused by the adaptive hypersensitivity response to fungal and bacterial spores[194]. Agricultural workers are also highly susceptible to a specific form of allergies known as farmer's hypersensitivity pneumonitis (FHP), caused by inhalation of mold spores from animal feed[60]. Dendritic cells and eosinophils respond to the allergen to cause an immune response and tissue damage[38,193]. Eosinophils degranulate and release tissue-damaging substances while dendritic cells prime T cells to continue the immune response and cause further tissue damage and severe symptoms such as difficulty breathing[38,193].

Allergic reactions are characterized by an early and late phase. The early phase begins within minutes of exposure and involves cross-linking of IgE, and degranulation of mast cells and basophils to release histamines, leukotrienes, and prostaglandins and can last up to 3 hours[130,194,214]. The early phase is the main contributor to rhinorrhea symptoms[214]. The late phase occurs within 4 hours of exposure and can last up to 12 hours, It is characterized by the increase

of leukocyte adhesion molecules to promote recruitment of monocytes, eosinophils, T cells, and basophils to the pulmonary mucosa and increased production of TNF-α by mast cells[130,195,205]. Allergic reactions to the spores in organic dust can be acute or chronic and may be associated with higher risk of asthma[60,165]. Acute symptoms typically manifest within 4 hours of exposure, peaking at 12 hours, and lasting up to 48 hours; they include fever, chills, frequent productive cough, shortness of breath, and chest discomfort. Chronic FHP can last significantly longer and presents as a long chest cold. These symptoms can decrease a patient's quality of life and reduce their ability to perform necessary tasks[60].

Interestingly, there are some groups of individuals that have increased immunity with exposure to agriculture dust. In Amish populations, the instances of allergies and other immune reactions to agriculture dust are 4-6 times lower than other populations[178]. Additionally, it appears that genetic factors and exposure windows are critical to developing allergic sensitization responses[178,182].

There are limited treatments for allergies, with most research focusing on food sensitivities[202]. Antihistamines are the recommended treatment for exposure allergies but often do not adequately control symptoms and may have adverse effects[114,202,250]. Immunotherapy is being explored for allergic rhinitis, where patients are inoculated sublingually with their sensitized agent to promote increased tolerance. However, in workers that develop FHP, these treatments are not effective, so exploration of other therapies is needed[116,197]. In workers with fungal sensitivities, immunotherapy has low efficacy in controlling rhinitis symptoms, requiring alternative treatments[23]. AT-RvD1 has demonstrated efficacy in reducing gut mucosal hypersensitivity through reduction of histamine release [149]. It has also shown to alter B cell class switching to inhibit IgE production while maintaining IgM, IgG, or IgA concentrations,

protecting against allergic reactions while maintaining mucosal barrier integrity, indicating it may be an effective treatment for respiratory allergies[93].

1.2.2 Asthma

Asthma is a disease characterized by coughing, wheezing, shortness of breath, and difficulty breathing[6]. It can be exacerbated by environmental triggers and cause significant detriment to patients' quality of life[6,67,236]. Asthma classically presents as eosinophil-mediated, with some dendritic and T cell involvement[79,110]. Some patients may also present with neutrophilic asthma, often during an attack and neutrophilic asthma is associated with reduced efficacy of steroid treatments and higher mortality than eosinophilic asthma[166].

As of 2020, there are currently 21 million adults in the US living with asthma, which makes up 8.4% of the population[6,67]. Females are more likely to be diagnosed with asthma than males, a statistic that is consistent with females experiencing higher prevalence and severity of chronic pulmonary diseases[6,14,18].

Work-related asthma (WRA) includes the exacerbation of pre-existing asthma or the new onset of asthma in patients who have never experienced it before, due to one's occupation[235]. The American Thoracic Society estimates that 15% of American adults with asthma can attribute their disease to their occupation[235]. Populations repetitively exposed to organic dust, whether from their occupation or residence, exhibited a positive correlation with increased severity of pre-existing asthma and increased development of new asthma patients[249]. In the US, adult asthma patients account for over 1 million emergency room visits per year, with over 100,000 patients requiring in-patient hospital stays to manage their symptoms, and approximately 4,000

patients dying from asthma each year[129]. Asthma treatment and related hospital stays are estimated to cost the US healthcare industry approximately $50 billion each year[32]. Development of new therapies to treat WRA is paramount to decreasing the monetary and labor burden on the healthcare system and reduce side effects of current therapies. There are many current treatments for asthma, all carrying side effects and risks, and some are only effective against some subtypes[64,166]. Corticosteroids are the most commonly prescribed treatment[67]. They reduce the Th2 inflammatory response and modulate the immune system to reduce inflammation from asthmatic triggers[64,67]. Long-acting β-agonists (LABAs) are often prescribed in combination with corticosteroids to reduce their side effects and reduce the risk of death associated with LABAs[67,121]. Leukotriene modifiers are prescribed to prevent the Th2 and Th17 responses, which can interfere with resolution actions of the Th17 pathway[67,227]. Theophyllines reduce symptoms through promotion of anti-inflammatory pathways through reduction of neutrophil recruitment and pro-inflammatory cytokine production[67].

Current treatments focus on anti-inflammatory therapies, which subsequently block the resolution response and return of tissue homeostasis[61,134]. IL-22 has been implicated as a regulator of asthma, and its production is thought to be driven by SPMs, therefore SPMs as a treatment would be effective to mediate the immune response to transition to a pro-resolution state, reducing symptoms and repairing tissues[15,84].

1.2.3 Chronic Obstructive Pulmonary Disease

COPD is a class of chronic irreversible lower respiratory diseases that include emphysema and chronic bronchitis. It is characterized by coughing and wheezing with increased

pulmonary mucus production, eventually leading to shortness of breath, and difficulty taking deep breaths[14].

COPD patients experience reduced quality of life, with difficulties performing normal activities[108], often not engaging in social activities, and experience additional comorbidities including cardiovascular diseases, asthma, and cognitive difficulties[69,232]. COPD has also been linked to increased risk of developing severe COVID-19 infections by 47.2%[167]. The cost of COPD medical bills increased from $32.1 billion to $49 billion in 2020. 51% of COPD medical bills were paid by Medicare, 25% by Medicaid, and 18% by private medical insurance, placing a significant burden on the state-funded medical system[39].

Organic dust-induced COPD is associated with high mortality rates[211]. As the disease progresses, patients experience reduced oxygen availability[14]. Mortality of COPD patients in agriculture occupations account for 11.3% of the chronic pulmonary disease-related deaths in the US[211]. COPD can also be associated with cardiovascular disease, heart failure, arrhythmia, and pulmonary embolism[18]. Women are affected more severely than men and have a higher mortality rate, and as of 2018, it is the 4th leading cause of death among adult women in the US[14,30].

The primary cause of COPD is smoking, but occupational pollutants such as agricultural dust, are also a significant contributing factor[14,211]. COPD is caused and perpetuated by chronic immune activation from foreign particles such as smoke or organic dusts[1]. The inflammation in COPD is initiated by macrophages and epithelial cells reacting to foreign material in the alveolar spaces[1]. Macrophages are the primary coordinators of the inflammatory response in COPD, but

other cells such as neutrophils, eosinophils, and lymphocytes also contribute to the chronic inflammation and tissue damage[52,233,239].

Neutrophils are recruited as part of the immune response but cause tissue damage through release of granules and neutrophil extracellular traps (NETs) when chronically activated[28]. There is conflicting evidence for the association of eosinophils and COPD. High eosinophil levels in the lung have previously been associated with exacerbated disease states and increased inflammation, contributing to eosinophilic COPD[52]. Eosinophilic COPD endotypes are associated with higher healthcare costs[143]. Recent studies have shown lung-resident eosinophils contribute to resolution of inflammation and the restoration of tissue homeostasis[123,124]. COPD histology is associated with increased lymphocyte infiltration and aggregation, tissue destruction, and signs of significant remodeling[57]. Patients exhibit elevated production of IL-6, TNF-α, and IL-10[224]. As the disease progresses, serum IL-10 levels decrease while IL-6 levels increase[86,199]. Chronic inflammation in COPD leads to fibroblasts activating the remodeling process in excess, causing tissue thickening in the airways and obstructed breathing[1].
Due to its negative effects on patient quality of life, exploring effective therapies to slow the progression of the disease and prolong the patient's quality of life is of increasing interest in biomedical and pharmacological research groups. Current treatments aim to control the symptoms through bronchodilators such as β-agonists, and anti-inflammatory drugs including corticosteroids, phosphodiesterase inhibitors, and macrolides[52]. However, these therapies have not been shown to reduce the progression of the disease or impact mortality rates[52]. β-agonists often have severe side effects and risk of death, requiring combinational therapy with

corticosteroids[67,121]. Corticosteroids and other anti-inflammatory drugs block the inflammatory response, which leads to a reduction of the resolution response and prevents tissue repair[61,134]. Control of the inflammatory response to prevent chronic activation and promote resolution is preferred to prevent progression of the disease[83]. SPMs have been implicated in aiding the transition of the inflammatory response to resolution, increasing tissue repair, and reducing chronic inflammation-caused pathology[83,192]. Resolvins have demonstrated pro-resolution properties in a wide range pulmonary injury models, suggesting they could be a viable treatment for COPD[48,54,190]. We hypothesize that these compounds would work differently than the established treatments by reducing the progression of the disease and decreasing mortality rates.

1.2.4 Organic Dust Toxic Syndrome

Organic dust toxic syndrome (ODTS) is an acute respiratory disease mediated by a severe immune reaction to organic dust[59]. Symptoms appear within 4-6 hours of exposure and include flu-like symptoms: fever, chills, cough, muscle aches, weakness and fatigue, and loss of appetite[60].

The disease is primarily facilitated by the innate immune response to fungal spores and endotoxins in organic dust[10,115,170]. Pathophysiological effects of ODTS are primarily facilitated by the release of chemotactic molecules from alveolar macrophages to initiate neutrophil recruitment to the lungs from the vasculature[58]. Febrile symptoms are the result of the production of pyrogenic cytokines such as IL-6 by pulmonary epithelial cells and alveolar macrophages[173].

Bronchoalveolar lavage fluid (BALF) from patients with ODTS revealed increased neutrophil counts, IL-6, and TNF-α[58,234].

Patients are often misdiagnosed with infectious diseases due to the presenting symptoms and laboratory tests[132]. They often recover without medical attention but are left with increased risk of chronic bronchitis[59,97]. Current routine treatment for ODTS is acetaminophen for febrile symptoms and generic non-steroidal anti-inflammatory drugs (NSAIDs) to treat the other symptoms, which reduce the immune response[172]. Attenuation of the immune response is not desired as its processes are critical to clear the tissue-damaging foreign substances[61,134].
Use of PPE such as respirators was associated with reduced neutrophil recruitment, IL-6 nasal lavage levels and, reduced endotoxin levels in the human subjects who were wearing respirators and exposed to swine dust compared to participants who were not wearing a respirator and exposed to swine dust[49,146]. Supplemental DHA has been associated with reduced neutrophil recruitment to injured tissues within 4 hours by blocking chemotaxis[71,206]. Resolution of the immune response and transition to repair processes has previously been demonstrated to be mediated and enhanced by SPMs, including AT-RvD1, indicating it could be a viable treatment for ODTS[54,188].

1.2.5 Neurological Disease and Agriculture Dust

Particulate matter (PM) exposure, such as air pollution, wildfire smoke, and industrial dusts cause irreversible inflammatory lung disease in those exposed[27,40,127,163,164]. Agricultural workers are exposed to many toxic assaults including chemicals and PM as organic dust[91,160,163,176,236]. Organic dust exposure (ODE) has been demonstrated as a leading cause of chronic inflammatory respiratory diseases such as chronic obstructive pulmonary disease

(COPD)[29,136,138,210]. An epidemiological study has significantly linked ODE from agricultural operations with increased risk of dementia (HR, 1.13; 95% CI, 1.01-1.27)[245]. PM has demonstrated the ability to travel through the nasal epithelium and olfactory nerve to the brain, as well as through the pulmonary lung-blood barrier, into circulation, and through the blood brain barrier (BBB), leading to neurological inflammation[103,141,150,164].

Inhaled PM exposure has been recently linked to an increased risk of developing dementia, with the greatest risk being associated with agricultural organic dust exposure over all other PM exposures [246]. COPD patients have documented increases in depressive symptoms, confusion, memory loss, and mental functional decline as their disease progresses (13,14). A study conducted by the CDC analyzed comorbidities of 8,094 patients in resident care facilities diagnosed with CLRDs including chronic bronchitis, emphysema, and COPD [232]. This study found that 51.4% of patients with one more CLRD also presented with Alzheimer's disease or dementia ($p < 0.001$), 27.4% were diagnosed with depression ($p=0.012$), 7.7% were diagnosed with multiple sclerosis, Parkinson's disease, or epilepsy ($p= 0.020$), and 11.7% presented with other mental disorders ($p=0.007$) [232]. Overall, the authors found that 64.9% of patients with more CLRD experienced a mental or behavioral health disorder, and 11.6% experienced a nervous system disorder [232]. Agriculture workers often experience high levels of mental disorders including anxiety (males: 22% females: 39%, total: 31%) and depression (males: 35%, females: 42%, total: 39%) [131]. Additionally, air pollution exposure has been linked to neurological inflammation in murine models but has not been assessed in the specific context of agricultural organic dust exposure [27,105,180].

1.3 The Pulmonary and Neurological Response to Organic Dusts

The pulmonary system is consistently exposed to microorganisms and toxins in the air we breathe, and maintaining the integrity of the mucosal barrier and immune response is essential to prevent chronic infections and diseases. It is critical to maintain tissue integrity in the pulmonary system due to its close interface with the circulatory system to prevent transfer of foreign particles or pathogens into systemic circulation[4]. The pulmonary system is comprised of mucosal tissue with resident immune cells positioned to patrol for foreign particles and pathogens[11]. Cells involved in the immune response to particulate exposure such as agriculture dust include macrophages, neutrophils, eosinophils, and lymphocytes[124,126,158,226].

Macrophages are the primary coordinators of the pulmonary immune system, producing IL-6 and TNF-α in response to foreign particles[80,179]. After resolution of inflammation, they will also produce IL-10 to initiate tissue repair[177,196]. Recruited macrophages and lymphocytes produce IL-22 to aid in the resolution of inflammation and tissue repair processes[153,158].

1.3.1 Signaling Molecules in the Pulmonary and Neurological Immune Response

Pro-inflammatory cytokines such as IL-6 and TNF-α are common indicators of acute inflammation which, after repeated exposure to toxins or particles, can progress to chronic inflammatory diseases [54]. Pro-inflammatory cytokines are produced by epithelial cells, monocytes, and macrophages during an inflammatory response initiated by pathogen associated molecular patterns (PAMPs) and/or damage associated molecular patterns (DAMPs)[98,213].

In the case of organic dust exposure, damage to the epithelial cells from the dust particles causes apoptosis and the release of cellular contents as DAMPs, such as mitochondrial DNA (mtDNA) and cellular proteins that are recognized by toll-like receptors on macrophages, which induces

IL-6 and TNF-α production[248]. Organic dusts may also contain microorganisms such as bacteria, viruses, and fungal spores which activate PAMP pathways to initiate an immune response with the release of IL-6 and TNF-α[98].

IL-6 can be produced by monocytes, macrophages, T cells, B cells, and epithelial cells[94,242]. IL-6 is produced by macrophages and monocytes at the initiation of the immune response to signal the maturation of B cells into antibody-producing plasma cells[75,212]. It also functions to increase pulmonary vascular permeability to aid the recruitment of other immune cells[70].

TNF-α is produced by monocytes and macrophages in response to infection or injury to activate neutrophils and natural killer (NK) cells and increase macrophage phaocytosis[62,80]. Excessive production can result in apoptosis or necrosis, damaging tissues and furthering the immune response to a chronic state[20].

The cytokines IL-10 and IL-22 are regarded as anti-inflammatory and pro-resolution, promoting epithelial repair and homeostasis after inflamamtion[144]. IL-10 is produced by monocytes and macrophages during the immune response to promote the transition to resolution and aid in tissue repair[196]. IL-22 has been implicated in promoting tissue repair and epithelial barrier integrity[153]. Studies indicate that attenuation of IL-22 is associated with worse disease state outcomes[220]. It is widely regarded as being exclusively produced by lymphocytes, but macrophages have been implicated as a possible source in our previous studies[51,220]. IL-22 is not always shown to be universally anti-inflammatory. In other studies, IL-22 production has been shown to correlate with some diseases, and that polymorphisms in certain patients can enhance susceptibility to secondary exposures[46,207,244,247]. This conflicting data makes IL-22 an important

cytokine target to understand the inflammatory response and regulation in agriculture dust exposure.

1.3.2 Immune Cells in the Pulmonary and Neurological Response to Organic Dusts

Alveolar macrophages are located in the alveoli and airways and function to patrol for foreign materials and pathogens, acting as the primary initiators and coordinators of the pulmonary immune response[45]. Macrophages, including alveolar macrophages, exist in an anti-inflammatory basal state to protect the delicate tissues from immune-modulated injury, but like all macrophages, exist on a spectrum which allows for the production of both pro-inflammatory and anti-inflammatory mediators as needed[125].

Neutrophils are circulating granulocytes that are recruited from the vasculature by chemokines secreted from macrophages and damaged epithelial cells during an immune response[28,175]. They produce and release cytotoxic compounds to assist in the elimination of pathogens and foreign material, but often cause tissue collateral damage in the process[226]. They also assist in phagocytosis of foreign particles and pathogens, as well as produce NETs to trap foreign materials for phagocytosis and elimination by macrophages and neutrophils[28]. Recent evidence has implicated them in resolution and repair processes, indicating they may not only serve a damaging role[226].

Eosinophils are granulocytes involved in many inflammatory processes, most notably in parasitic infections and allergies, but are also elevated in COPD and asthma[12,38]. They can be tissue-resident or recruited from the vasculature during inflammation and are involved in the complement cascade to assist in pathogen clearance as well as secrete cytokines and chemokines to coordinate immune functions[38,124,230]. Recruitment of eosinophils into the pulmonary tissues

depends on IL-22 signaling from T lymphocytes[19]. They have also been implicated in the repair process after allergic reactions[38].

Lymphocytes are recruited from the blood during inflammation by chemotactic molecules[17]. αβ $CD4^+$ T cells are upregulated in dust exposure mouse models and are primarily polarized to Th1 and Th17 responses[158]. In organic dust-exposed COPD patients, NK cells and $CD8^+$ T cells are significantly decreased compared to non-COPD patients[91]. COPD patients in general have elevated lymphocyte populations compared to non-COPD patients, which contributes to the chronic inflammation and tissue damage[91].

1.3.3 IL-22 In the Pulmonary and Neurological Immune Response to Organic Dust

IL-22 is a cytokine in the IL-10 superfamily, which are generally described as being anti-inflammatory[51,144]. Previous evidence has indicated that increased expression of IL-22 may aid in reduction of inflammation[84]. Its role in controlling inflammation is demonstrated by its correlation with reduced neutrophil infiltration in a murine *Pseudomonas aeruginosa* pneumonia model[25]. Therapies that increase this cytokine could aid in preventing the inflammatory response from progressing to chronic pulmonary disease[48,78].

Previous studies have indicated that IL-22 is produced exclusively by lymphocytes, however, the investigators gated only on the lymphoid lineage, excluding myeloid populations in their exploration of IL-22 expression, therefore this study was limited by the investigators only considering the lymphocytic population when gating for IL-22[2,51]. In the pulmonary system, IL-

22 is produced by innate lymphoid cells during the innate immune response and Th17 αβ T cells, γδ T cells, and NK cells during the adaptive immune response[124,126,153,158,226].

The IL-22 receptor IL22Ra1 is present on pulmonary epithelial cells and acts to direct repair and maintain mucosal homeostasis[135,153]. The IL-22 receptor is comprised of two subunits, the IL10R2 subunit and the IL22R1 subunit, suggesting it would have similar downstream intracellular functions as IL-10[128]. IL-22 acts on receptors on ciliated airway epithelial cells to promote epithelial repair and inflammatory resolution[8,153]. During inflammation, IL22Ra1 is upregulated on parenchymal epithelial cells, indicating IL-22 is critical to restoring and maintaining epithelial homeostasis[153].

Studies have demonstrated neutralization of IL-22 increases mucosal susceptibility to microbial challenge by reducing neutrophil recruitment and infiltration into pulmonary tissues, indicating its role in mucosal barrier maintenance and microbial resistance[25]. IL-22 also has pro-inflammatory roles in the presence of IL-17, recruiting eosinophils in asthma models of mice sensitized to ovalbumin[19].

IL-22 also plays a role in the neuroinflammatory response via receptors on microglia. There is debate for whether IL-22 is protective or inflammatory, as some studies have shown that IL-22 is involved in TNF-α production and that IL-22 mRNA is elevated in Alzheimer's patients [34,101]. Other studies have found that IL-22$^{-/-}$ mice are more susceptible to neuroinflammatory insults and have increased disease severity [117].

1.4 Lipids in the Pulmonary and Neurological Inflammatory Response

Polyunsaturated fatty acids (PUFAs) perform many functions in the immune response as mediators for both inflammation and resolution and repair including activating, modulating, and

resolving inflammation[8,43,81,183,185,186,189,200]. During inflammation, omega-6 (ω-6) PUFAs are cleaved from immune and epithelial cell membranes and metabolized to pro-inflammatory mediators, and both ω-6 and ω-3 PUFAs are cleaved to be metabolized to SPMs, which initiate repair and resolution (Figure 3)[8,81,184].

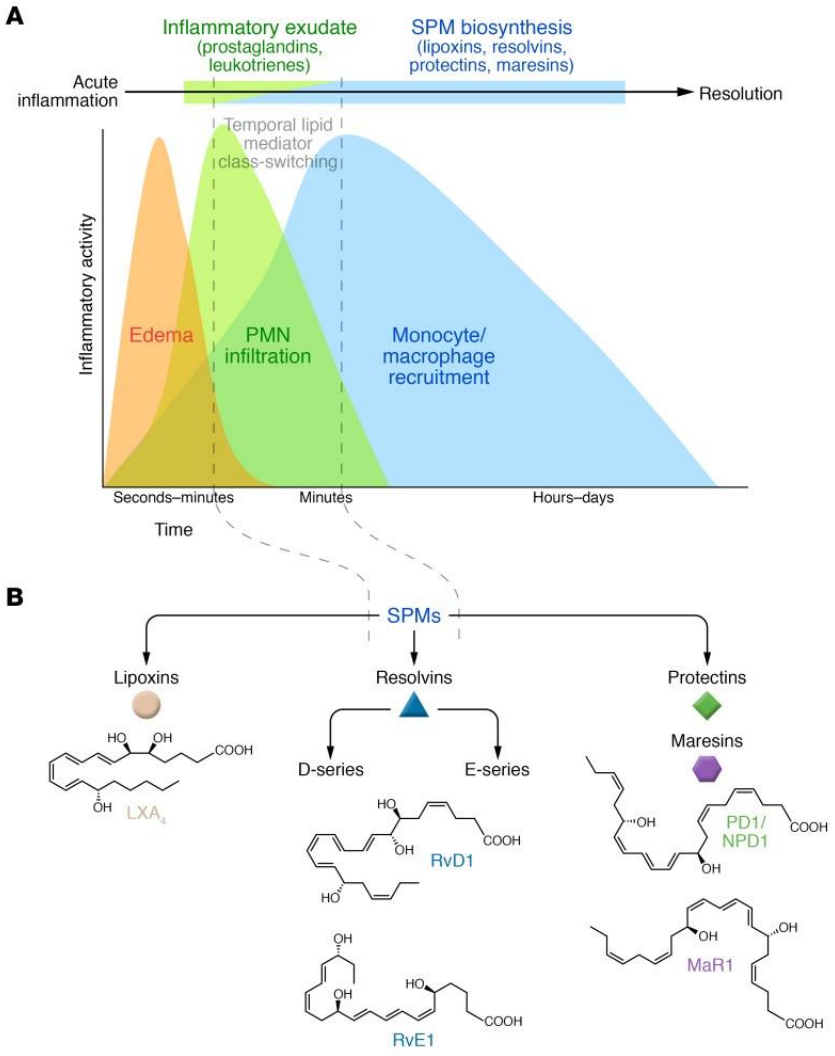


Figure 3. Inflammation-Resolution Relationship Mediated by SPMs[189]

1.4.1 Omega-6 Fatty Acids in Inflammation

Omega-6 (ω-6) fatty acids are metabolized by leukocytes during inflammation to produce pro-inflammatory lipid mediators that act on other immune cells to induce the production of pro-inflammatory cytokines[113,225].

The primary substrate is arachidonic acid (AA), which is cleaved from the cell's plasma membrane and acted on by cyclooxygenases (COX), lipoxygenases (LOX), and cytochrome P450 (CYP) enzymes. COX reactions produce prostaglandins, LOX reactions produce

leukotrienes, and P450 reactions produce hydroxyeicosatetraenoic acids (HETEs)[113,218,225]. Prostaglandins and HETEs are chemotactic for circulating immune cells, driving leukocyte infiltration into tissues[113]. Leukotrienes enhance leukocyte adhesion to vessels, aids infiltration into tissues during inflammation[113]. HETEs aid in vasodilation, an important factor in facilitating immune cell infiltration into tissues[218].

1.4.2 Omega-3 Fatty Acids in Inflammation

ω-3 fatty acids are known to control inflammation and aid in reducing symptoms of chronic diseases[122]. Diets high in the ω-3 PUFA DHA have been shown to be protective in a murine model of chronic organic dust exposure and other chronic inflammatory diseases by increasing the concentration of substrates necessary to transition the immune response to a pro-resolution state[122,219].

ω-3 fatty acids are cleaved from immune cell membranes during the resolution phase of inflammation to be metabolized into SPMs, which act on macrophages and lymphocytes to induce the production of anti-inflammatory and pro-resolution cytokines and increase phagocytosis and other antimicrobial functions[35,43,187]. They also act on receptors on epithelial cells to initiate tissue repair processes[153]. SPMs function during the peak of the inflammatory response to control and mitigate tissue damage and restore homeostasis[189].

1.4.3 Specialized Pro-Resolving Mediators

The resolution of inflammation has traditionally been considered a passive process but has since been demonstrated to be highly bioreactive[183]. SPMs are produced from

polyunsaturated ω-3 fatty acids in response to inflammation by cleavage from epithelial, macrophage, and other immune cell membranes[186].

Inflammation is protective but can become damaging if left unresolved[189]. Resolution of inflammation is critical to restoring tissue homeostasis and preventing further tissue damage[189]. SPMs are considered anti-inflammatory and pro-resolution because they control the severity of the response by restricting immune cell recruitment and cytokine production to only what is necessary to clear the trigger while limiting tissue damage[41,102,112,189]. SPMs decrease the time interval of inflammation by limiting immune cell infiltration while enhancing efferocytosis, phagocytosis, and microbial elimination (Figure 4)[35,44]. In contrast, administration of NSAIDs and other anti-inflammatory drugs can cause immunosuppression, reducing the effectiveness of the immune response during pathogen or particle challenge[189]. SPMs drive the polarization of immune cells to a pro-resolution state, inhibiting the production of pro-inflammatory cytokines and upregulating the production of pro-resolution cytokines to promote tissue repair[9,35]. Cytokine production alteration by SPMs acts on innate lymphocytes, NK cells, T cells, and B cells[13,93,96].

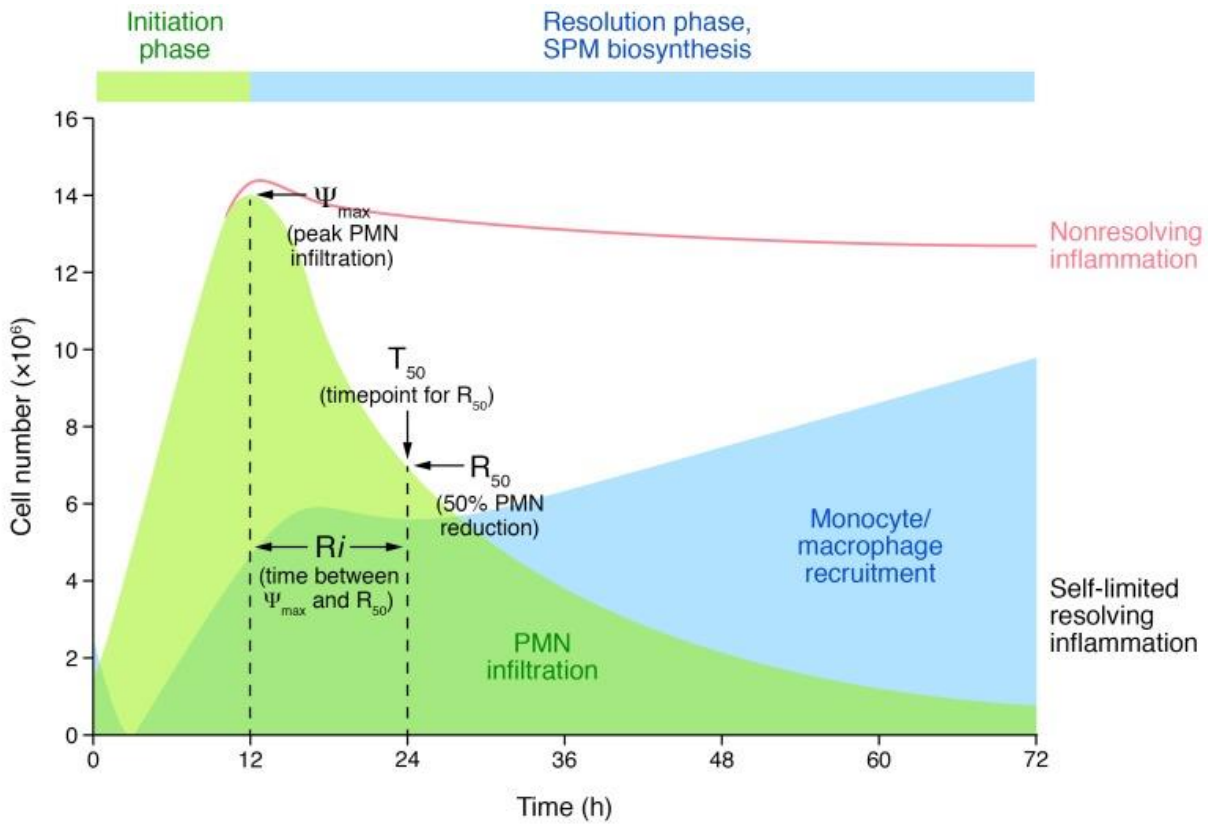


Figure 4. Resolution of Inflammation vs Nonrevolving Inflammatory Response[189]

1.4.4 Resolvin D1 and Aspirin-Triggered Resolvin D1

Resolvin D1 (RvD1) is an SPM produced by macrophages and neutrophils in response to inflammation[43,186]. RvD1 has been demonstrated to peak 5 hours post-DE exposure and continue into the resolution phase in a murine model or agricultural dust exposure[43,219]. RvD1 is produced by pulmonary mucosal tissues in response to acute lung injury following hydrochloric acid challenge and reduces pro-inflammatory cytokine production[54]. It is produced *in vivo* and rapidly inactivated by eicosanoid oxidoreductase to significantly less bioactive metabolites 8-oxo-RvD1 and 17-oxo-RvD1[208].

Aspirin-Triggered Resolvin D1 (AT-RvD1) is an epimer of RvD1 produced through acetylation of the cyclooxygenase-2 (COX-2) enzyme by aspirin, causing a conformational

change in the enzyme and altering the metabolism of docosahexaenoic acid (DHA) to form 17(R)-RvD1 instead of RvD1 (Figure 5)[181,208]. AT-RvD1 is converted to its 8-oxo-RvD1 and 17-oxo-RvD1 metabolites at a reduced rate, so has longer-lasting, more potent pharmacological activity[1,208]. RvD1 is converted to these metabolites within 25 minutes, whereas AT-RvD1 was shown to be resistant to this degradation pathway[208]. Stereochemistry is critical to biological activity and potency, with the 17(R) conformation being favored biologically and 17(R)-AT-RvD1 being favored in studies[48,54,77,185]. The half-life of RvD1 and AT-RvD1 are also significantly different, with RvD1 having a half-life of 5.5 hours, while AT-RvD1 has a half-life of 105 hours, allowing it to remain in the tissues longer [240,241]. However, these studies were

performed using predictive computational modeling and only in female NOD/ShiLtJ mice given only one dosage of 0.1 mg/kg, which may not translate to our mouse models [240,241].

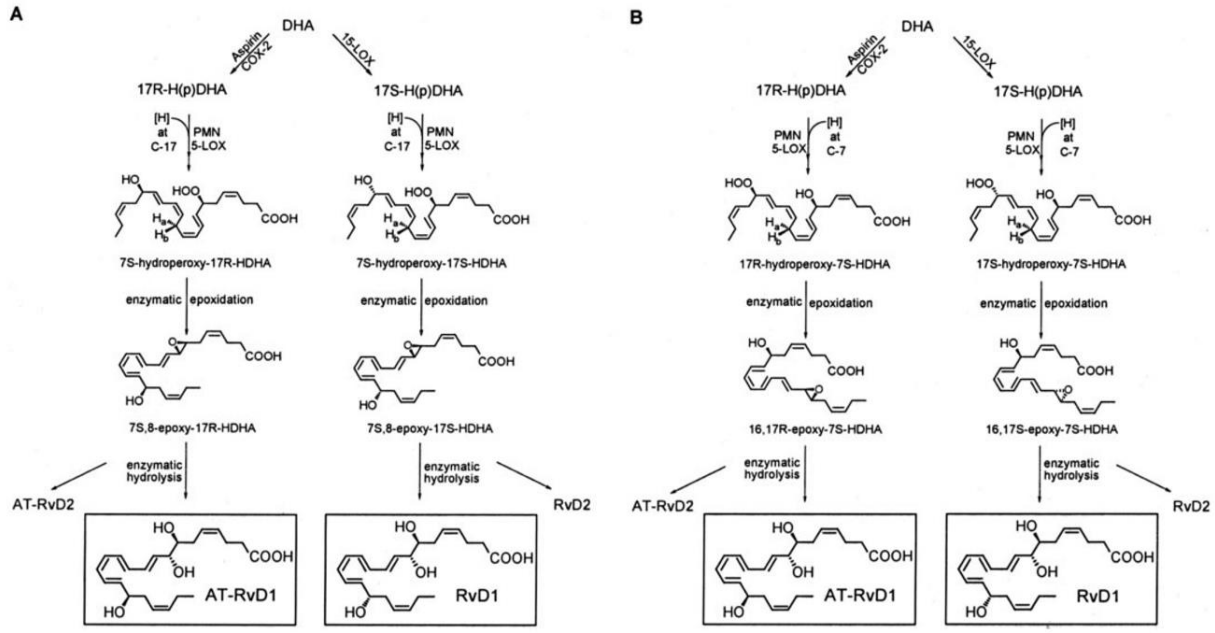


Figure 5. Metabolic pathway for formation of RvD1 and AT-RvD1[208]

(A) Formation of 7(S),17(R) AT-RvD1 by acetylation of COX-2 by aspirin and 7(S),17(S) RvD1 by 15-LOX.; (B) Formation of 17(R),7(S) AT-RvD1 by acetylation of COX-2 by aspirin and 17(S),7(S) RvD1 by 15-LOX.

RvD1 production and tissue concentrations are correlated with disease outcomes in acute and chronic inflammatory disease as well as autoimmune diseases[145,189]. In an acute lung injury murine model, AT-RvD1 reduced BALF IL-6 and TNF-α concentrations and histology displayed higher epithelial integrity compared to those without RvD1 treatment[54]. It has also demonstrated significantly reduced infiltration of macrophages, neutrophils, eosinophils, and lymphocytes[48]. In a murine cancer model of chronic dust exposure, AT-RvD1 administration was correlated with reduced neutrophil and lymphocyte infiltration and increased IL-10 concentrations in BALF[48].

RvD1 has also exhibited a protective role in neutrophil-mediated reperfusion injury[208]. These studies indicate it may assist in maintaining homeostasis between inflammation and resolution.

1.5 Justification and Specific Aims

Organic dust exposure in agriculture workers is a leading cause of COPD and other acute and chronic respiratory diseases, of which there are limited treatments with many side effects[23,82,132,136,203]. Studies have shown low compliance with PPE in agricultural workers, leading to higher prevalence of chronic inflammatory diseases, and highlighting the need for improved treatments for organic dust-induced chronic inflammatory diseases[29,56,90,224]. Recent studies have also linked agriculture dust exposure to an increased risk of developing dementia, and COPD patients have reported increased symptoms of memory loss, depression, and anxiety, and approximately 60% of patients with COPD or a related chronic inflammatory pulmonary disease are also diagnoses with a nervous system disorder [29,211,232,246]. The cytokine IL-22 functions to maintain the mucosal barrier and restore tissue homeostasis after an inflammatory response and the literature primarily accepts it is produced by lymphocytes[51,84]. RvD1 is an SPM derived from the ω-3 PUFA, DHA that has exhibited a protective role in a murine acute lung injury model and a murine chronic dust exposure cancer model[48,54].

Our previous findings indicate that knock-out of IL-22 is associated with worse disease outcomes in a repetitive organic dust exposure model with IL-22 knock out mice[220]. We have also demonstrated ω-3 fatty acid metabolites may contribute to increased IL-22 production by macrophages, as have other researchers of acute and chronic lung injury[54,220]. Disruptions in SPM production are associated with attenuated IL-22 production and correlate with worse outcomes in a murine sepsis model[36]. SPMs, specifically RvD1, have been previously shown to

induce a pro-resolution response after initiation of inflammation and play a protective role in tissue repair[54].

This project aims to characterize the neuroinflammatory response to agriculture dust via *in vitro* exposure of macrophages and microglia to agriculture dust and treatment with AT-RvD1 and an *in vivo* mouse model of repetitive agriculture dust exposure and determine the therapeutic potential of AT-RvD1. We hypothesize that our *in vitro* studies will reveal increased inflammatory mediator production including IL-6 and TNF-α in cells exposed to agriculture dust and a reduction of these mediators in cells co-treated with AT-RvD1. Our hypothesis was that animals exposed to agriculture dust will display neuroinflammatory pathology and that this inflammation will be reduced in animals co-treated with AT-RvD1. We expect these studies to contribute to the greater understanding of how inhaled environmental exposures contribute to neurotoxicity and determine if AT-RvD1 could be a viable novel therapeutic for the reduction of agriculture dust-induced pulmonary and neurological inflammation. We expect this to translate to better patient outcomes including but not limited to reduction of cough, increased oxygen saturation, improved reported emotional status, and increased memory and mentation outcomes.

CHAPTER 2: OPTIMIZING ASPIRIN-TRIGGERED RESOLVIN D1 FOR *IN VIVO* APPLICATIONS

2.1 Introduction

Agriculture workers are exposed to organic dusts that lead to chronic inflammatory lung diseases such as allergies, asthma, chronic obstructive pulmonary disease (COPD), and organic dust toxic syndrome (ODTS)[7,48,60,136,220,249]. These diseases are progressive and ultimately fatal, with limited treatments currently available. Development of improved pharmacological interventions is of increasing concern in public health[59,110,111,202,203].

Omega-3 (ω-3) fatty acids and their metabolites have been shown to reduce inflammation *in vitro* and *in vivo*, making them promising candidates for novel therapeutics for chronic inflammatory diseases such as COPD [8,181,183,185,189,191]. The docosahexaenoic acid (DHA) metabolite, AT-RvD1 has previously demonstrated anti-inflammatory and pro-resolution properties in many murine models of acute lung injury, sepsis, and chronic organic dust exposure[48,54,99,220]. We have also previously shown that AT-RvD1 assists in the production of IL-22 and modulates the pulmonary immune response to organic dust[220]. AT-RvD1 has been shown to modulate several cellular processes in order to facilitate its anti-inflammatory and tissue repair functions. These processes include the attenuation of pro-inflammatory cytokines and chemokines, the polarization of macrophages and microglia to pro-resolution states, and the reduction of neutrophil lymphocyte recruitment [48,50,208,216].

We aimed to understand the effects of AT-RvD1 on *in vitro* cultures of macrophages and microglia and determine the therapeutic effects of this SPM in an *in vivo* mouse model of repetitive agriculture dust exposure. We also aimed to determine an effective dosage amount and schedule for our *in vivo* model by utilizing various dosages and dosing schedules. We aimed to

utilize this final dose in a larger *in vivo* study to better understand the therapeutic potential of AT-RvD1 in an *in vivo* mouse model of repetitive agriculture dust exposure.

2.2 Materials and Methods

2.2.1 Hog Dust Extract Preparation

Dust was collected at least one meter above the ground from enclosed swine confinement facilities in the Midwest US and stored at -20 °C for later use. 10 g of collected dust was added to 100 mL of Hank's Balanced Salt Solution (HBSS) (HyClone Laboratories; Logan, Utah, USA) and stirred for one hour on a magnetic stir plate at room temperature. The solution was transferred to 50 mL conical tubes and centrifuged at 2500 rpm at 4 °C for 20 minutes. Supernatant was transferred to new 50 mL conical tubes, and the pellets were discarded. The solution was centrifuged again at 2500 rpm at 4 °C for 20 minutes. The supernatant was filtered through 0.22 μm syringe filters into new 50 mL conical tubes and aliquoted into microcentrifuge tubes at 1 mL 100% DE per tube and stored at -20 °C.

2.2.2 Mouse Alveolar Macrophage Culture and Co-Exposure Model

A mouse alveolar macrophage immortalized cell line (MH-S ATCC CRL-2019) was cultured in RPMI-1640 medium (Mediatech Inc.; Virginia, USA) with 10% fetal bovine serum (FBS) (Mediatech Inc.; Virginia, USA), 1% penicillin-streptomycin (Life Technologies Corporation, New York, USA), and 1% L-glutamine solution (HyClone Laboratories; Logan, Utah, USA) at 37 °C with 5% CO_2. Medium was refreshed every 2-3 days. Cells were harvested from culture flasks with 0.25% trypsin, 0.53 mM ethylenediaminetetraacetic acid (EDTA) solution (HyClone Laboratories; Logan, Utah, USA) and counted via hemocytometer to seed 24-

well plates (Fisher Brand) at a density of $1x10^6$ cells per well. Plates were incubated overnight in growth medium and no more than 24 hours before treatment. Solutions for treatments with hog dust extract (DE) and 17(R)-AT-RvD1 (AT-RvD1) (Caymen Labs) were prepared: medium with no additives, medium with 1% DE, medium at 10 nM AT-RvD1, medium at 100 nM AT-RvD1, medium at 10 nM AT-RvD1 with 1% DE co-exposure, and medium at 100 nM AT-RvD1 with 1% DE co-exposure were prepped. Overnight growth medium was aspirated, and the treatments were added with four replicates each and incubated for 1, 2, 6, 18, or 24 hours. All studies were repeated twice for a total number of 8 wells per treatment. A schematic of the 24-well plate set-up is detailed in Figure 6.

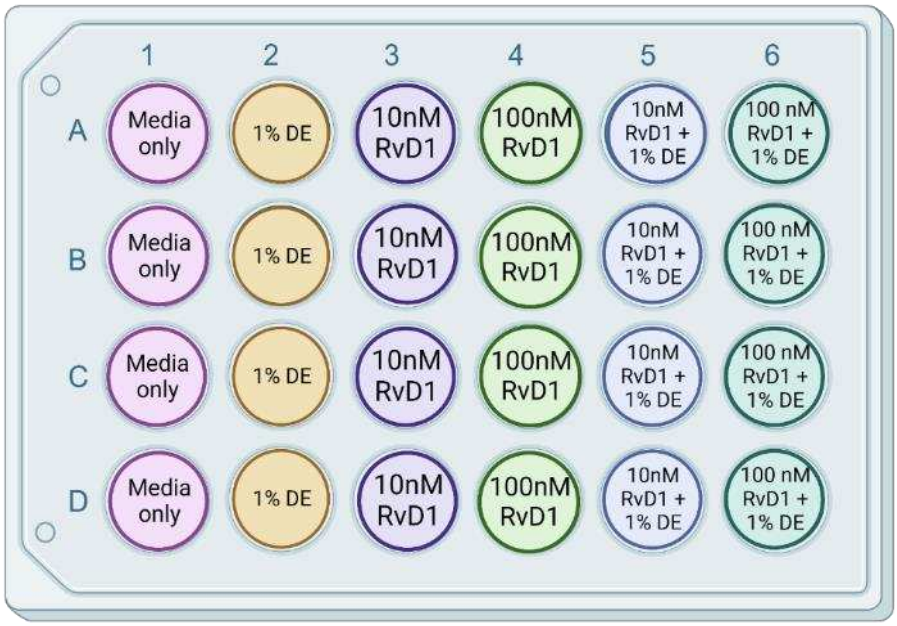


Figure 6. Experimental Plate Set-Up for Cultured Macrophages

2.2.3 Mouse Microglia Culture Maintenance

Mouse immortalized microglia (BV2 line) were purchased from ATCC and cultured with company recommendations. Briefly, culture medium was comprised of DMEM (Mediatech Inc.;

Virginia, USA), with 10% FBS (Mediatech Inc.; Virginia, USA), 1% penicillin-streptomycin (Life Technologies Corporation, New York, USA), and 1% L-glutamine solution (HyClone Laboratories; Logan, Utah, USA) at 37 °C with 5% CO_2. Medium was refreshed every 2-3 days.

2.2.4 Mitochondrial Function (MTT) Assay

Mitochondria function was assessed in cultured microglia to determine the effects of DE on cellular functions in cells exposed to increasing concentrations of DE. Cells were exposed to the following conditions: media only, 0.025% DE, 0.05% DE, 1% DE, 0.2% DE, 0.25% DE, 0.5% DE, 1% DE, 2% DE, and 2.5% DE. Cells were harvested from culture flasks using 0.25% trypsin, 0.53 mM ethylenediaminetetraacetic acid (EDTA) solution (HyClone Laboratories; Logan, Utah, USA) and counted via hemocytometer to seed 24-well plates (Fisher Scientific) at a density of 10,000 cells per well in a 96-well plate. Plates were incubated overnight in growth medium and no more than 24 hours before treatment. Overnight growth medium was aspirated, and the treatments were added with four replicates each and incubated for 6 hours. After the incubation period was complete, the culture media was aspirated and 100 µl of 3-(4,5-dimethylthiazol-2-yl)-2,5-diphenyltetrazolium bromide (MTT) was added to each well and the liquid was pipetted up and down to mix. The plates were then returned to the incubator for 2 hours at 37 °C with 5% CO_2. Following incubation, 50 µl of dimethyl sulfoxide (Fisher Scientific) was added to each well and mixed thoroughly. The plates were then analyzed on a

FLUOstar Omega spectrophotometer at 570 nm using Omega software version 5.7. A schematic of the 96-well plate set-up is provided in Figure 7.

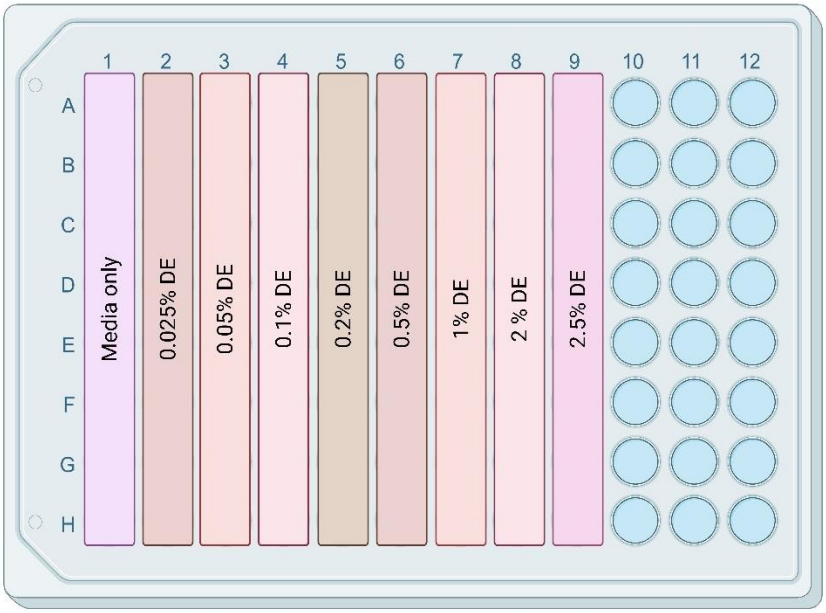


Figure 7. Experimental set-up for MTT assay

2.2.5 Lactate Dehydrogenase (LDH) Assay

Supernate lactate dehydrogenase (LDH) concentrations were assessed in cultured microglia to determine cytotoxicity percentage in cells exposed to increasing concentrations of DE. Cells were exposed to the following conditions: media only, 0.025% DE, 0.05% DE, 1% DE, 0.2% DE, 0.25% DE, 0.5% DE, 1% DE, 2% DE, and 2.5% DE. Cells were harvested from culture flasks using 0.25% trypsin, 0.53 mM ethylenediaminetetraacetic acid (EDTA) solution (HyClone Laboratories; Logan, Utah, USA) and counted via hemocytometer to seed 24-well plates (Fisher Scientific) at a density of 10,000 cells per well in a 96-well plate. Plates were incubated overnight in growth medium and no more than 24 hours before treatment. Overnight growth medium was aspirated, and the treatments were added with four replicates each and incubated for 6 hours. A CyQUANT™ LDH Cytotoxicity Assay Kit was purchased from

Thermo Fisher and used as directed by the manufacturer. The resulting plates were read on a FLUOstar Omega spectrophotometer at 490 and 680 nm using Omega software version 5.7. Cytotoxicity percentage was calculated via manufacturer recommendations in the kit manual. A schematic of the 96-well plate set-up is provided in Figure 8.

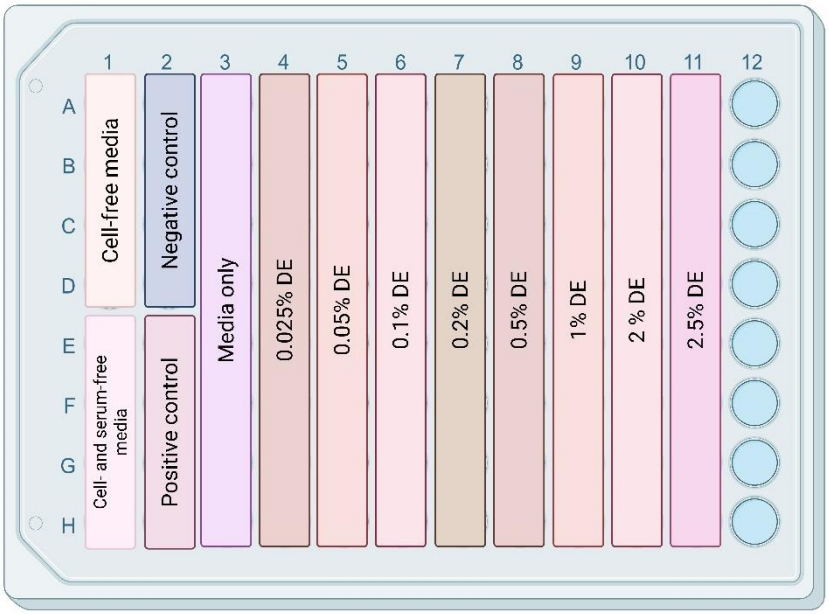


Figure 8. Experimental set-up for LDH assay

2.2.6 DE and AT-RvD1 Microglia Co-Exposure Model

Cells were harvested from culture flasks using 0.25% trypsin, 0.53 mM ethylenediaminetetraacetic acid (EDTA) solution (HyClone Laboratories; Logan, Utah, USA) and counted via hemocytometer to seed 24-well plates (Fisher Scientific) at a density of 2.5 x10^5 cells per well in a 24-well plate. Plates were incubated overnight in growth medium and no more than 24 hours before treatment. Overnight growth medium was aspirated, and the treatments were added with four replicates each and incubated for 6 hours. All studies were repeated twice for a total number of 8 wells per treatment. A schematic of the 24-well plate set-up is detailed in Figure 9.

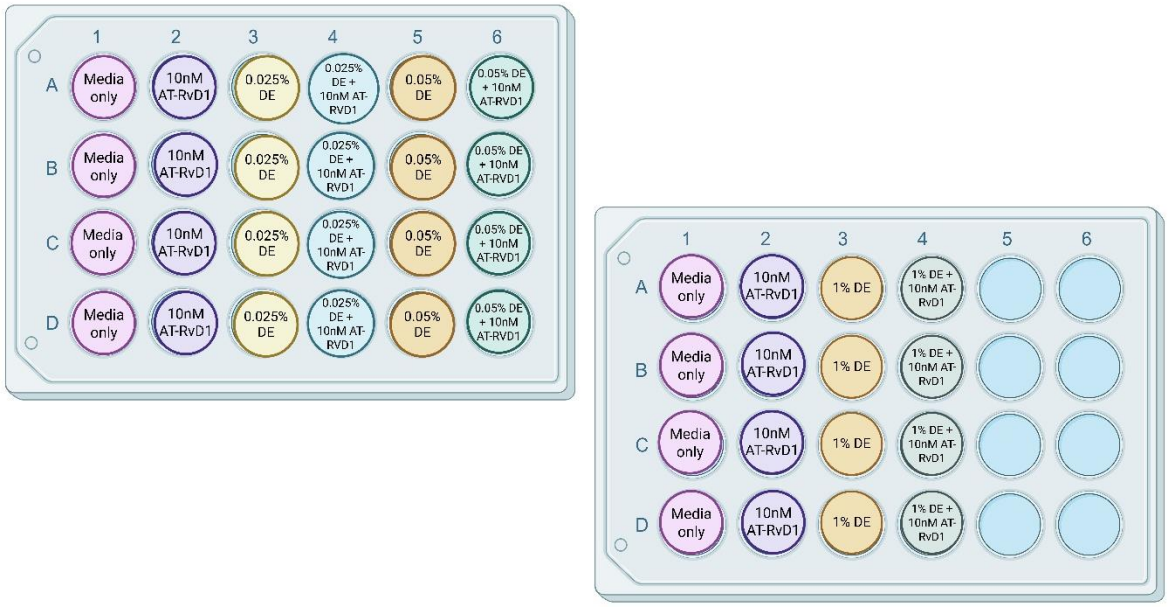


Figure 9. Experimental plate set-up for co-exposed cultured microglia.

2.2.7 Supernatant Fractions and Cell Lysate Collection

Supernatant fractions were aspirated at 1, 2, 6, 18, and 24 hours post co-exposure, placed in 1.5 mL microcentrifuge tubes (VWR), centrifuged at 5000 rpm at 4 °C for 10 minutes, and stored at -20 °C for future assays. Cell lysates were collected for analysis of intracellular IL-22 production. Supernatant fractions were aspirated as previously discussed and cells were washed twice with 500 µl ice-cold PBS. 150 µl of ice-cold radioimmunoprecipitation assay (RIPA) lysis buffer (Thermo Fisher) with 100 µl/ml protease inhibitor (Thermo Fisher) was added to each well. The plate was rocked gently, placed on ice for 30 minutes, then rocked gently every 10 minutes during incubation. Lysate was aspirated, centrifuged at 5000 rpm at 4 °C for 10 minutes, and stored at -20 °C for later use[85].

2.2.8 Enzyme-Linked Immunosorbent Assays

Cytokine protein concentrations in culture media and bronchoalveolar lavage fluids (BALF) were quantified using sandwich enzyme-linked immunosorbent assays (ELISAs). Kits were purchased from DuoSet (R&D Systems) with the modification of capture antibody diluted in BupH Carbonate-Bicarbonate Buffer (Voller's Coating Buffer, Thermo Scientific). High-binding half-well 96-well plates (VWR) were coated with capture antibody and incubated for 24 hours before progression of assay. Samples were removed from -20 °C storage and placed on ice for 1 hour to thaw before centrifugation at 5000 rpm at 4 °C for 10 minutes prior to addition to the plates in duplicate. The protocol was completed as outlined by DuoSet with no other modifications. Peroxidase substrate with peroxide (Thermo Scientific) was used as the indicator and 2N sulfuric acid (Sigma-Aldrich) was used as stop solution. Plates were read on a FLUOstar Omega spectrophotometer at 450 nm using Omega software version 5.7. ELISA data were analyzed using Omega MARS software version 4.0 to calculate concentration based on 4-parameter calculations of a standard concentration curve. Averages of technical replicates were used for statistical analysis. Concentration readings below the level of detection were set to 0.0001 for statistical analysis and graphing to indicate the analyte may be present but was not detectable by the assay.

2.2.9 *In Vivo* Repetitive Organic Dust Extract Exposure Model

In vivo studies were conducted at the Colorado State University Laboratory Animal Resources Painter Facility and approved by the Institutional Animal Care and Use Committee (IACUC, Protocol Number 2887). C57BL/6 (WT) and whole-body IL-22 knock-out (IL22KO) mice 8-12 weeks of age were housed in the Painter Facility in a pathogen free environment with

free access to standard mouse feed and water. We utilized a 3-week 5 days/week repetitive DE instillation study design extensively utilized in our laboratory to determine an optimal dosing regimen for AT-RvD1 treatment in mice[48,209,216,219–221]. Treatment groups included:

- 50 µl intranasal (i.n.) instillation of saline with 50 µl intraperitoneal (i.p.) injection of saline with 5% ethanol (EtOH) (EtOH is the vehicle for AT-RvD1)
- 50 µl i.n. instillation of saline with 50 µl i.p. injection of 50 ng AT-RvD1 in saline
- 50 µl i.n. instillation of saline with 50 µl i.p. injection of 100 ng AT-RvD1 in saline
- 50 µl i.n. instillation of saline with 50 µl i.p. injection of 250 ng AT-RvD1 in saline
- 50 µl i.n. instillation of 12.5% hog dust extract (DE) with 50 µl i.p. injection of saline with 5% EtOH
- 50 µl i.n. instillation of 12.5% hog dust extract (DE) with 50 µl i.p. injection of 50 ng AT-RvD1
- 50 µl i.n. instillation of 12.5% hog dust extract (DE) with 50 µl i.p. injection of 100 ng AT-RvD1
- 50 µl i.n. instillation of 12.5% hog dust extract (DE) with 50 µl i.p. injection of 250 ng AT-RvD1

Mice were instilled i.n. 5 days/week for 3 weeks under light isoflurane sedation using SomnoSuite Small Animal Anesthesia System (Kent Scientific Cooperation). Animals were placed into the anesthesia receptacle and parameters were set at a flow rate of 100 mL/minute at 2-4% anesthesia depending on the size and tolerance of the animal. Animals were removed for instillation once breathing appeared slowed and even. 50 µl of the appropriate treatment was

loaded into a pipette and deposited at the tip of the animal's nose to allow the animal to naturally inhale the liquid. Following installation, DE animals were marked on their tails with sharpie for later identification and tracking of exposure groups. Animals were returned to their enclosures on their backs to encourage recovery from the anesthesia and monitored to ensure return of normal behaviors. Injections were prepared with the appropriate dosages of 17(R) AT-RvD1 or ethanol in PBS per mouse to produce solutions of 50-250 ng/50 µl of AT-RvD1 or .5-5% EtOH. EtOH is the vehicle for AT-RvD1 and was chosen as the control as EtOH exposure in lung models has been shown to affect pathological outcomes [119,237]. A dosing scheme is provided in Figure 10.

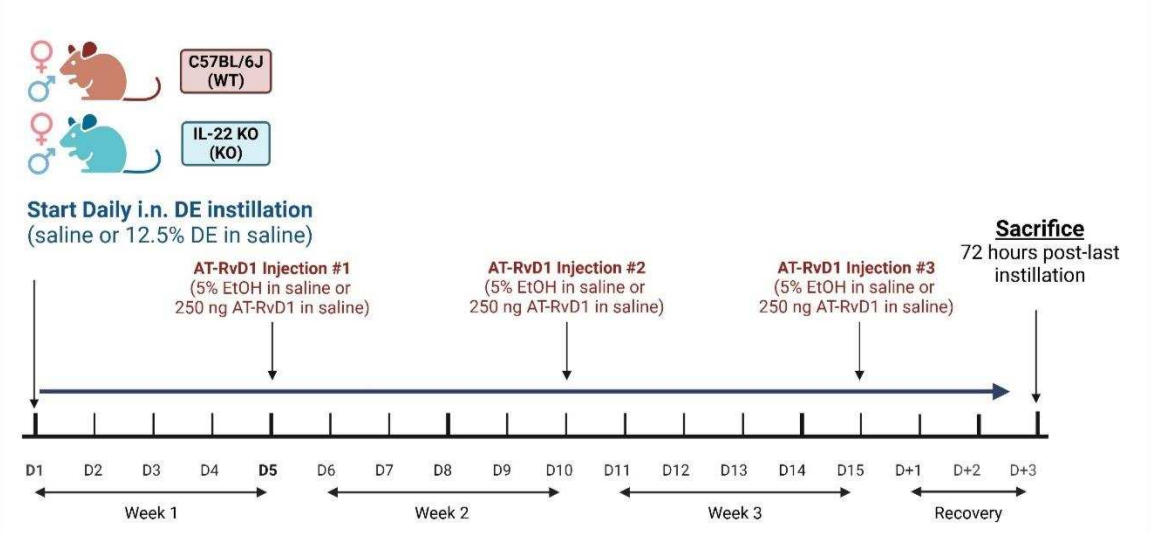


Figure 10. AT-RvD1 dosing strategy in WT and IL-22 KO mice.

Once weekly AT-RvD1 dosing strategy; WT and KO animals were instilled intranasally (i.n.) with 12.5% DE 5 days/week for 3 weeks and treated with 250 ng AT-RvD1 intraperitoneally (i.p.) once/week on day 5 for 3 weeks. Created with BioRender.com.

2.3.10 Animal Sacrifice Sample Collection

Animals were euthanized by isoflurane followed by cervical dislocation. Dissection of the chest and neck was performed to expose the lungs and trachea. Bronchoalveolar lavage fluid (BALF) was collected by inserting a 25 g catheter into the trachea and securing it with suture

followed by lavage of the lung three times with 1 mL sterile saline for each wash. The first wash was collected in one tube while washes 2 and 3 were pooled in the same tube. The left lung lobe was tied off with suture, extracted, placed in a 1.5 mL microcentrifuge tube (VWR) with 400 µl RNAlater solution, and stored at -20 °C for later use. The right lobes, trachea, and heart were removed from the animals and inflated with 0.7 mL 10% formalin (Fisher Scientific), hung submerged in 10% formalin overnight at 20 cm H_2O pressure, then placed in tissue cassettes and stored in 10% formalin for further histological analysis.

2.3.11 Bronchoalveolar Lavage Cellular Infiltrate Analysis

BALF was centrifuged at 1200 rpm at 4 °C for 5 minutes. Supernatant fractions of the first wash were retained and aliquoted at 105 µl in 1.5 ml microcentrifuge tubes (VWR) for cytokine analyses by ELISA. Supernates of pooled washes two and three were discarded. Cell pellets of all washes were combined with 400 µl of red blood cell lysis buffer (Life Technologies Corporation, New York, USA) and placed on ice to incubate. After 5 minutes, the washes were checked for red color and the process was repeated if necessary. After incubation, washes were centrifuged at 1200 rpm at 4 °C for 5 minutes. Supernatant fractions were discarded and cell pellets were reconstituted in 200 µl PBS and counted on a hemocytometer to determine the total number of cells present and to calculate the additional volume of PBS necessary to bring the concentration to $1x10^6$ cells/mL. 200 µl were then added to a cytocentrifuge (Thermo Cytospin 4, Thermo Scientific) and spun at 600 rpm for 5 minutes. Slides were dried overnight and differentially stained using Volu-Sol dip-stain kit for microscopic analysis (Volu-Sol; Salt Lake City, Utah, USA). Differential counts were performed by counting 300 cells on each slide to

assess the types of immune cell infiltrations present. Macrophages, lymphocytes, and polymorphonuclear cells were reported. Counts were assisted by Fiji Cell Counter version 1.54b.

2.3.12 Lung Pathology

Whole right lung coronal sections, collected as previously described above, were stained with hematoxylin and eosin (H&E) following deparaffinization and rehydration with xylene and graded EtOH solutions (xylene, 100% EtOH, 95% EtOH, 80% EtOH, 50% EtOH, and finally 1X PBS). Slides were scanned at 40X on a Vectra Polaris scanning microscope. Images of lungs from animals administered weekly AT-RvD1 injections were blinded and manually scored using a well-established semiquantitative scoring method [48,137,220,221,229]. Images from animals administered daily AT-RvD1 injections were imported into VisioPharm version 2023.09.3.15043 x64 and processed through an artificial intelligence (AI) workflow for quantitative assessment of alveolar space, alveolar septa thickness, peribronchiolar inflammation, perivascular inflammation, total alveolar septa nuclei, and percentage of inducible bronchus-associated lymphoid tissue (iBALT) formations relative to tissue area. AI quantification was performed on the whole lung tissue with output measurements including area, percentages of parameters to total tissue area or total parameter counts. VisioPharm is one of the leading AI histopathology analysis software available. Our workflow and applications were designed, annotated, trained, and verified by a board-certified veterinary anatomic pathologist to identify our desired readouts and ensure accurate results. The workflow is then trained through a large set of sample images by a board-certified veterinary anatomic pathologist where structures are identified by the software and confirmed by the pathologist, allowing the software to “learn” how structures are organized and are identified in the experimental images. Briefly, the workflow consisted of

multiple stepwise applications of increasing specificity, starting with identification of the lung tissue, followed by identification of airways and vessels, then inflammation and iBALT, and finally identification of airways epithelial cells and alveolar nuclei. During each step of the workflow, the results are confirmed manually to ensure accurate detection of structures. All parameters are normalized to tissue area to mitigate size and artifact skewing.

2.3.13 Immunohistochemistry

Whole brain sagittal paraffin embedded tissue sections were deparaffinized by baking slides at 60 °C for 20 minutes, followed by rehydration through an EtOH gradient (xylene, 50% xylene/50% EtOH, 100% EtOH, 95% EtOH, 70% EtOH), and then incubated in 1.0 M Tris buffered saline (TBS). Antigen retrieval was achieved using 0.01 M sodium citrate, pH 6.0 at 95 °C for 20 minutes in a Biocare Medical Decloaking Chamber™ NxGen (Biocare Medical). Slides were incubated in 0.3% hydrogen peroxide solution at room temperature for 30 minutes. Tissues were permeabilized and blocked using 0.1% Triton-X in 1 M Tris Buffered Saline (TBS) with 10% donkey serum. Astrocytes were identified using rabbit anti-S100 calcium-binding protein β (S100β) antibody (1:750; Abcam, Cat #: ab41548) diluted in 1.0 M TBS and incubated overnight at 4 °C. Tissues were then washed three times for two minutes each with 2% bovine serum albumin and 2% Triton-X in 1 M TBS before incubating slides with secondary antibody at room temperature for 1 hour. Slides were washed again three time for two minutes and incubated in ABC HRP peroxidase detection kit (Vector Laboratories, Cat #: pk-4,000) and ImmPACT DAB Substrate, Peroxidase (HRP) Kit (Vector Laboratories, Cat #: sk-4,105). Slides were counterstained with hematoxylin before undergoing dehydration with 95% EtOH, 100% EtOH,

and xylene before applying a coverslip. Slides were imaged using a Vectra Polaris microscope at 40X magnification and cells were counted in QuPath using the cell detection plugin.

2.3.14 Statistical Analysis

Significance was determined with two-way ANOVA for *in vitro* experiments and three-way ANOVA for *in vivo* experiments with post-hoc Tukey tests using GraphPad Prism Version 9. Temporal relationships of cytokine concentrations were determined by mixed effects analysis and graphed as averages of all replicates. For all *in vivo* study data, males and females were combined and differentiated on graphs to show sex differences but were calculated together for statistical analysis. Males were defined as filled shapes and females were defined as open shapes on graphs. Significance was determined by a p-value < 0.05. GraphPad Prism Version 9 was used for production of all data figures. On graphs, significance is denoted by, * = $p \leq 0.05$; ** = $p \leq 0.01$; *** = $p \leq 0.001$; **** = $p \leq 0.0001$.

2.3 Results:

2.3.1 Effects of AT-RvD1 on cytokine production in DE-exposed alveolar macrophages

IL-6 is widely considered to be a marker for inflammation produced by macrophages in the immune response[213]. In an alveolar macrophage model, we aimed to determine how treatment of RvD1 in concentrations of 10 nM and 100 nM would alter the production of this cytokine. The results of the Tukey post-hoc test revealed that exposure to 1% DE and addition of 10 nM ($p<0.0001$) and 100 nM ($p<0.0001$) AT-RvD1 treatment significantly reduced production of IL-6 at 6 hours post co-exposure (Figure 11). Although these data were statistically significant, the variability of our datapoints and the lack of total reduction of IL-6 concentrations

relative to baseline may indicate a lack of biological relevance. A high dosage of AT-RvD1 may be needed to achieve a more robust reduction in IL-6 production in alveolar macrophages exposed to DE.

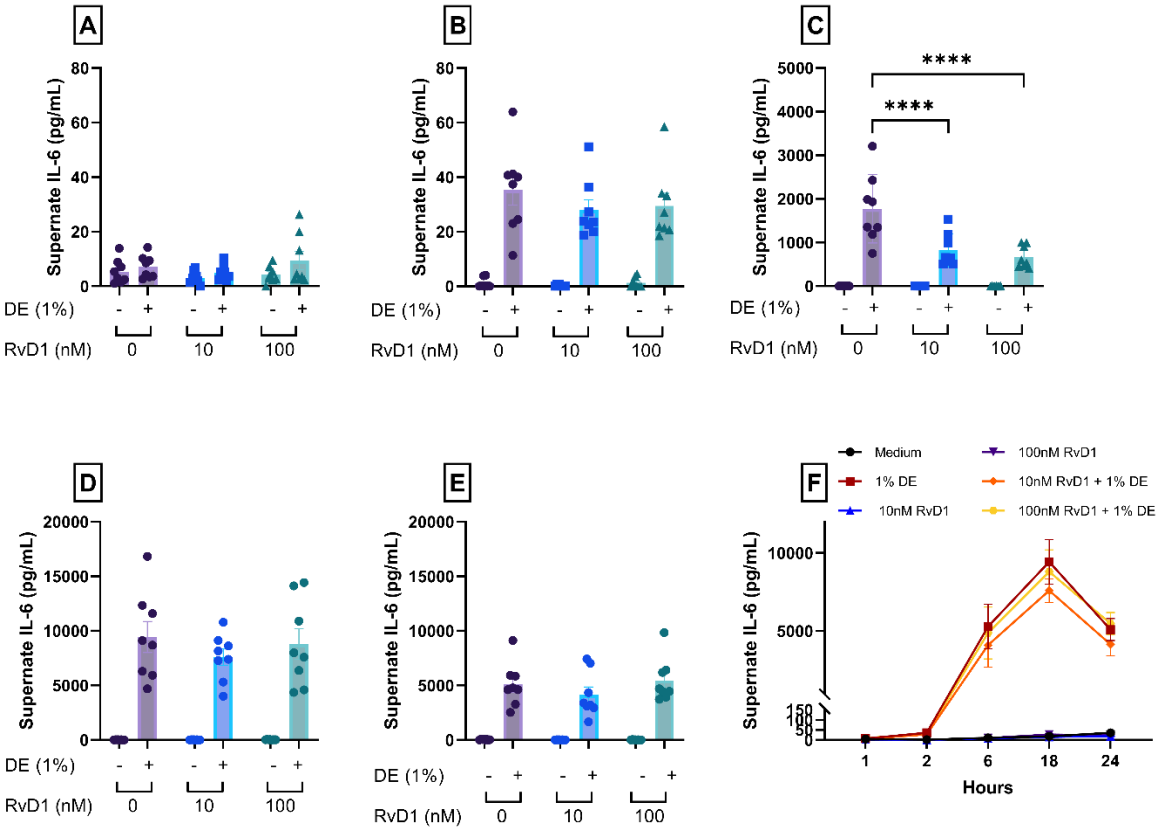


Figure 11. Effects of DE exposure and AT-RvD1 treatment on IL-6 induction in alveolar macrophages over 24 hours.

Levels of IL-6 at (A) 1 hour post co-exposure; (B) 2 hours post co-exposure; (C) 6 hours post co-exposure; (D) 8 hours post co-exposure; (E) 24 hours post co-exposure; (F) temporal relationships of treatment groups over 24 hours. 3-way ANOVA with Tukey post-hoc analysis, error bars = SEM; * = $p \leq 0.05$; ** = $p \leq 0.01$; *** = $p \leq 0.001$; **** = $p \leq 0.0001$. Sample sizes: 12 per treatment condition.

TNF-α is another pro-inflammatory cytokine produced by macrophages in response to organic dust exposure[238]. We aimed to determine the effects of AT-RvD1 on TNF-α production by alveolar macrophages *in vitro*. Statistical significance was observed between DE-exposed cells and DE-exposed cells treated with 100 nM AT-RvD1 at 6 hours (Figure 12). There is only a small change in the TNF-α production in cells exposed to DE and treated with 100 nM AT-RvD1 compared to the DE-only treated controls, which may not translate to being biologically relevant. A high dose of AT-RvD1 may be necessary to achieve greater reduction in TNF-α production.

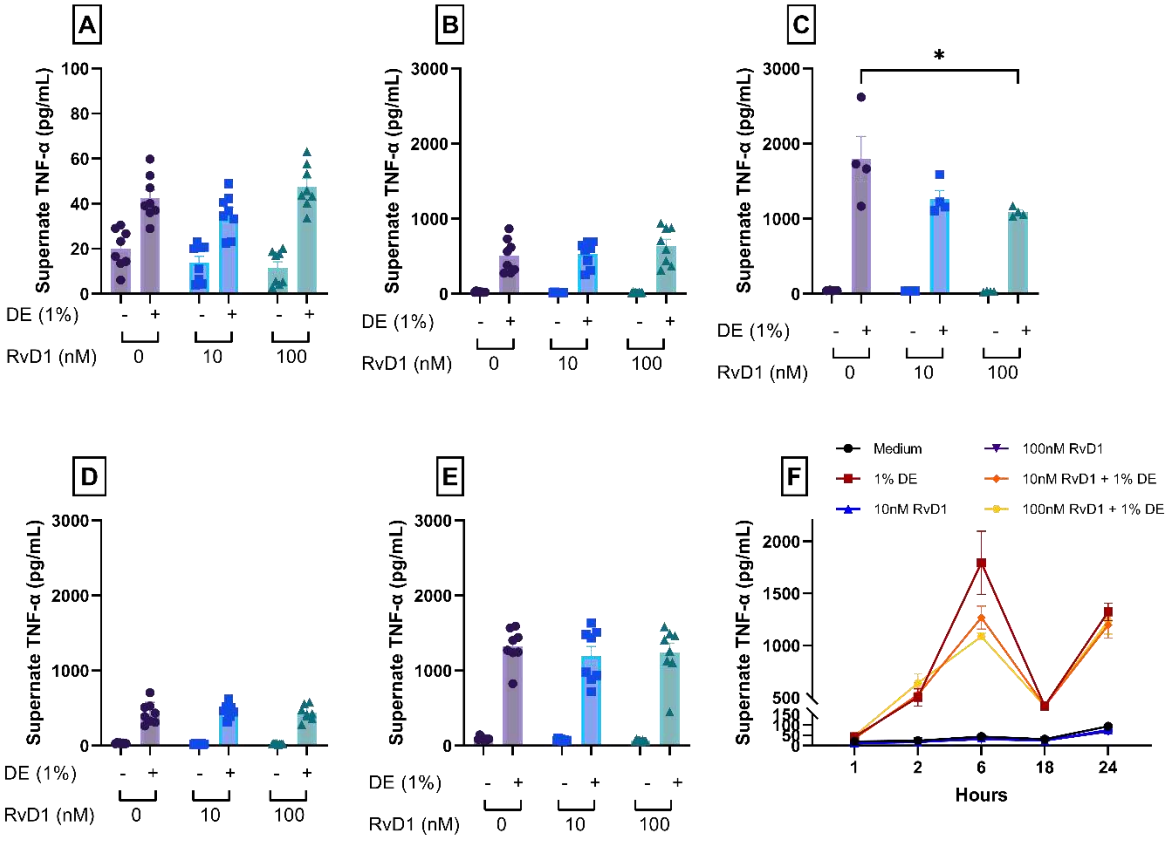


Figure 12. Effects of DE exposure and AT-RvD1 treatment on TNF-α induction in alveolar macrophages over 24 hours.

Levels of TNF-a at (A) 1 hour post co-exposure; (B) 2 hours post co-exposure; (C) 6 hours post co-exposure; (D) 8 hours post co-exposure; (E) 24 hours post co-exposure; (F) temporal relationships of treatment groups over 24 hours. 3-way ANOVA with Tukey post-hoc analysis, error bars = SEM; * = $p \leq 0.05$; ** = $p \leq 0.01$; *** = $p \leq 0.001$; **** = $p \leq 0.0001$. Sample sizes: 12 per treatment condition.

IL-10 was evaluated as a marker for resolution of inflammation and the anti-inflammatory effects of AT-RvD1 in alveolar macrophages[144]. Treatment of AT-RvD1 in DE-exposed cells did not significantly alter the production of IL-10 (Figure 13).

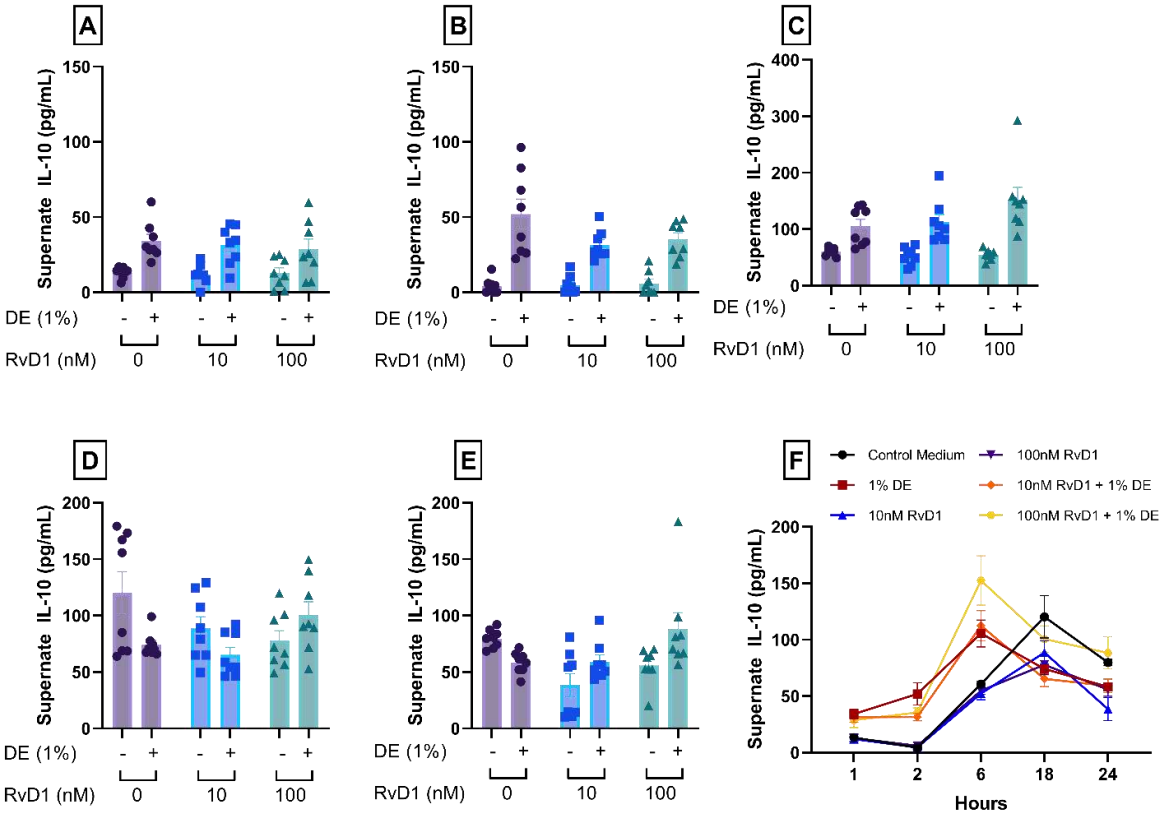


Figure 13. Effects of DE exposure and AT-RvD1 treatment on IL-10 induction in alveolar macrophages over 24 hours.

Levels of IL-10 at (A) 1 hour post co-exposure; (B) 2 hours post co-exposure; (C) 6 hours post co-exposure; (D) 8 hours post co-exposure; (E) 24 hours post co-exposure; (F) temporal relationships of treatment groups over 24 hours. 3-way ANOVA with Tukey post-hoc analysis, error bars = SEM; * = $p \leq 0.05$; ** = $p \leq 0.01$; *** = $p \leq 0.001$; **** = $p \leq 0.0001$. Sample sizes: 12 per treatment condition.

Our recent studies have shown alveolar macrophages produce IL-22 in response to organic dust and that it was Golgi-localized [220]. We tested induction of IL-22 in mouse alveolar macrophages exposed to DE and treated with AT-RvD1. We also evaluated lysate concentrations

to determine intracellular localization of IL-22 during the immune response to organic dust extract.

Supernate concentrations after 1 hour demonstrated significant differences between cells exposed to DE and cells exposed to DE and treated with 10 nM AT-RvD1 ($p=0.0399$) and 100 nM AT-RvD1 ($p<0.0001$). After 2 hours, these changes were also observed at both 10 nM and 100 nM AT-RvD1 concentrations with the same significance ($p=0.0002$) (Figures 14 and 15).

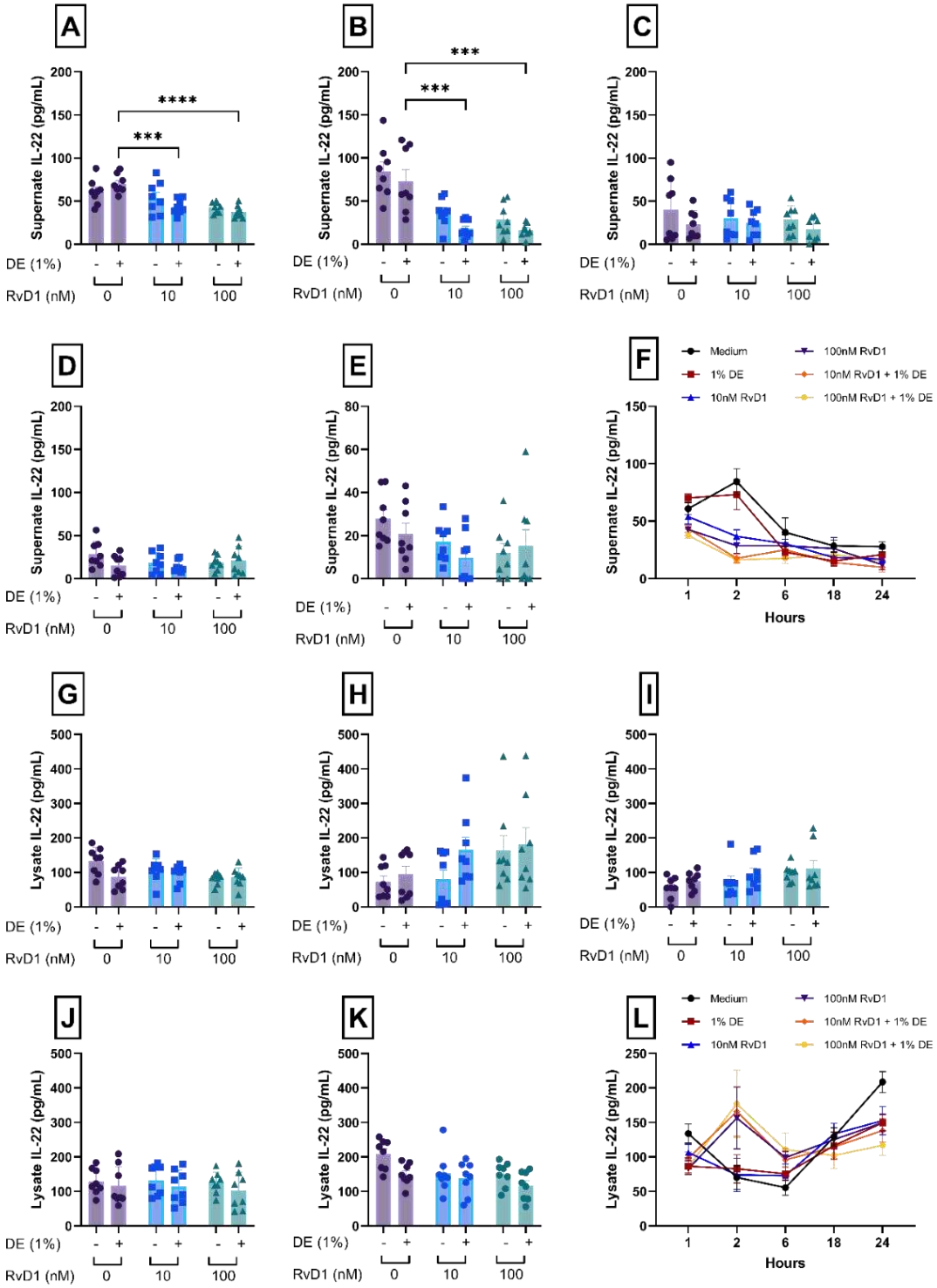


Figure 14. Effects of DE exposure and AT-RvD1 treatment on IL-22 induction in alveolar macrophages over 24 hours.

Supernatant concentrations of IL-22 at (A) 1 hour post co-exposure; (B) 2 hours post co-exposure; (C) 6 hours post co-exposure; (D) 18 hours post co-exposure; (E) 24 hours post co-exposure; (F) temporal relationships of treatment groups. Cell lysate or protein levels of IL-22 at (G) 1 hour post co-exposure; (H) 2 hours post co-exposure; (I) l 6 hours post co-exposure; (J) l18 hours post co-exposure; (K) 24 hours post co-exposure; (L) lysate temporal relationships of treatment groups over 24 hours. 3-way ANOVA with Tukey post-hoc analysis, error bars = SEM; * = $p \leq 0.05$; ** = $p \leq 0.01$; *** = $p \leq 0.001$; **** = $p \leq 0.0001$. Sample sizes: 12 per treatment condition.

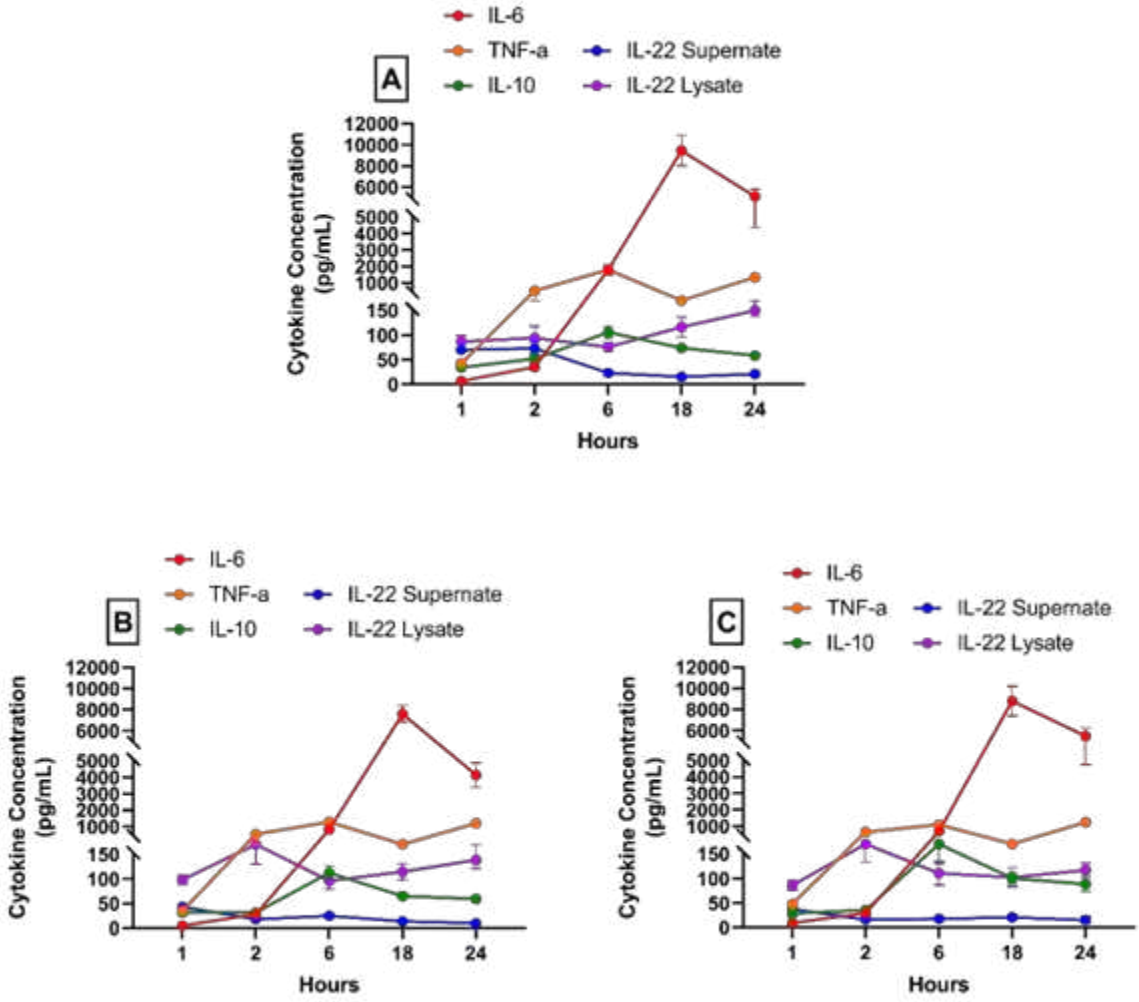


Figure 15. Effects of DE exposure and AT-RvD1 treatment on IL-6, TNF-α, IL-10, and IL-22 in alveolar macrophages over 24 hours.

(A) IL-6, TNF-α, IL-10, IL-22 supernate, and IL-22 lysate concentrations in cells exposed to 1% DE without AT-RvD1 over 24 hours; (B) IL-6, TNF-α, IL-10, IL-22 supernate, and IL-22 lysate concentrations in cells co-exposed to 10 nM AT-RvD1 with 1% DE over 24 hours; (C) IL-6, TNF-α, IL-10, IL-22 supernate, and IL-22 lysate concentrations in cells co-exposed to 100 nM AT-RvD1 with 1% DE over 24 hours. 3-way ANOVA with Tukey post-hoc analysis, error bars

= SEM; * = $p \leq 0.05$; ** = $p \leq 0.01$; *** = $p \leq 0.001$; **** = $p \leq 0.0001$. Sample sizes: 12 per treatment condition.

2.3.2 Effects of DE exposure and AT-RvD1 treatment in cultured microglia

After our observations of the cytokine modulating effects of AT-RvD1 in alveolar macrophages, we aimed to determine the response of microglia to DE and assess the effects of AT-RvD1 on inflammatory mediator production in these cells. Since DE had not previously been tested in microglial cultures, a series of assays were chosen to assess the cellular response to DE and AT-RvD1 in various DE concentrations to determine an optimal protocol. The MTT assay was chosen as a marker of mitochondrial function to determine if there was significantly disruptive cytotoxicity observed in microglia as they were exposed to increasing concentrations of AT-RvD1. The LDH assay was chosen as a marker of cytotoxicity to assess the toxicity of DE in increasing concentrations. Both of these assays together with the evaluation of TNF-α secretion were utilized to determine a dosage of DE in microglia cultures that would elicit a strong immune response but would not induce significant cellular toxicity and/or death. Assay results revealed that mitochondrial function decreased with a low dose of 0.025% DE (p) but then increased with a higher dose of 0.25% (p). Low doses between 0.025%-0.2% DE ($p<0.0001$, $p=0.0070$, $p=0.0001$, $p<0.0001$) decreased cytotoxicity, however we did not see any significant cytotoxicity in higher doses. We found that all doses of DE above 0.5% elicited a significant increase in TNF-α production ($p<0.0001$). We also found that cells cultured with 0.1% DE and 10nM AT-RvD1 had reduced TNF-α production compared to cells cultured with only 1% DE ($p=0.0089$) (Figure 16). Although we saw a reduction in TNF-α production in microglia exposed to DE and treated with AT-RvD1 compared to their DE exposed controls, it is

only a slight decrease and may not translate to biologically relevant patient outcomes. A larger dose of AT-RvD1 may be necessary to elicit a stronger reduction in TNF-α production.

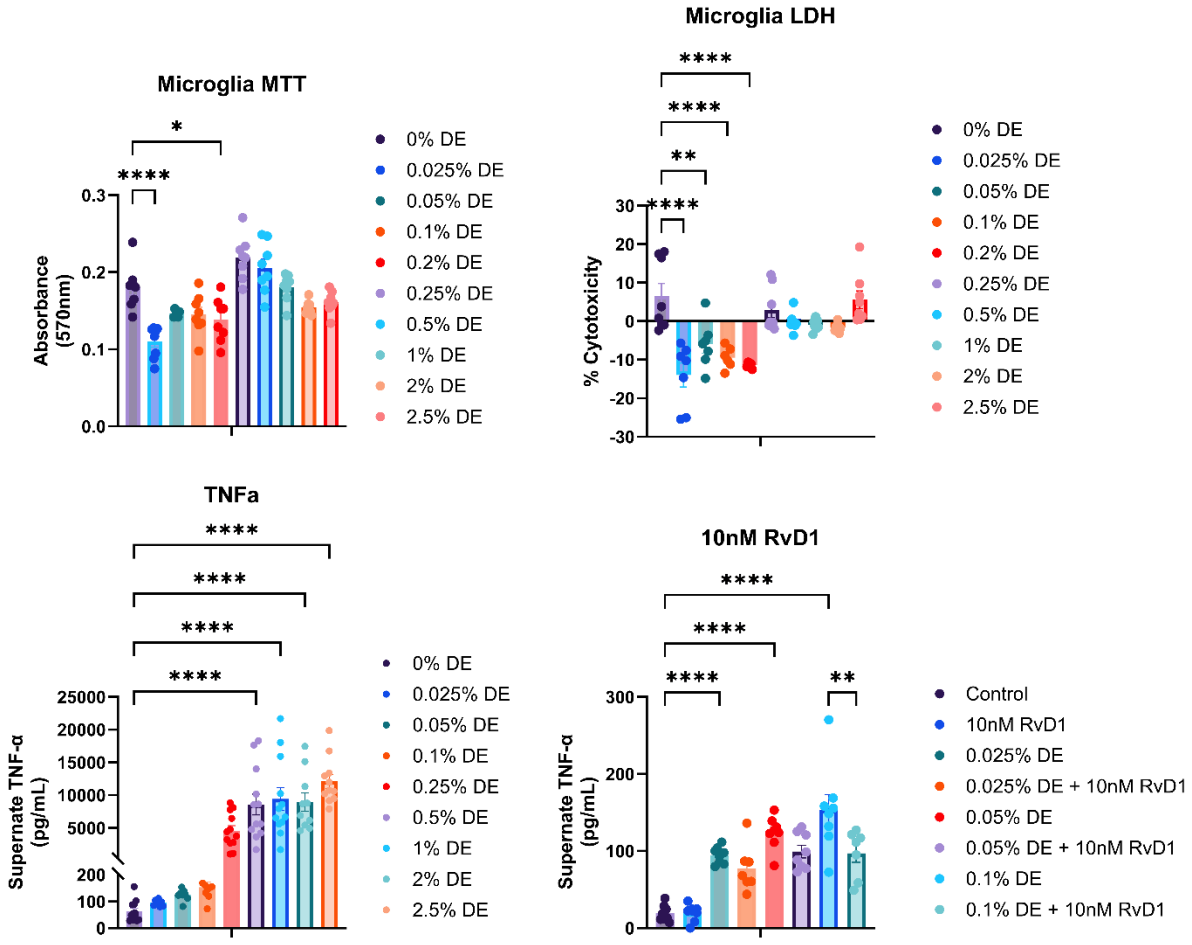


Figure 16. Effects of dust exposure on cultured microglia.

(A) MTT assay results; (B) LDH assay results; (C) TNF-α production in cells exposed to various concentrations of DE; (D) TNF-α production in cells exposed to DE and treated with 10 nM AT-RvD1. 3 way ANOVA with Tukey post-hoc analysis, error bars = SEM; * = $p \leq 0.05$; ** = $p \leq 0.01$; *** = $p \leq 0.001$; **** = $p \leq 0.0001$. Sample sizes: 6 per treatment condition.

2.3.3 Effects of various AT-RvD1 dosages on BALF cellular infiltrates

Through our cellular culture experiments, we determined that AT-RvD1 has a significant effect on the production of pro-inflammatory cytokines in both macrophages and microglia. We then aimed to understand its functions in an *in vivo* model of repetitive agriculture dust exposure

and AT-RvD1 treatment. We utilized a 3-week DE exposure model extensively utilized in our laboratory coupled with a daily AT-RvD1 injection model at various doses: saline control, 50 ng, 100 ng, or 250 ng. We then assessed previously utilized targets for determining pulmonary and neurological inflammation including BALF cellular infiltrates, pulmonary pathological markers, and astrocyte numbers.

Although we found no significant differences in the cell infiltrate profiles in dust exposed, AT-RvD1 treated animals compared to saline exposed, saline treated animals, we can appreciate the slight increase in total cells, macrophages, and lymphocytes in dust exposed, saline treated animals, which may confirm continued immune involvement following a 72-hour recovery period (Figure 17). This study had a very low sample size which could contribute to our lack of statistical and biologically relevant findings.

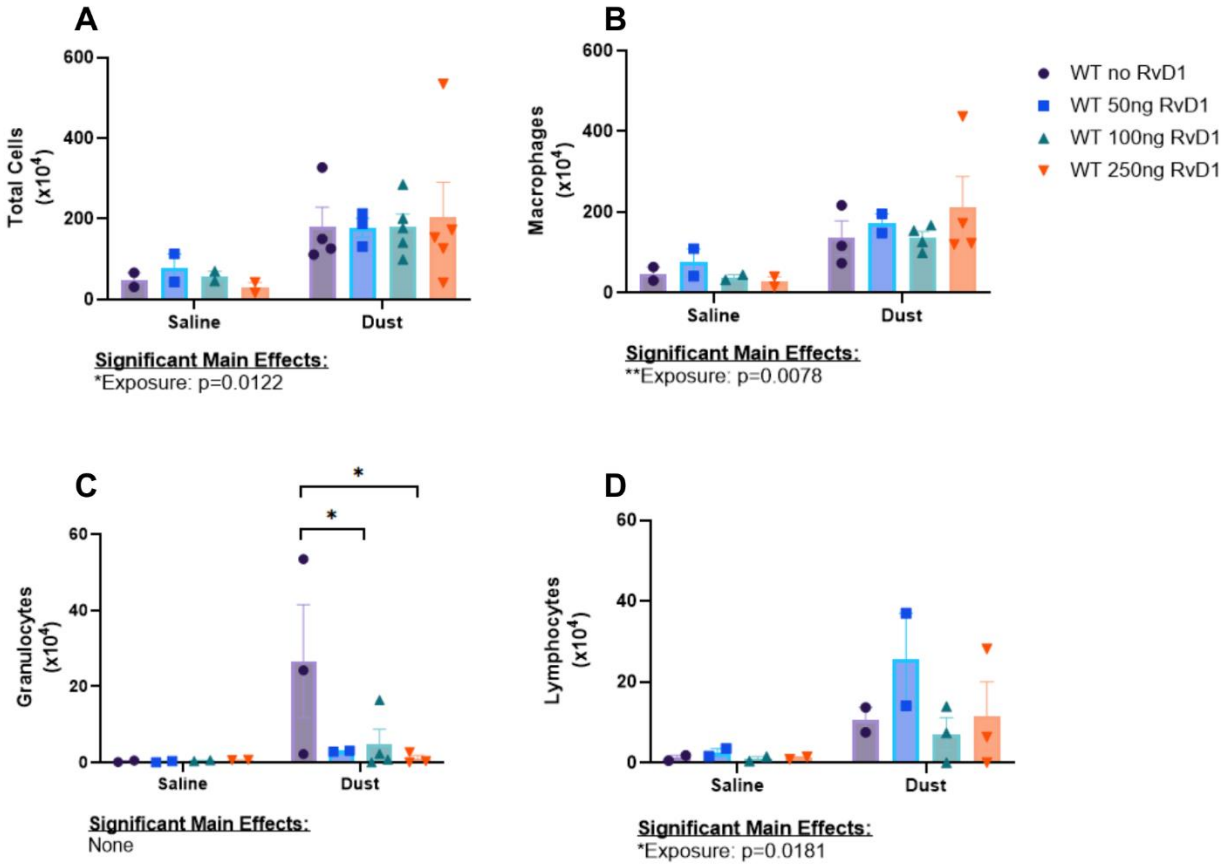


Figure 17. BALF Cellular infiltrate profiles in mice exposed to DE and treated with various doses of AT-RvD1.

(A) Total Cellular Counts in BALF; (B)Macrophages in BALF; (C) Granulocytes in BALF; (D) Lymphocytes in BALF.3-way ANOVA with Tukey post-hoc analysis, error bars = SEM; * = $p \leq 0.05$; ** = $p \leq 0.01$; *** = $p \leq 0.001$; **** = $p \leq 0.0001$. Sample sizes: WT Saline i.n./Saline i.p. (2 female); WT Saline i.n./50 ng AT-RvD1 i.p. (2 female); WT Saline i.n./100 ng AT-RvD1 i.p. (2 female); WT Saline i.n./250 ng AT-RvD1 i.p. (2 female); WT Dust i.n./Saline i.p. (2 female/2 male); WT Dust i.n./50 ng AT-RvD1 i.p. (2 female/1 male); WT Dust i.n./100 ng AT-RvD1 i.p. (2 female/2 male); WT Dust i.n./250 ng AT-RvD1 i.p. (2 female/1 male).

2.3.4 Effects of various AT-RvD1 dosages on lung pathology

We then evaluated pulmonary pathology to first determine if our instillations were successful and if the pathological results were consistent with expected findings, and second, to determine if AT-RvD1 treatment reduces pulmonary inflammation. We assessed iBALT and peribronchiolar/perivascular inflammation, both markers of inflammation expected in this

model[48,174,216,220,221]. Following evaluation of iBALT and peribronchiolar/perivascular inflammation, we found that dust exposed animals had increased iBALT production (p=0.0295), with a significant decrease in iBALT production in animals exposed to dust and treated with 100 ng or 250 ng AT-RvD1 (p=0.0045) (Figure 18).

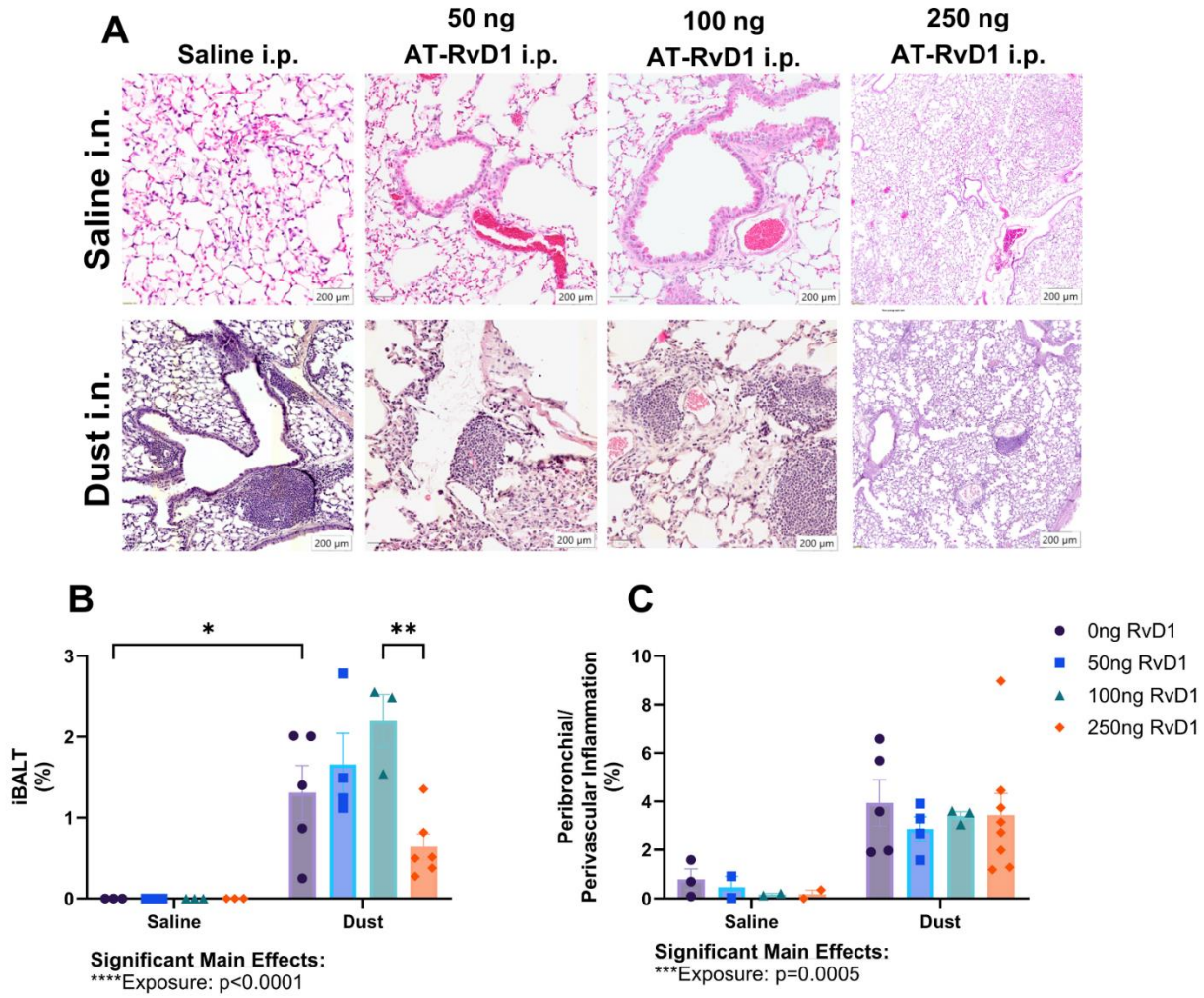


Figure 18. Effects of DE exposure and AT-RvD1 treatment on iBALT and peribronchiolar and perivascular inflammation in WT mice.

(A) Representative images at 40X magnification; (B) iBALT percentage; (C) peribronchiolar/perivascular inflammation percentage. 3 way ANOVA with Tukey post-hoc analysis, error bars = SEM; * = $p \leq 0.05$; ** = $p \leq 0.01$; *** = $p \leq 0.001$; **** = $p \leq 0.0001$. Sample sizes: WT Saline i.n./Saline i.p. (2 female); WT Saline i.n./50 ng AT-RvD1 i.p. (2 female); WT Saline i.n./100 ng AT-RvD1 i.p. (2 female); WT Saline i.n./250 ng AT-RvD1 i.p. (2

female); WT Dust i.n./Saline i.p. (2 female); WT Dust i.n./50 ng AT-RvD1 i.p. (2 female); WT Dust i.n./100 ng AT-RvD1 i.p. (2 female); WT Dust i.n./250 ng AT-RvD1 i.p. (2 female).

2.3.5 Effects of DE and AT-RvD1 on neuroinflammatory markers

To determine the neuroinflammatory effects of DE we assessed proliferation of microglia and astrocytes, common targets for neuroinflammation [26,65,66,106,147,171]. Microglia numbers were analyzed and found to be elevated in the olfactory bulb ($p<0.0001$), frontal cortex ($p=0.0094$), and isocortex ($p=0.0051$) of animals exposed to DE. Additionally, we also observed a decrease in microglia numbers in these brain regions ($p=0.0090$, $p=0.0633$, $p=0.0051$) in animals treated with 250 ng AT-RvD1 (Figure 19).

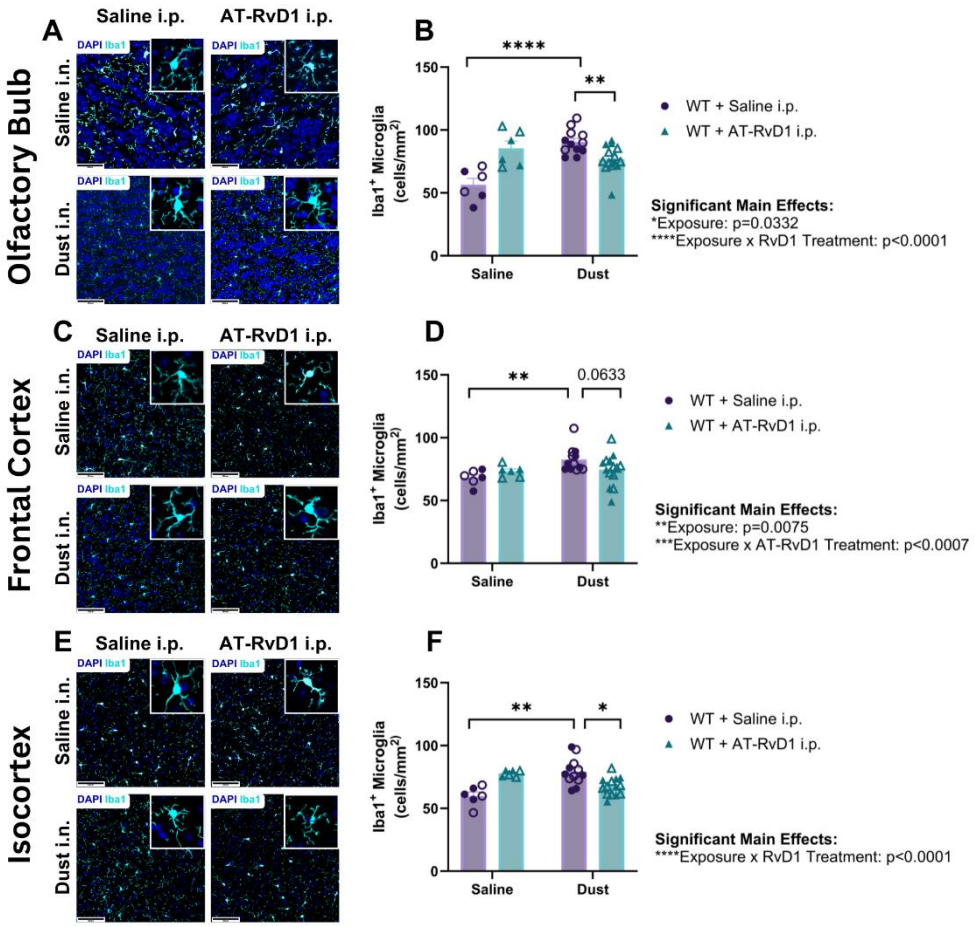


Figure 19. Microglia counts in mice exposed to DE and treated with 250ng AT-RvD1. (A) Representative images of the olfactory bulb at 40X magnification; (B) microglia counts in the olfactory bulb; (C) Representative images of the frontal cortex at 40X magnification; (D) microglia counts in the frontal cortex; (E) Representative images of the isocortex at 40X magnification; (F) microglia counts in the isocortex 3-way ANOVA with Tukey post-hoc analysis, error bars = SEM; * = $p \leq 0.05$; ** = $p \leq 0.01$; *** = $p \leq 0.001$; **** = $p \leq 0.0001$. Sample sizes: WT Saline i.n./Saline i.p. (3 female/3 male); WT Saline i.n./250 ng AT-RvD1 i.p.

(3 female/3 male); WT Dust i.n./Saline i.p. (6 female/6 male); WT Dust i.n./250 ng AT-RvD1 i.p. (6 female/6 male).

Astrocytes numbers were also evaluated and found to be increased in the frontal cortex of animals exposed to DE ($p<0.0001$) with a decrease in astrocyte counts in the frontal cortex of animals exposed to DE and treated with 250ng AT-RvD1 ($p=0.0004$) (Figure 20)

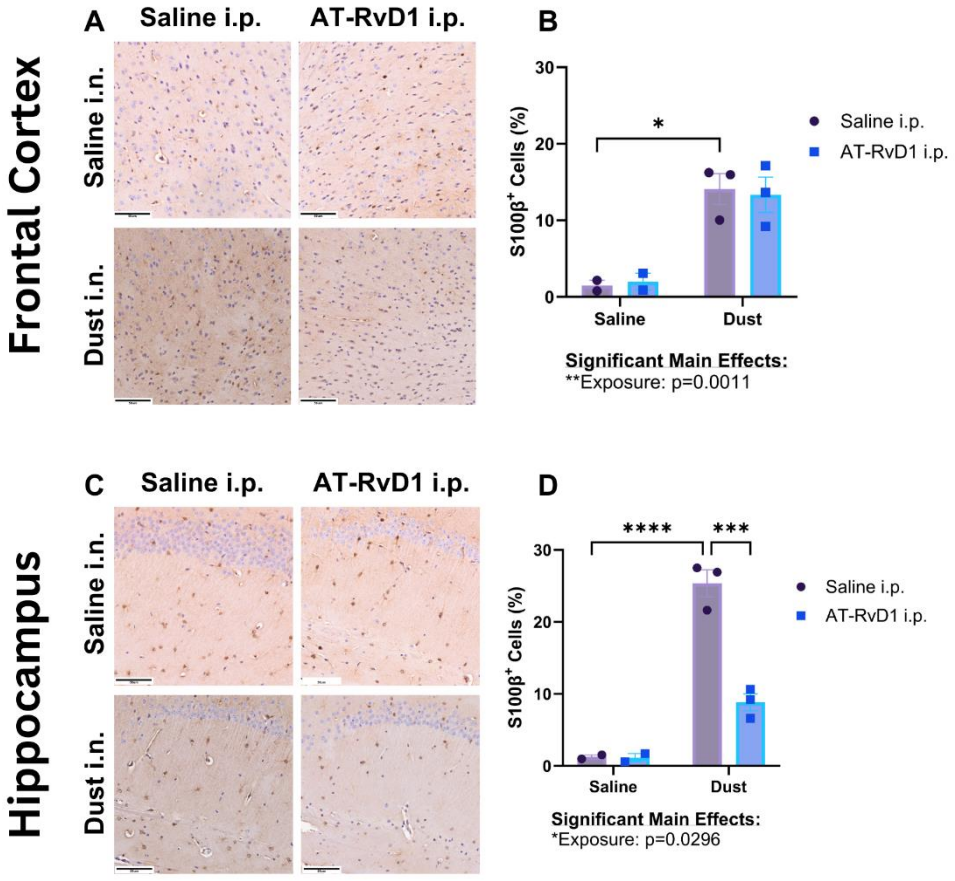


Figure 20. Astrocyte counts in mice exposed to DE and treated with 250 ng AT-RvD1. (A) Representative images of the frontal cortex at 40X magnification; (B) astrocyte counts in the frontal cortex; (C) Representative images of the hippocampus at 40X magnification; (D) Astrocyte counts in the hippocampus. 3-way ANOVA with Tukey post-hoc analysis, error bars = SEM; * = $p \leq 0.05$; ** = $p \leq 0.01$; *** = $p \leq 0.001$; **** = $p \leq 0.0001$. Sample sizes: WT Saline

i.n./Saline i.p. (2 female); WT Saline i.n./250 ng AT-RvD1 i.p. (2 female); WT Dust i.n./Saline i.p. (3 female); WT Dust i.n./250 ng AT-RvD1 i.p. (3 female).

2.4 Discussion

The pulmonary inflammatory response to agriculture dust has been well established by our and other laboratories, but the neuroinflammatory response to this toxicant has not been investigated[136,160,174]. Recent studies have linked exposure to agriculture dust to an increased risk of developing dementia. Additionally, patients with COPD have reported increased memory loss, confusion, depression, and anxiety, and 60% of patients with severe chronic inflammatory pulmonary diseases are also diagnosed with a nervous system disorder [29,232,246]. These symptoms lead to reduced social interaction and quality of life in these patients, and treatment for these diseases is urgently needed [108]. We have previously assessed the usage of AT-RvD1 *in vivo* in a 24-week repetitive dust exposure model and found reduction of pulmonary pathology in this model [48]. We aimed to test the inflammatory modulating effects of AT-RvD1 in macrophages and microglia and aimed to optimize the dosage for usage in a larger *in vivo* study to better understand the link between inhaled agriculture dust exposure, neuroinflammation, and AT-RvD1.

Cellular inflammatory responses to ODE and the efficacy of adjuvant treatment with AT-RvD1 were evaluated in cultured macrophages and microglia via pro-inflammatory and anti-inflammatory cytokine production. In macrophages, ODE elicited a strong inflammatory response characterized by increased production of IL-6 and TNF-α, which was reduced in cells co-treated with AT-RvD1, independent of dose. Microglia exposed to DE also produced a strong TNF-α response which was dampened by the addition of AT-RvD1. These data indicate that AT-

RvD1 alters the pro-inflammatory cytokine production of both macrophages and microglia, which contributes to the reduction of pathology seen in other models [48,216].

In our pathological assessment, we did not observe significantly reduced pathology between DE-exposed and AT-RvD1 treated animals and DE-exposed and saline-treated controls. However, this may be due to a low sample size since we observed a reduction in iBALT percentage in animals exposed to DE and treated with 250 ng AT-RvD1 compared with animals exposed to DE and treated with 100 ng AT-RvD1. This led us to prefer the daily 250 ng dosage as opposed to 50 ng or 100 ng AT-RvD1 daily, but more robust evidence was needed to make a final determination of an effective AT-RvD1 dose for a larger study.

We therefore turned to our neurological pathology targets to determine if agriculture dust exposure elicited an immune response in the brain and if our preferred dosage of 250 ng AT-RvD1 was effective at reducing neuroinflammation. Other models of neuroinflammation perpetuated by pulmonary inflammation found that microglia and astrocytes were elevated, therefore we also assessed microglia and astrocyte numbers to evaluate neuroinflammation in our agriculture dust exposure model. Microglia and astrocyte counts are a common marker of neuroinflammation and have been extensively used to test neuroinflammatory responses to toxicants [27,40,100,105,215]. We observed an increase in microglia numbers in the olfactory bulb, frontal cortex, and isocortex in animals exposed to DE, with reductions in these same regions in animals treated with 250 ng AT-RvD1. Additionally, we observed the same trend regarding astrocyte numbers in the frontal cortex and hippocampus of DE-exposed, AT-RvD1-treated

animals. These data confirmed that 250 ng AT-RvD1 daily was an effective dosing strategy in our model of repetitive agriculture dust exposure.

Through our investigations, we found that even low doses of AT-RvD1 in cultured microglia reduced TNF-α production, and that 250 ng of AT-RvD1 in mice was effective in reducing DE-induced neuroinflammation. Through these studies, we determined that this dosage would likely be effective for further *in vivo* studies.

CHAPTER 3: ASPIRIN-TRIGGERED RESOLVIN D1 MODULATES PULMONARY AND NEUROLOGICAL INFLAMMATION IN AN IL-22 KNOCK-OUT ORGANIC DUST EXPOSURE MOUSE MODEL

3.1 Introduction

The Centers for Disease Control and Prevention ranked chronic lower respiratory diseases (CLRD) as a leading cause of death in the United States (US) with 147,367 deaths in 2023 [33]. Chronic inflammatory lung diseases have also been linked to neuroinflammation and the development of neurodegenerative diseases such as Alzheimer's [100,105,164,243]. In 2023, 6.7 million people were reported as diagnosed and living with Alzheimer's disease in the US, and estimates project that number to increase to 14 million people by 2060 [31,33]. CLRDs include chronic obstructive pulmonary disease (COPD), asthma, and allergies [138,176,198]. Particulate matter (PM) exposure is a significant occupational hazard for agriculture workers, with organic dust exposure strongly linked to occupational-associated CLRDs [136,236]. Organic dusts contain a variety of particulate matter (PM) sizes from 100 μm to 0.25 μm, microbes, and many immunogenic compounds such as microbial components, endotoxins, and metals that contribute to the pulmonary immune response [22,155].

Our laboratory has extensively characterized the pulmonary immunological and pathological effects of organic dust exposure in a murine model of repetitive dust exposure, but the secondary neuroinflammatory effects of inhaled organic dust exposure have not been explored [136,160,161,219,221]. Inhaled PM exposure has been recently linked to an increased risk of developing dementia, with the greatest risk being associated with agricultural organic dust exposure over all other PM exposures [246]. COPD patients have documented increases in depressive symptoms, confusion, memory loss, and mental functional decline as their disease

progresses (13,14). A study conducted by the CDC analyzed comorbidities of 8,094 patients in resident care facilities diagnosed with CLRDs including chronic bronchitis, emphysema, and COPD [232]. This study found that 51.4% of patients with one more CLRD also presented with Alzheimer's disease or dementia ($p < 0.001$), 27.4% were diagnosed with depression ($p=0.012$), 7.7% were diagnosed with multiple sclerosis, Parkinson's disease, or epilepsy ($p= 0.020$), and 11.7% presented with other mental disorders ($p=0.007$) [232]. Overall, the authors found that 64.9% of patients with more CLRD experienced a mental or behavioral health disorder, and 11.6% experienced a nervous system disorder [232]. Agriculture workers often experience high levels of mental disorders including anxiety (males: 22% females: 39%, total: 31%) and depression (males: 35%, females: 42%, total: 39%) [131]. Additionally, air pollution exposure has been linked to neurological inflammation in murine models but has not been assessed in the specific context of agricultural organic dust exposure [27,105,180].

Both COPD and Alzheimer's are incurable, progressive, and ultimately fatal diseases with severe symptoms that reduce patients' quality of life during the progression of disease [27,69,108]. The search for therapies that combat these diseases is thus at the forefront of immunotoxicological research. Omega-3 fatty acid metabolites termed specialized pro-resolving mediators (SPMs), have been proposed as exogenous therapies for a variety of inflammatory diseases, suggesting they may be effective in reducing inflammation in a repetitive organic dust exposure model of pulmonary and neurological inflammation [183,187]. Aspirin-Triggered Resolvin D1 (AT-RvD1), a SPM, has demonstrated restorative functions in pulmonary and neuroinflammation models [48,54,189,217]. Specifically, the aspirin-triggered 17(R)-RvD1 epimer has shown increased stability and pharmacological efficacy compared to its 17(S)-RvD1 epimer in

murine models of acute lung injury and a chronic organic dust exposure-mediated pulmonary inflammation murine model [48,78,184,208].

Interleukin-22 (IL-22), an interleukin-10 (IL-10)-family cytokine has been implicated in inflammation modulation, tissue repair, and antimicrobial defense [51]. Murine models investigating the inflammatory consequence of IL-22 knock-out in infection, allergy, and organic dust exposure models have demonstrated increased disease severity in animals lacking IL-22 [2,3,25,118,153,220]. We recently demonstrated that whole-body IL-22 knock-out mice exhibit increased pathology severity, cellular infiltrate counts, pro-inflammatory cytokine production, and altered tissue pathology following repetitive organic dust exposure [220]. We aimed to investigate the link between attenuation of IL-22 and the tissue repair functions of AT-RvD1 in an IL-22 knock-out mouse model repetitively exposed to organic dust exposure.

We explored the link between inhaled organic dust exposure-induced pulmonary and neurological inflammation via a mouse model repetitively exposed to aqueous agriculture organic dust extract (DE). We also aimed to investigate the SPM AT-RvD1 as an exogenous therapy for pulmonary and neurological inflammation utilizing an IL-22 knock-out transgenic mouse model of severe pulmonary inflammation to explore its role in modulating lung-brain axis inflammation. To investigate our hypotheses, we evaluated the inflammatory response to organic dust exposure and the immune modulation of AT-RvD1 in an IL-22 knock-out model repetitively exposed to DE through evaluation of lung immune cell infiltrates, bronchoalveolar

lavage fluid (BALF) and lung tissue cytokines, lung pathology, brain microglia quantification, and transcript evaluation in lung and brain tissue via RNAscope technology.

3.2 Materials and Methods

3.2.1 Dust Extract Preparation

Dust was collected from hog confinement facilities in the Midwest, United States from surfaces at least 1 meter off the ground to represent the respirable fraction. Dust aliquots were stored at -20 °C until use. Dust extracts were prepared as previously described [137,219]. Briefly, whole dust was combined with Hank's balanced saline solution (HBSS) (HyClone Laboratories) at a ratio of 1 g dust to 10 mL HBSS on a magnetic stir plate for 1 hour at room temperature. The resulting mixture was centrifuged at 2500 rpm for 20 minutes at 4 °C. The supernate was collected, while the pellet was discarded. Supernate was transferred to a new tube and centrifuged again at 2500 rpm for 20 minutes at 4 °C. Supernate was collected and filtered through 0.22 μm syringe filters to produce 100% dust extract (DE) and stored at -20 °C. The resulting extract contains predominantly gram-positive bacterial components, endotoxins, and trace metals [155]. Complete analysis of dust extract can be found at Online Repository Methods at www.jacionline.org [155].

3.2.2 Animal Husbandry and Care

All animal protocols were reviewed and approved by the Institutional Animal Care and Use Committee (Protocol Number 2887). C57BL/6J (WT) and whole-body IL-22 knock-out [C57BL/6-Il22tm1.1(icre)Stck/J] (KO) (Jackson Labs) mice aged 8-12 weeks were housed in the Colorado State University Painter Facility in a specific pathogen-free environment with free

access to standard mouse feed and water. Three pairs of KO animals were purchased to establish a breeding colony of IL-22cre x IL-22cre that produced all experimental animals. Animals from the original breeding pairs and all offspring were genotyped through TransnetYX (Memphis, TN) genotyping PCR service to ensure accurate genotypes. WT mice were purchased directly from Jackson Laboratories, age and sex matched to KO mice. Purchased mice were acclimated for at least 7 days before performing any procedures.

3.2.3 *In Vivo* Repetitive DE Exposure and AT-RvD1 Treatment Model

Mice were intranasally (i.n.) instilled with 50 µl 12.5% DE or sterile saline 5 days/week for 3 weeks under light isoflurane sedation. The concentration of DE was previously determined by a dose-response study, which was found to elicit a strong pulmonary inflammatory response without the risk of mortality [174]. Sedation for instillations was achieved using a SomnoSuite Small Animal Anesthesia System (Kent Scientific Corporation) fitted with a small animal anesthesia box. Animals were placed into the box with a flow rate of 100 mL/minute at 2.0-3.0% anesthesia. Animals were removed for instillations once breathing appeared slowed and even. Animals were held in a supine position and 50 µl of the appropriate exposure was loaded into a pipette tip and deposited at the tip of the animal's nose one drop at a time to allow natural inhalation. Afterwards, animals were returned to their enclosures in a supine position to encourage recovery and monitored for several minutes to ensure return of normal behaviors. AT-RvD1 treated mice were administered intraperitoneal (i.p) injections of 50 µl of 250 ng AT-RvD1 or 5% ethanol (EtOH) (AT-RvD1 vehicle) in sterile saline either once per week after the 5th DE instillation (weekly, for a total of 3 injections) or 5 times per week (daily, for a total of 15 injections) (Figure 21A-B). Dosages and controls were determined based on previously

published data and a dose-response pilot study (data not shown) [48,54,119,120]. Animals were allowed to recover for 72 hours past-last DE instillation and AT-RvD1 injection before sacrifice.

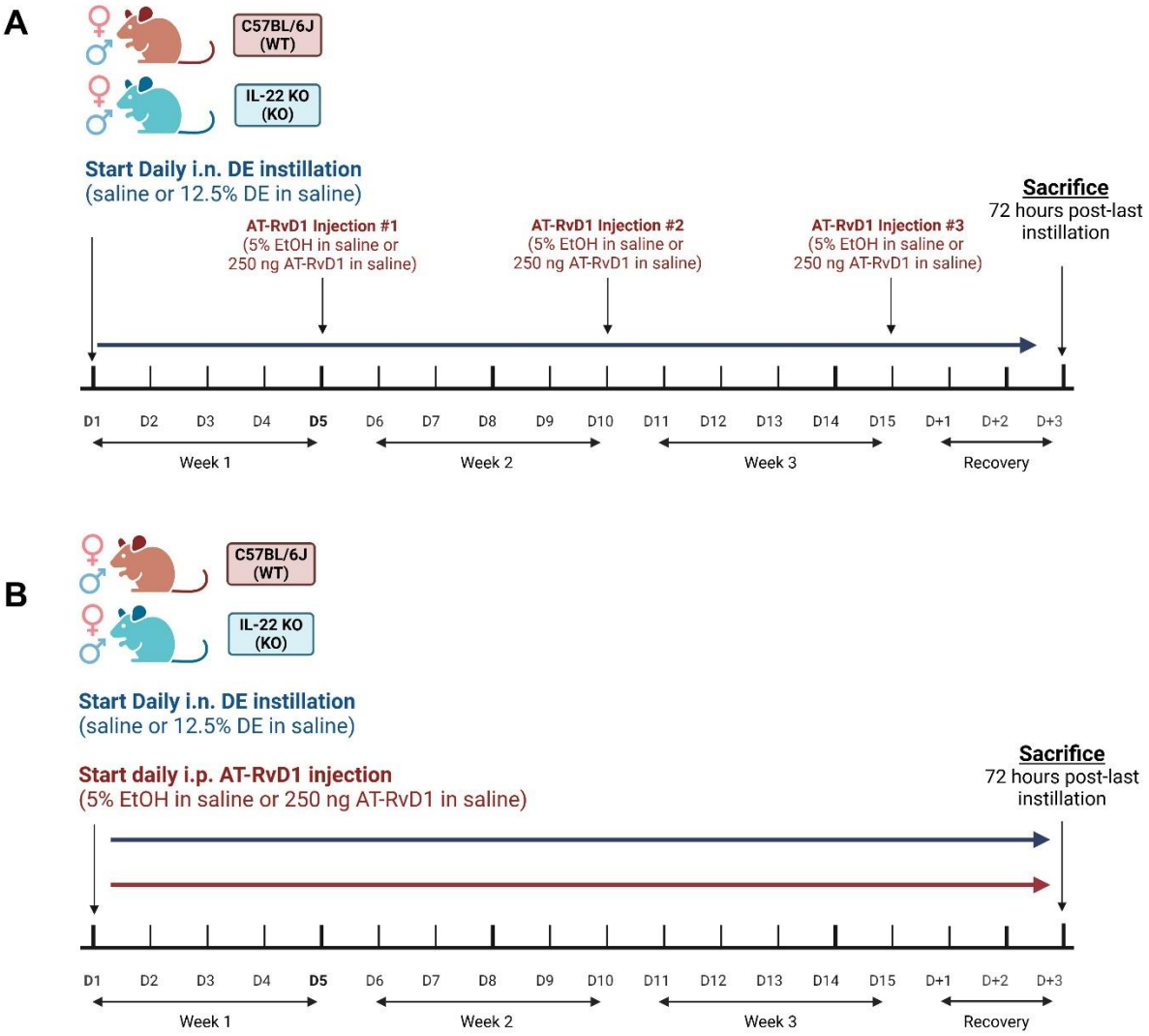


Figure 21. AT-RvD1 dosing strategies in WT and IL-22 KO mice.
(A) once weekly AT-RvD1 dosing strategy timeline; WT and KO animals were instilled i.n. with 12.5% DE 5 days/week for 3 weeks and treated with 250 ng AT-RvD1 i.p. once/week for 3 weeks, (B) Once daily AT-RvD1 dosing strategy timeline; WT and KO animals were instilled

i.n. with 12.5% DE 5 days/week for 3 weeks and treated with 250 ng AT-RvD1 i.p. 5 days/week for 3 weeks. Created with BioRender.com.

3.2.4 Animal Sacrifice and Sample Collection

Animals were euthanized in accordance with the American Veterinary Medical Association guidelines by isoflurane overdose immediately followed by cervical dislocation, 72 hours following the final DE instillation and AT-RvD1 injection. Bronchoalveolar lavage fluid (BALF) was obtained by inserting a 25G catheter into the trachea, tying it off with suture, and lavaging the lungs three times with 1 mL of ice-cold phosphate-buffered saline (PBS) (HyClone Laboratories) for each wash. The first wash was collected in one 5 mL FACS tube while washes two and three were collected in a second 5 mL FACS tube. Both tubes were centrifuged at 300 x g for 8 minutes to pellet the cells. The supernatant fraction from wash 1 was aliquoted into a separate tube and stored at -80 °C for cytokine analysis by enzyme-linked immunosorbent assay (ELISA). The supernates from washes two and three were discarded, and cell pellets from both tubes were combined with 400 µl of red blood cell lysis buffer (Life Technologies Corporation), placed on ice for 5 minutes, then centrifuged at 300 x g for 8 minutes at 4 °C. The supernatant fraction was discarded, and the cell pellets were resuspended with 200 µL of PBS. A 10 µl aliquot of the cell suspension was then collected for counting using a Countess 3 FL automatic cell counter to generate total cell infiltrate values. The cell suspensions were diluted with PBS to achieve a concentration of $1x10^6$ cells/mL. 200 µl of the final cell suspension was then added to a Thermo Cytospin 4 cytocentrifuge and centrifuged at 600 rpm for 5 minutes. Slides were dried overnight for further staining and analysis. The left lobes of the lungs were tied off with suture, removed, placed in 800 µl of RNAlater (Invitrogen), and stored at -80 °C until use. The right lung lobes were extracted along with the heart and tracheal tissue, then inflated with 10%

neutral-buffered formalin (NBF) (Cancer Diagnostics Inc.) before hanging under 20 cm of pressure and submerged in 10% NBF overnight. They were then transferred to cassettes and stored in 10% NBF for at least 48 hours before further processing. Brains were extracted *en bloc* and immediately fixed whole in tissue cassettes in 10% NBF for at least 48 hours before further processing. All tissues were submitted to the Colorado State University Veterinary Diagnostic Laboratory Experimental Pathology Facility (EPF) for paraffin embedding and sectioning at 5 μm.

3.2.5 Cellular Infiltrate Analysis

Staining was performed on dried slides using a Volu-Sol dip-stain kit, with methanol as the fixative, and eosin and methylene blue (Volu-Sol) as the differential stains. Slides were imaged at 20X magnification using an Olympus BX35 microscope and cellSense software version 4.1. Differential counts were performed by counting 300 cells on each image to evaluate macrophages, neutrophils, eosinophils, and lymphocytes, assisted by QuPath version 0.5.1.

3.2.6 Cytokine Quantification

Bronchoalveolar lavage fluid (BALF) was collected, processed, and stored as previously described above. Left lung lobes in RNAlater were homogenized with lysis buffer containing PBS, 1X RIPA lysis buffer (Thermo Scientific, Cat#: J62524.AE), and 1X proteinase inhibitor cocktail (Thermo Scientific, Cat#: 1861279) at a ratio of 50 mg tissue to 1 mL buffer. A Bead Mill 24 bead homogenizer was used to break up the tissues (speed: 5.00, time: 0:05, cycles: 3, duration: 0:03). The samples were then incubated on ice for 30 minutes, with agitation every 10 minutes. Homogenate aliquots were stored at -80 °C until use. Cytokine protein concentrations in

BALF and lung tissue were quantified using sandwich ELISAs. Kits were purchased from DuoSet (R&D Systems) and used according to the manufacturer's recommendations with the modification of capture antibody diluted in BupH Carbonate-Bicarbonate Buffer (Voller's Coating Buffer, Thermo Scientific). High-binding half-well 96-well plates (Greiner Biotech) were coated with manufacturer-specified capture antibody concentrations and incubated overnight at room temperature before progression of assay. All washes were performed using a Tecan HydroFlex™ plate washer. After completion of the assay, plates were read on a FLUOstar Omega spectrophotometer at 450 nm using Omega software version 5.7. Concentration values were calculated from standards using a four-parameter fit model in Omega MARS Software Version 4.00.

3.2.7 Lung Histopathology

Whole right lung coronal sections, collected as previously described above, were stained with hematoxylin and eosin (H&E) following deparaffinization and rehydration with xylene and graded EtOH solutions (xylene, 100% EtOH, 95% EtOH, 80% EtOH, 50% EtOH, and finally 1X PBS). Slides were scanned at 40X on a Vectra Polaris scanning microscope. Images of lungs from animals administered weekly AT-RvD1 injections were blinded and manually scored using a well-established semiquantitative scoring method [48,137,220,221,229]. Images from animals administered daily AT-RvD1 injections were imported into VisioPharm version 2023.09.3.15043 x64 and processed through an artificial intelligence (AI) workflow for quantitative assessment of alveolar space, alveolar septa thickness, peribronchiolar inflammation, perivascular inflammation, total alveolar septa nuclei, and percentage of inducible bronchus-associated lymphoid tissue (iBALT) formations relative to tissue area. AI quantification was performed on

the whole lung tissue with output measurements including area, percentages of parameters to total tissue area or total parameter counts. VisioPharm is one of the leading AI histopathology analysis software available. Our workflow and applications were designed, annotated, trained, and verified by a board-certified veterinary anatomic pathologist to identify our desired readouts and ensure accurate results. The workflow is then trained through a large set of sample images by a board-certified veterinary anatomic pathologist where structures are identified by the software and confirmed by the pathologist, allowing the software to "learn" how structures are organized and are identified in the experimental images. Briefly, the workflow consisted of multiple stepwise applications of increasing specificity, starting with identification of the lung tissue, followed by identification of airways and vessels, then inflammation and iBALT, and finally identification of airways epithelial cells and alveolar nuclei. During each step of the workflow, the results are confirmed manually to ensure accurate detection of structures. All parameters are normalized to tissue area to mitigate size and artifact skewing.

3.2.8 Immunofluorescence

Whole brain sagittal paraffin embedded tissue sections, as previously described above, were deparaffinized by baking slides at 60 °C for 20 minutes, followed by rehydration through an EtOH gradient (xylene, 50% xylene/50% EtOH, 100% EtOH, 95% EtOH, 70% EtOH), and then incubated in 1.0 M Tris buffered saline (TBS). Antigen retrieval was achieved using 1 nM EDTA buffer with 0.05% Tween20, pH 8.0 at 95 °C for 20 minutes in a Biocare Medical Decloaking Chamber™ NxGen (Biocare Medical). Tissues were washed three times for 10 minutes each with 0.05M TBS and blocked using 2% donkey serum in 0.2% Triton-X in 1.0 M TBS for 1 hour at room temperature. Microglia were identified using rabbit anti-ionized calcium

binding adaptor molecule 1 (Iba1) (1:1000; Abcam, Cat #: ab178846) diluted in 1.0 M TBS and incubated overnight at 4 °C. Tissues were then washed four times for 10 minutes each with 0.05 M TBS. A goat anti-rabbit Alexa Fluor 647 secondary antibody (Invitrogen, Cat#: A21244) diluted 1:500 in 2% donkey serum in 1.0 M TBS, was applied and incubated for 1 hour at room temperature. Sections were washed three times for 10 minutes each with 0.05 M TBS. Nuclear staining was achieved by incubation with Hoechst 33342, diluted 1:2000 in PBS (Invitrogen, Cat #: H3570), for three minutes, then washed three times for 10 minutes each with 0.05 M M TBS. ProLong Diamond Antifade Mountant (Fisher Scientific, Cat #: P36970) was then applied before mounting with glass coverslips. Slides were kept at room temperature, protected from light, for 24 – 48 hours to cure mounting medium, then stored at 4 °C in the dark prior to imaging. Stained sections were scanned at 40X using a Vectra Polaris microscope, and the number of microglia per area of each brain region of interest were quantified using QuPath Version 0.5.1. All sections were imaged on the same day with the same exposure settings for each channel.

3.2.9 RNAscope

RNAscope® assays were performed according to the formalin-fixed, paraffin-embedded (FFPE) tissue protocol provided in the RNAscope™ Multiplex Fluorescent Reagent Kit v2 Assay Manual (Document Number: UM 323100). Mouse lung and brain sections previously described above were utilized, with 3 animals per sex, per treatment condition, per genotype selected. Probes for IL-1β (Cat #: 316891-C3), CXCL10 (Cat #: 408921-C3), IL-10 (Cat #: 317261-C2), TGF-β (Cat #: 407751), and AREG (Cat #: 430501) were purchased from Advanced Cell Diagnostics, Inc. TSA Vivid Fluorophore dyes 570 (Cat #: 323272) and 650 (Cat #: 232273) were purchased from Advanced Cell Diagnostics, Inc. and diluted in TSA buffer

1:1500 (Cat #: 322809). Opal Polaris 780 Fluorophore Reagent Pack was purchased from Akoya Biosciences (Cat #: FP1501001KT). TSA-DIG was diluted 1:1500 in TSA buffer for lung sections and 1:750 for brain sections. Opal Polaris 780 Fluorophore was diluted 1:500 in Antibody Diluent/Block (Akoya Biosciences, Cat #: ARD1001EA) for lung sections and 1:200 for brain sections. Positive control slides using RNAscope™ 3-plex positive control probes (CAT #: 320881) and negative control slides using RNAscope™ 3-plex negative control probes (Cat#: 320871) were utilized to validate the assay and results. After completion of the RNAscope® protocol, sections were incubated with RNAscope® DAPI (Advanced Cell Diagnostics, Inc.) for 30 seconds, then mounted on glass coverslips with ProLong Diamond Antifade mounting medium (Invitrogen). The mounted sections were kept at room temperature, protected from light, for 24–48 hours to cure mounting medium, before being stored at 4 °C until imaging. Slides were scanned at 40X using a Vectra Polaris microscope, with all sections imaged on the same day using the same exposure settings for each channel. QuPath Version 0.5.1 was used according to manufacturer protocols to detect the cell nuclei and quantify subcellular dots per nucleus for the entirety of the lung tissue and for each of the brain regions of interest.

3.2.10 Statistical Analysis

All statistical and graphical analyses were performed using GraphPad Prism Version 10. A power analysis was performed using an alpha = 0.05 based on histopathological scoring from our pilot study which indicated 8-10 mice per group would be sufficient to achieve 85-90% power to identify significant differences between groups. Outliers were tested for and removed from the datasets using ROUT analysis with Q=1%. Statistical significance was determined by performing 3-way ANOVA analyses with Benjamini, Krieger and Yekutieli post-hoc analysis for

pairwise comparisons to reduce false discovery rate. A p-value of less than or equal to 0.05 was used to determine significance and a p-value of less than or equal to 0.1 was considered a trend. Individual animals are represented by a single symbol on figures, with filled shapes representing male animals and unfilled shapes representing female animals. On figures, significance is denoted by, * = $p \leq 0.05$; ** = $p \leq 0.01$; *** = $p \leq 0.001$; **** = $p \leq 0.0001$.

3.3 Results

3.3.1 IL-22 KO alters lung immune cell trafficking and weekly AT-RvD1 administration reduces cellular infiltration in IL-22 KO mice following repetitive organic dust exposure

We have previously demonstrated that DE exposure leads to increased infiltration of immune cells into the airways [48,162,221]. One well-established mechanism of AT-RvD1 is its ability to modify immune cell recruitment to sites of infection and injury (33). We aimed to establish an effective dosing strategy to assess the therapeutic applications of AT-RvD1 in a model of repetitive ODE. WT and IL-22 KO mice were instilled i.n. with 50 µl of either 12.5% DE in sterile saline or sterile saline for 5 days per week for 3 weeks (15 total installations) and injected i.p. with 50 µl of either 250 ng AT-RvD1 in sterile saline or 5% EtOH (AT-RvD1 carrier) in sterile saline once per week following the 5th DE instillation each week (3 total injections) (Figure 22A). To determine the impact of AT-RvD1 treatment on immune cell recruitment following DE, we examined cellular infiltration into the airway via BALF cellular analysis (Figures 22A-E) and lung histopathology (Figures 22A-D).

Upon analysis of BALF cellular infiltrates, we observed an increase in the total number of cellular infiltrates in both WT ($p=0.0011$) and KO ($p<0.0001$) mice exposed to DE compared to saline controls (Figure 22A). Additionally, we observed a trend of increased total cells in KO

mice exposed to DE compared to WT mice exposed to DE ($p=0.0702$) (Figure 22A). KO mice exposed to DE and treated with AT-RvD1 exhibited reduced total cell counts compared to KO mice exposed to DE and treated with saline ($p=0.0265$) (Figure 22A). Macrophage differential counts revealed increased influx in WT ($p=0.0162$) and KO ($p=0.0015$) mice exposed to DE compared to WT and KO mice exposed to saline, respectively (Figure 22B). We also observed a trend between KO mice exposed to DE and WT mice exposed to DE ($p=0.0966$) (Figure 22B). KO mice exposed to DE and treated with AT-RvD1 demonstrated significantly reduced macrophage differential counts compared to KO mice exposed to DE and treated with AT-RvD1 ($p=0.0457$) (Figure 22B). We did not observe any significant differences or trends in the number of neutrophils, regardless of exposure or treatment condition (Figure 22C). Eosinophil differential counts revealed a decrease in the number of eosinophil influx in KO mice exposed to DE and treated with AT-RvD1 compared to KO mice exposed to DE and treated with saline ($p=0.0180$) (Figure 22D). We also observed elevated trafficking of lymphocytes in WT ($p=0.0013$) and KO ($p<0.0001$) mice exposed to DE compared to saline exposed controls as well as significantly increased lymphocyte counts in KO mice exposed to DE compared to WT mice exposed to DE ($p=0.0454$) (Figure 22E).

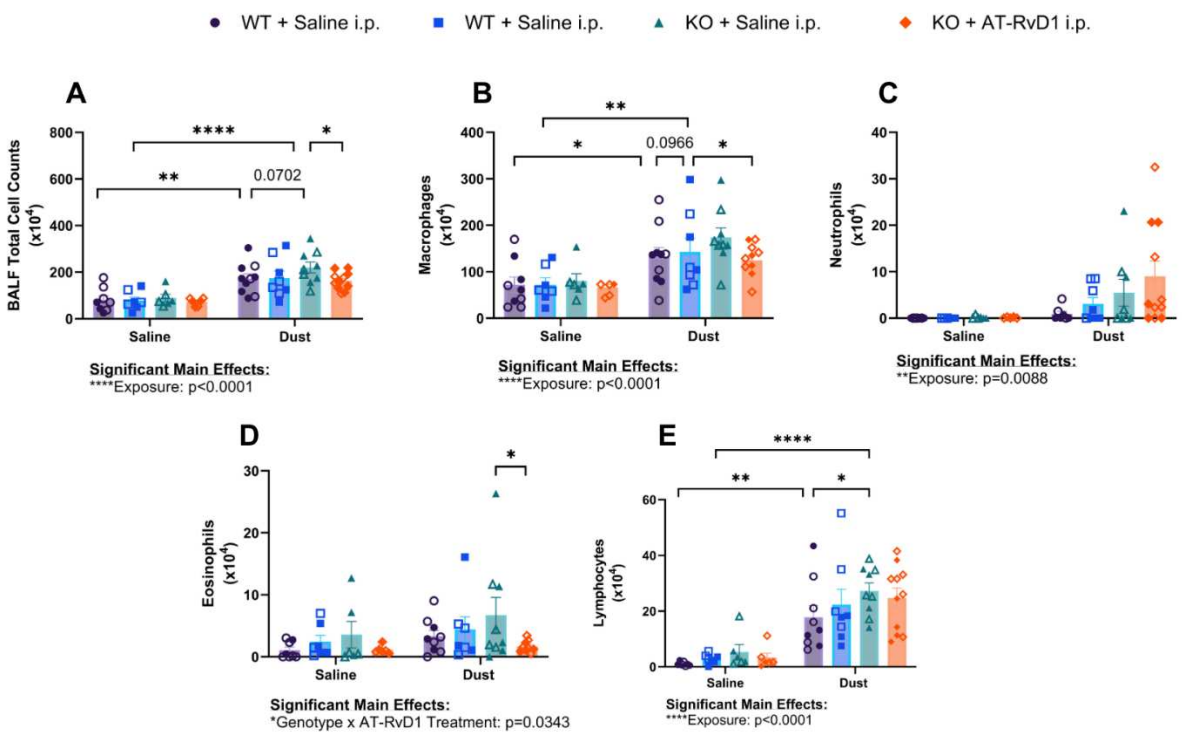


Figure 22. Impacts of DE and AT-RvD1 on BALF immune cellular infiltrates in WT and IL-22 KO animals.
WT and KO animals were instilled i.n. with 12.5% DE 5 days/week for 3 weeks and treated with 250 ng AT-RvD1 i.p. once/week for 3 weeks. (A) total cell counts, (B) macrophages, (C) neutrophils, (D) eosinophils, (E) lymphocytes. 3 way ANOVA with Benjamini, Krieger and Yekutieli post-hoc analysis, error bars = SEM; * = $p \leq 0.05$; ** = $p \leq 0.01$; *** = $p \leq 0.001$; **** = $p \leq 0.0001$. Sample sizes: WT Saline i.n. + Saline i.p (3 female/3 male), WT Saline i.n. + AT-RvD1 i.p (3 female/3 male), WT Dust i.n. + Saline i.p (5 female/5 male), WT Dust i.n. + AT-RvD1 i.p (4 female/4 male), KO Saline i.n. + Saline i.p (3 female/3 male), KO Saline i.n. + AT-RvD1 i.p (3 female/3 male), KO Dust i.n. + Saline i.p (5 female/4 male), KO Dust i.n. + AT-RvD1 i.p (6 female/5 male).

We also examined lung pathology of mice injected with 250 ng AT-RvD1 once per week to assess the effectiveness of AT-RvD1 at reducing DE-induced lung pathology. We evaluated inducible bronchus associated lymphoid tissue (iBALT), peribronchiolar inflammation, and alveolar inflammation using a semiquantitative scoring method previously utilized in our laboratory [47,48,157,221,229]. Statistical analysis revealed a significant main effect of DE exposure in all three parameters evaluated: iBALT ($p=0.0002$), peribronchiolar inflammation ($p<0.0001$) and alveolar inflammation ($p<0.0001$) (Figures 23B-D). However, on post-hoc analysis, we observed

no statistically significant differences or trends between AT-RvD1 i.p. and saline i.p. treatment groups (Figures 23B-D). Interestingly, we observed a similar pattern in all parameters evaluated. We found a significant increase in the mean inflammatory score of iBALT in both WT (p=0.0446) and KO (p=0.0025) animals exposed to DE compared to saline-exposure controls (Figure 23B). Additionally, we observed a significantly increased peribronchiolar inflammation in WT (p=0.0064) and KO (p=0.0005) animals exposed to DE compared to saline-exposed controls (Figure 23C), as well as a significant increase in the mean score for alveolar inflammation in KO animals exposed to DE compared to saline-exposure controls (p=0.0004) and a trend in WT animals exposed to DE compared to saline-exposure controls (p=0.0596) (Figure 23). We also did not observe any significant changes in mean pathological scores of WT compared to KO animals regardless of exposure or treatment group.

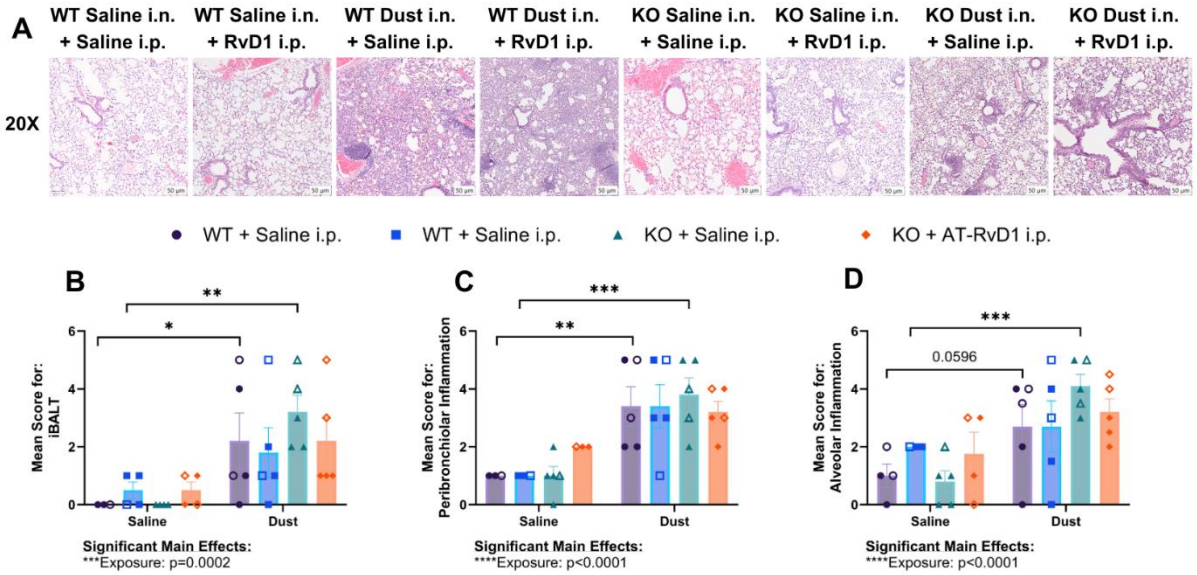


Figure 23. AT-RvD1 administration once weekly does not improve lung pathology. WT and KO animals were instilled i.n. with 12.5% DE 5 days/week for 3 weeks and treated with 250 ng AT-RvD1 i.p. once/week for 3 weeks. (A) representative images at 20X magnification, (B) mean inflammatory score for iBALT, (C) mean inflammatory score for peribronchiolar inflammation, (D) mean inflammatory score for alveolar inflammation. Scale bar = 50 μm. 3 way ANOVA with Benjamini, Krieger and Yekutieli post-hoc analysis, error bars = SEM; * = $p \leq 0.05$; ** = $p \leq 0.01$; *** = $p \leq 0.001$; **** = $p \leq 0.0001$. Sample sizes: WT Saline i.n. + Saline

i.p (2 female/2 male), WT Saline i.n. + AT-RvD1 i.p (2 female/2 male), WT Dust i.n. + Saline i.p (2 female/3 male), WT Dust i.n. + AT-RvD1 i.p (3 female/3 male), KO Saline i.n. + Saline i.p (3 female/3 male), KO Saline i.n. + AT-RvD1 i.p (2 female/2 male), KO Dust i.n. + Saline i.p (3 female/3 male), KO Dust i.n. + AT-RvD1 i.p (3 female/3 male).

Following our observations of no statistically significant changes in animals exposed to DE and treated with AT-RvD1 once weekly (Figures 23A-D), we developed a 5 day/week AT-RvD1 injection regimen, which we found yielded more significant therapeutic efficacy, through histopathology resolution, and was thus employed as our model for further analysis of the pulmonary and neurological inflammatory response to DE. Briefly, WT and IL-22 KO mice were instilled i.n. with 50 µl of either 12.5% DE in sterile saline or sterile saline for 5 days per week for 3 weeks, and then injected i.p. with 50 µl of either 250 ng AT-RvD1 in sterile saline or 5% EtOH (AT-RvD1 carrier) in sterile saline 5 days per week for 3 weeks (Figure 21B).

Our analysis of lung histopathology via VisioPharm AI applications revealed an increase in the percentage of iBALT relative to lung tissue area in both WT ($p=0.0014$) and KO mice ($p<0.0001$) exposed to DE (Figure 24B). Interestingly, we also observed a significant increase in iBALT percentage in KO mice compared to WT mice exposed to DE ($p=0.0002$) (Figure 24B). Additionally, KO mice exposed to DE and treated with AT-RvD1 displayed a significant decrease in iBALT percent of lung tissue compared to KO mice exposed to DE and treated with saline ($p<0.0001$) (Figure 24B). Furthermore, we discovered significant sex differences in the iBALT percentages displayed by both WT and KO animals. We found that female animals exposed to DE and treated with saline exhibited a significantly higher iBALT percentage than male animals exposed to DE and treated with saline in both WT ($p<0.0001$) and KO ($p<0.0001$) animals (Figures 24C,D). Additionally, both WT ($p=0.0021$) and KO ($p<0.0001$) female animals exposed to dust and treated with AT-RvD1 displayed significantly reduced iBALT compared to saline treated female animals (Figures 24C,D). Evaluation of peribronchiolar and perivascular

inflammation percentage revealed a significant increase in both WT ($p=0.0013$) and KO ($p<0.0001$) mice exposed to DE (Figure 24E). We observed a trend of reduced peribronchiolar and perivascular inflammation in KO animals exposed to DE and treated with saline and KO mice exposed to DE and treated with AT-RvD1 ($p=0.0791$) (Figure 24E). Bronchiolar epithelium area in KO mice exposed to DE was significantly increased compared to KO mice exposed to saline ($p=0.0474$) and was further increased in KO mice exposed to DE and treated with AT-RvD1 compared to KO mice exposed to DE and treated with saline ($p=0.0233$) (Figure 24F). Bronchiolar epithelium area was also decreased in WT mice exposed to DE and treated with AT-RvD1 compared to KO mice exposed to DE and treated with AT-RvD1 ($p=0.0353$) (Figure 24F). We observed a significant decrease in alveolar air space in KO mice exposed to saline compared to WT mice exposed to saline ($p=0.0301$) (Figure 24G). Total alveolar nuclear counts were observed to be elevated in WT mice exposed to DE compared to WT mice exposed to saline ($p=0.0377$), with an observed trend of increased nuclei in KO mice exposed to DE compared to KO mice exposed to saline ($p=0.0598$) (Figure 24H).

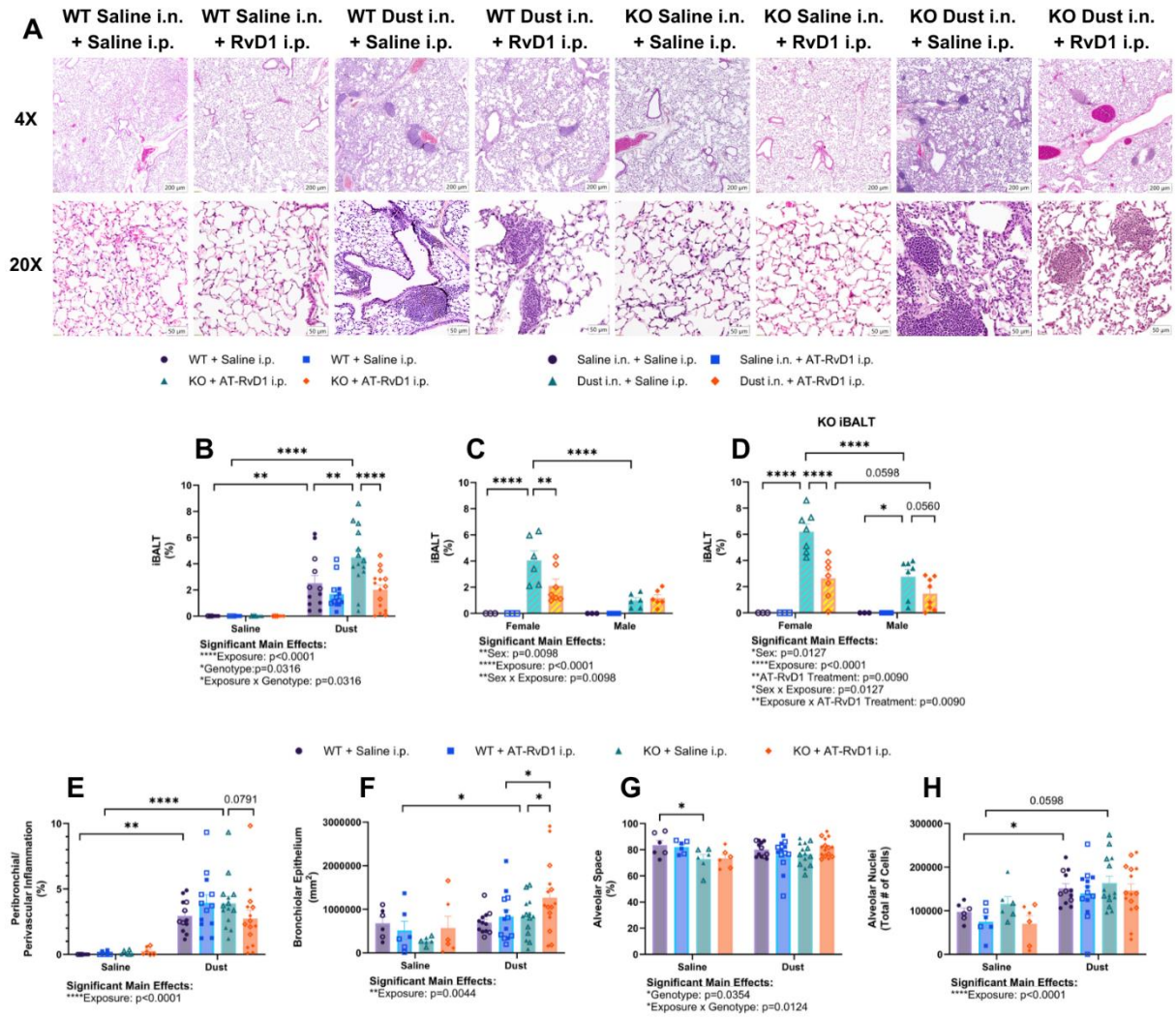


Figure 24. AT-RvD1 treatment daily reduces iBALT in animals exposed to DE. WT and KO animals were instilled i.n. with 12.5% DE 5 days/week for 3 weeks and treated with 250 ng AT-RvD1 i.p. 5 days/week for 3 weeks. (A) representative images at 4X and 10X magnification, (B) iBALT percentage in all animals, (C) iBALT percentage in WT animals by sex, (D) iBALT percentage in KO animals by sex, (E) combined peribronchiolar and perivascular inflammation percentage in all animals, (F) bronchiolar epithelium area, (G) alveolar space percentage, (H) total alveolar nuceli. Scale bar = 50 µm. 3 way ANOVA with Benjamini, Krieger and Yekutieli post-hoc analysis, error bars = SEM; * = $p \leq 0.05$; ** = $p \leq 0.01$; *** = $p \leq 0.001$; **** = $p \leq 0.0001$. Sample sizes: WT Saline i.n. + Saline i.p (3 female/3 male), WT Saline i.n. + AT-RvD1 i.p (3 female/3 male), WT Dust i.n. + Saline i.p (6 female/6 male), WT Dust i.n. + AT-RvD1 i.p (6 female/6 male), KO Saline i.n. + Saline i.p (3 female/3

male), KO Saline i.n. + AT-RvD1 i.p (3 female/3 male), KO Dust i.n. + Saline i.p (7 female/7 male), KO Dust i.n. + AT-RvD1 i.p (7 female/8 male).

3.3.2 Impacts of AT-RvD1 on lung inflammatory mediator production in WT and IL-22 KO mice during recovery following repetitive DE exposure

We have previously demonstrated that ODE in mice increases both pro- and anti-inflammatory cytokine production [48,174,220]. In our recovery model, we found that after 15 DE instillations, mice displayed altered cytokine and inflammatory mediator production in the airway and pulmonary tissue compartments at the protein level (Figure 25A-F). Evaluation of amphiregulin (AREG) concentrations in BALF showed that KO mice exposed to DE exhibited decreased concentrations compared to saline controls ($p=0.0130$) and that KO mice exposed to DE displayed a trend of decreased AREG concentrations compared to WT mice exposed to DE ($p=0.0887$) (Figure 25A). Concentrations of interleukin-10 (IL-10), a classic anti-inflammatory, pro-resolution cytokine was decreased in the BALF of WT mice exposed to DE compared to saline controls ($p=0.0009$) and a trend of decreased concentrations in KO mice exposed to DE compared to saline controls ($p=0.0535$) was also observed (Figure 25B). Transforming growth factor-β (TGF-β) concentrations in BALF did not yield any significant differences regardless of genotype or treatment groups, however we did observe a significant main effect of DE exposure ($p=0.0021$) (Figure 25C). In the tissue compartment, IL-10 was observed to be elevated in KO mice exposed to saline compared to WT mice exposed to saline ($p=0.0003$) and in KO mice exposed to DE compared to WT mice exposed to DE ($p=0.0002$). WT mice exposed to DE and treated with AT-RvD1 exhibited increased tissue IL-10 concentrations compared to WT mice exposed to DE and treated with saline ($p=0.0070$) (Figure 25D). AREG quantification in lung tissues of WT mice exposed to DE displayed increased

concentrations compared to WT saline controls ($p=0.0005$) and were observed to be decreased in KO mice exposed to DE compared to WT mice exposed to DE ($p=0.0051$) (Figure 25E). We also observed a significant decrease in AREG concentrations in KO mice exposed to DE and treated with AT-RvD1 compared to WT mice exposed to DE and treated with AT-RvD1 ($p<0.0001$). Lung tissue TGF-β concentrations demonstrated a trend of increased concentrations in KO mice exposed to saline compared to WT mice exposed to saline ($p=0.0533$) and a significant increase in KO mice exposed to DE and treated with AT-RvD1 compared to WT mice exposed to DE and treated with AT-RvD1 ($p<0.0003$) (Figure 25F).

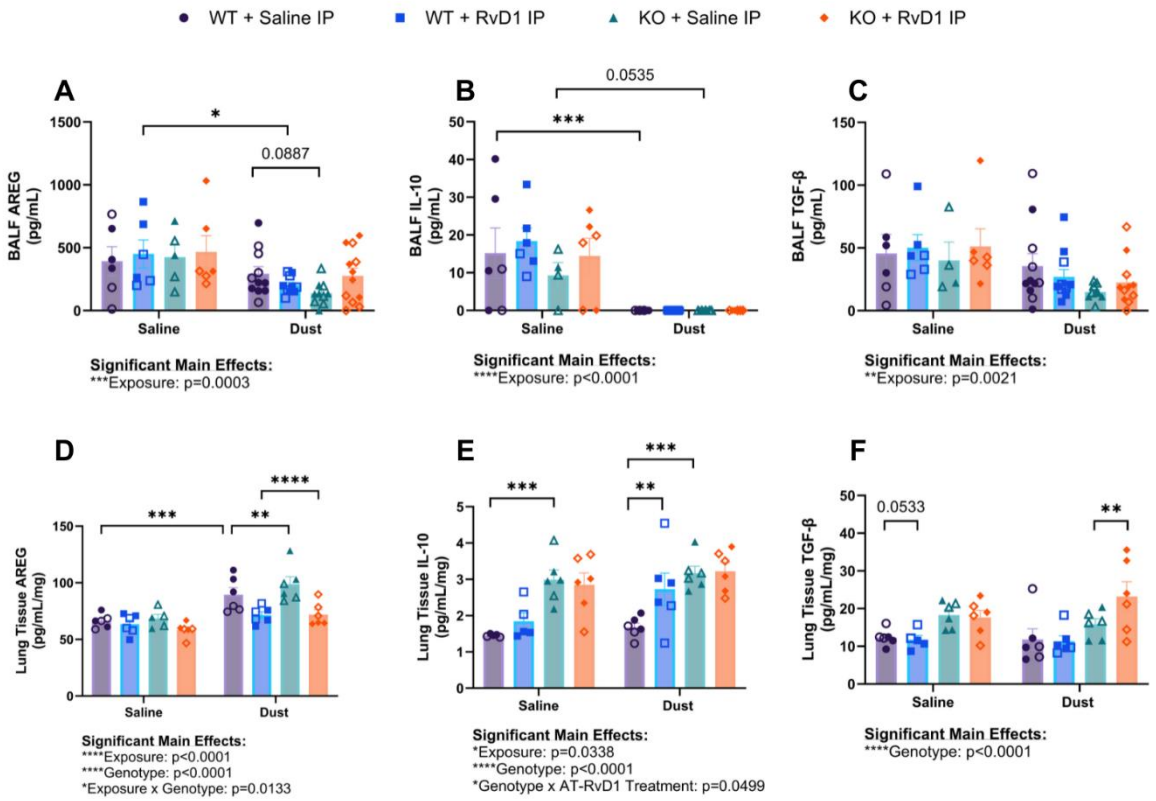


Figure 25. Effects of repetitive dust exposure and RvD1 treatment on bronchoalveolar lavage fluid (BALF) and lung tissue homogenate cytokines.
WT and KO animals were instilled i.n. with 12.5% DE 5 days/week for 3 weeks and treated with 250 ng AT-RvD1 i.p. 5 days/week for 3 weeks. (A) amphiregulin (AREG) concentrations in BALF, (B) interleukin-10 (IL-10) concentrations in BALF, (C) transforming growth factor-β (TGF-β) concentrations in BALF, (D) AREG concentrations in lung tissue, (E) IL-10 concentrations in lung tissue, and (F) TGFβ concentrations in lung tissue. 3 way ANOVA with Benjamini, Krieger and Yekutieli post-hoc analysis, error bars = SEM; * = $p \leq 0.05$; ** = $p \leq 0.01$; *** = $p \leq 0.001$; **** = $p \leq 0.0001$. BALF sample sizes: WT Saline i.n. + Saline i.p (3 female/3 male), WT Saline i.n. + AT-RvD1 i.p (3 female/3 male), WT Dust i.n. + Saline i.p (6 female/6 male), WT Dust i.n. + AT-RvD1 i.p (6 female/6 male), KO Saline i.n. + Saline i.p (3 female/3 male), KO Saline i.n. + AT-RvD1 i.p (3 female/3 male), KO Dust i.n. + Saline i.p (7 female/7 male), KO Dust i.n. + AT-RvD1 i.p (7 female/8 male). Lung tissue sample sizes: WT Saline i.n. + Saline i.p (3 female/3 male), WT Saline i.n. + AT-RvD1 i.p (3 female/3 male), WT Dust i.n. + Saline i.p (3 female/3 male), WT Dust i.n. + AT-RvD1 i.p (3 female/3 male), KO Saline i.n. + Saline i.p (3 female/3 male), KO Saline i.n. + AT-RvD1 i.p (3 female/3 male), KO Dust i.n. + Saline i.p (3 female/3 male), KO Dust i.n. + AT-RvD1 i.p (3 female/3 male).

To evaluate mRNA transcript expression in animals exposed to DE and treated with AT-RvD1, we utilized RNAscope technology to visualize and quantify mRNA transcripts in whole lung tissue sections. We evaluated *areg*, *il10*, and C-X-C motif chemokine ligand 10 (*cxcl10*)

transcripts in the alveolar and airway compartments to assess the recovery of IL-22 KO mice and the therapeutic impacts of AT-RvD1 and to assess the differences between alveolar and airway inflammatory markers. In the alveolar compartment, we observed a significant increase in *areg* expression in KO mice exposed to saline and treated with AT-RvD1 compared to KO mice exposed to saline and treated with saline ($p=0.0051$) (Figure 26B). Assessment of *il10* expression in the alveolar compartment yielded no significant differences or trends of, regardless of DE exposure or AT-RvD1 treatment or genotype (Figure 26C). Expression of *cxcl10* in the alveolar compartments of KO mice exposed to DE displayed a trend of increased expression compared to saline-exposed KO controls ($p=0.0559$) (Figure 26D). In the airway compartment, we again observed a significant increase in *areg* expression in KO mice exposed to saline and treated with AT-RvD1 compared to KO mice exposed to saline and treated with saline ($p=0.0187$) (Figure 26F). We again observed no significant differences or trends of *il10* expression in the airway compartment (Figure 26G). Interestingly, we did observe significantly elevated *cxcl10* expression in WT mice exposed to DE compared to saline-exposed WT controls ($p=0.0156$),

which was then revealed to be decreased in WT animals exposed to DE and treated with AT-RvD1 (p=0.0107) (Figure 26H).

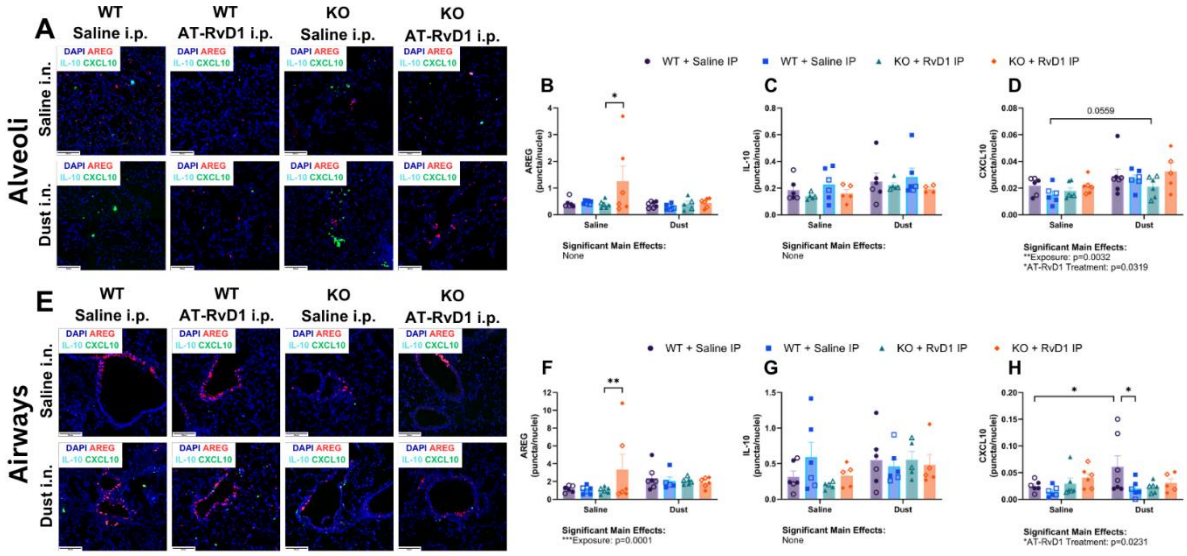


Figure 26. AT-RvD1 treatment reduces cxcl10 mRNA expression in WT animals exposed to DE.
WT and KO animals were instilled i.n. with 12.5% DE 5 days/week for 3 weeks and treated with 250 ng AT-RvD1 i.p. 5 days/week for 3 weeks. (A) representative images of the alveolar compartment at 40X magnification, (B) areg expression, (C) il10 expression, (D) cxcl10 expression, (E) representative images of the airway compartment at 40X magnification, (F) areg expression, (G) il10 expression, (H) cxcl10 expression. Scale bar = 50 µm. 3 way ANOVA with Benjamini, Krieger and Yekutieli post-hoc analysis, error bars = SEM; * = $p \leq 0.05$; ** = $p \leq 0.01$; *** = $p \leq 0.001$; **** = $p \leq 0.0001$. Sample sizes: WT Saline i.n. + Saline i.p (3 female/3 male), WT Saline i.n. + AT-RvD1 i.p (3 female/3 male), WT Dust i.n. + Saline i.p (4 female/3 male), WT Dust i.n. + AT-RvD1 i.p (3 female/3 male), KO Saline i.n. + Saline i.p (3 female/3 male), KO Saline i.n. + AT-RvD1 i.p (3 female/3 male), KO Dust i.n. + Saline i.p (3 female/3 male), KO Dust i.n. + AT-RvD1 i.p (3 female/3 male).

3.3.3 Agriculture dust exposure is associated with gliosis and AT-RvD1 administration reduces neuroinflammation

Brains of WT and IL-22 KO animals exposed to DE and treated with AT-RvD1 were assessed for microglia proliferation via immunofluorescence for $Iba1^+$ cells. Cells were counted and represented as a function of the area of each brain region of interest: olfactory bulb, frontal

cortex, isocortex, hippocampus, cerebellum, and hindbrain. The olfactory bulb was chosen due to its close proximity to the nasal passages and based upon previous investigations that have shown that intranasal instillations of other particulate matter sources result in gliosis in this region [142]. The frontal cortex, isocortex, and hippocampus regions of interest were evaluated due to their functions involving memory and cognition, the decline of which is a hallmark of neurodegenerative disease. The cerebellum was chosen as it controls motor function, and changes in motor function can also be a pathological marker seen in neurodegenerative disease. The hindbrain region of the brain stem is the innervation site for the vagus nerve, which has been implicated in neuroinflammatory models of chronic lung inflammation [100]. Increased numbers of $Iba1^+$ microglia were detected in areas involved in olfactory sensing and cognition including the olfactory bulb, frontal cortex, and isocortex in WT and KO mice (Figures 27A-F). KO mice displayed increased $Iba1^+$ microglia in the cerebellum, which is associated with motor function (Figures 27I, J). These data indicate that KO mice have altered responses to DE compared to WT controls, but that all mice regardless of genotype, experienced microgliosis in their brains following DE exposure. The increased number of microglia cells detected in brain tissue, is a hallmark sign of neuroinflammation and is a reliable marker for detecting neuroinflammatory processes [26,151,171].

Evaluation of the olfactory bulbs of animals exposed to DE revealed significant increases in the number of microglia in both WT ($p<0.0001$) and KO ($p=0.0109$) animals. We also observed an increase in the number of microglia in mice exposed to saline and treated with AT-RvD1 compared to with saline-exposed, saline-treated controls in both WT ($p=0.0002$) and KO ($p=0.0223$) genotypes (Figure 27B). Additionally, in the olfactory bulbs we observed a trend of increased microglia numbers in KO mice exposed to saline and treated with saline compared to

their WT saline-exposed, saline-treated controls (0.0645) (Figure 27B). Animals exposed to DE and treated with AT-RvD1 displayed decreased numbers of Iba1+ cells compared to DE-exposed, saline-treated controls in both WT (p=0.0090) and KO (p=0.0027) genotypes (Figure 27B). In the frontal cortex, both WT (p=0.0094) and KO (p=0.0009) animals exposed to DE displayed increased microglia numbers (Figure 27D). Saline-exposed, AT-RvD1-treated KO animals also displayed increased numbers compared to saline-exposed, saline-treated KO animals (p=0.0030) (Figure 27D). DE-exposed, AT-RvD1-treated WT animals displayed a trend of decreased numbers compared to WT DE-exposed, saline-treated animals (p=0.0633) (Figure 27D). Microglia numbers in the isocortex revealed a similar pattern as the olfactory bulb, with both WT (p=0.0051) and KO (p=0.0052) animals exposed to DE and treated with saline demonstrating increased microglia numbers compared to their saline controls (Figure 27F). We did not observe any significant differences in the number of microglia in the hippocampus, regardless of exposure or treatment condition (Figure 27H). Additionally, animals treated with AT-RvD1 exhibited decreased microglia numbers compared to their saline-treated controls for both WT (p=0.0247) and KO (p=0.0117) animals (Figure 27F). Saline-exposed KO animals displayed increased microglia counts in their cerebellums compared to WT saline-exposed animals (p=0.0093) and increased counts in DE-exposed, saline treated KO animals compared to saline-exposed controls (p=0.0313) (Figure 27J). WT animals exposed to saline and treated with AT-RvD1 displayed increased microglia numbers compared to saline-exposed, saline-treated WT animals in the hindbrain (p=0.0253) (Figure 27L).

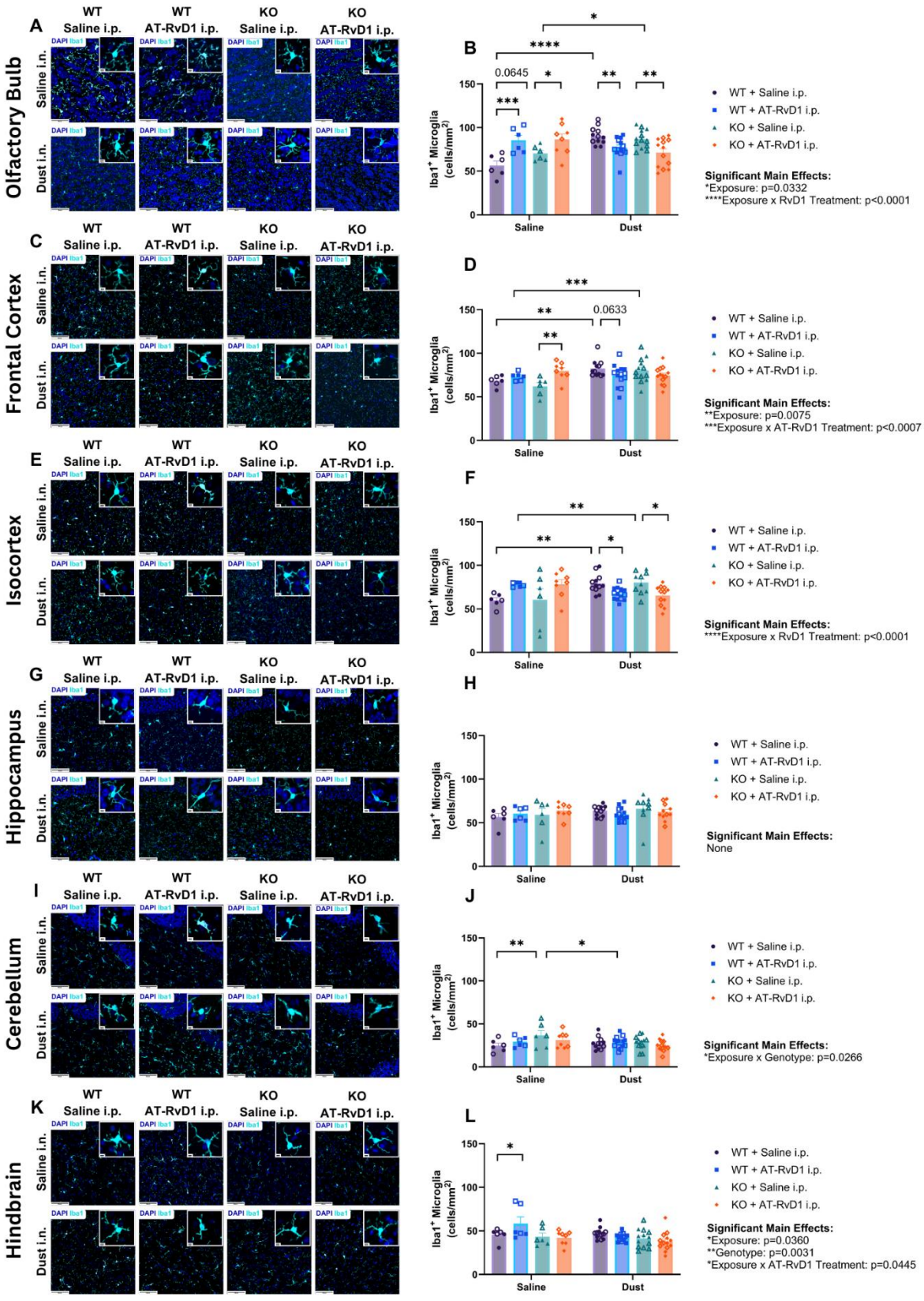

A
WT Saline i.p.
WT AT-RvD1 i.p.
KO Saline i.p.
KO AT-RvD1 i.p.
Olfactory Bulb
Saline i.n.
Dust i.n.
DAPI Iba1
B
Iba1+ Microglia (cells/mm2)
Saline
Dust
0.0645
WT + Saline i.p.
WT + AT-RvD1 i.p.
KO + Saline i.p.
KO + AT-RvD1 i.p.
Significant Main Effects:
*Exposure: p=0.0332
****Exposure x RvD1 Treatment: p<0.0001
C
Frontal Cortex
D
0.0633
Significant Main Effects:
**Exposure: p=0.0075
***Exposure x AT-RvD1 Treatment: p<0.0007
E
Isocortex
F
Significant Main Effects:
****Exposure x RvD1 Treatment: p<0.0001
G
Hippocampus
H
Significant Main Effects:
None
I
Cerebellum
J
Significant Main Effects:
*Exposure x Genotype: p=0.0266
K
Hindbrain
L
Significant Main Effects:
*Exposure: p=0.0360
**Genotype: p=0.0031
*Exposure x AT-RvD1 Treatment: p=0.0445

Figure 27. Gliosis is associated with agriculture dust exposure.
WT and KO animals were instilled i.n. with 12.5% DE 5 days/week for 3 weeks and treated with 250 ng AT-RvD1 i.p. 5 days/week for 3 weeks. (A) representative images of the olfactory bulb at 40X magnification, (B) microglia counts in the olfactory bulb, (C) representative images of the frontal cortex at 40X magnification, (D) microglia counts in the frontal cortex, (E) representative images of the isocortex at 40X magnification, (F) microglia counts in the isocortex, (G) representative images of the hippocampus at 40X magnification, (H) microglia counts in the hippocampus, (I) representative images of the cerebellum at 40X magnification, (J) microglia counts in the cerebellum, (K) representative images of the hindbrain at 40X magnification, (L) microglia counts in the hindbrain. Scale bar = 50 μm and 5 μm. 3 way ANOVA with Benjamini, Krieger and Yekutieli post-hoc analysis, error bars = SEM; * = $p \leq 0.05$; ** = $p \leq 0.01$; *** = $p \leq 0.001$; **** = $p \leq 0.0001$. WT Saline i.n. + Saline i.p (3 female/3 male), WT Saline i.n. + AT-RvD1 i.p (3 female/3 male), WT Dust i.n. + Saline i.p (6 female/6 male), WT Dust i.n. + AT-RvD1 i.p (8 female/6 male), KO Saline i.n. + Saline i.p (3 female/3 male), KO Saline i.n. + AT-RvD1 i.p (4 female/4 male), KO Dust i.n. + Saline i.p (7 female/6 male), KO Dust i.n. + AT-RvD1 i.p (6 female/7 male).

3.3.4 AT-RvD1 treatment alters brain transcript expression in animals exposed to DE

We again utilized RNAscope technology to visualize and quantify mRNA transcript expression in WT and KO animals exposed to DE and treated with AT-RvD1 using whole brain tissue sections to evaluate individual regions of interest. We evaluated *tgfb*, *il10*, and *il1β* transcripts in the olfactory bulb, frontal cortex, isocortex, hippocampus, cerebellum, and hindbrain.

Transcript quantification in the olfactory bulb revealed a trend of increased *tgfb* expression between WT saline-exposed mice and KO saline-exposed mice (p=0.0929) (Figure 28B). Additionally, a trend was observed for increased *il10* transcription in KO mice exposed to DE and treated with AT-RvD1 compared to WT mice exposed to DE and treated with AT-RvD1 (p=0.0669) (Figure 28C). Finally, *il1b* was significantly increased in WT DE-exposed, AT-RvD1-treated mice compared to KO DE-exposed, AT-RvD1-treated mice (p=0.0228) (Figure 28D). In the frontal cortex, tgfb displayed a trend of increased transcription between WT and KO mice exposed to saline (p=0.0600), and a trend of reduced transcription between KO mice

exposed to DE and KO mice exposed to saline (p=0.0560) (Figure 28F). Evaluation of the isocortex revealed significantly increased *tgfb* transcription between WT and KO saline-exposed mice (p=0. 0355), as well as significantly increased *tgfb* expression in KO mice exposed to DE compared to KO saline-exposed controls (p=0.0355) (Figure 28J). We also found that *il1b* expression was significantly reduced in WT DE-exposed, AT-RvD1 treated mice compared to KO DE-exposed, AT-RvD1 treated mice (p=0.0245) (Figure 28L). Transcript evaluation of the hippocampus revealed significantly increased *tgfb* expression in KO saline-exposed, saline-treated mice compared to WT saline-exposed, saline-treated mice (p=0.0049) (Figure 28N) and a significant decrease in *tgfb* expression in KO DE-exposed, saline-treated mice compared to KO saline-exposed, saline-treated controls (p=0.0198) (Figure 28N). We did not observe any significant differences or trends in the cerebellum. We did observe a change in the hindbrain, with *il1b* transcripts significantly decreased in WT saline-exposed and AT-RvD1 treated mice compared to WT saline-exposed, saline-treated (p=0.0252) (Figure 28X).

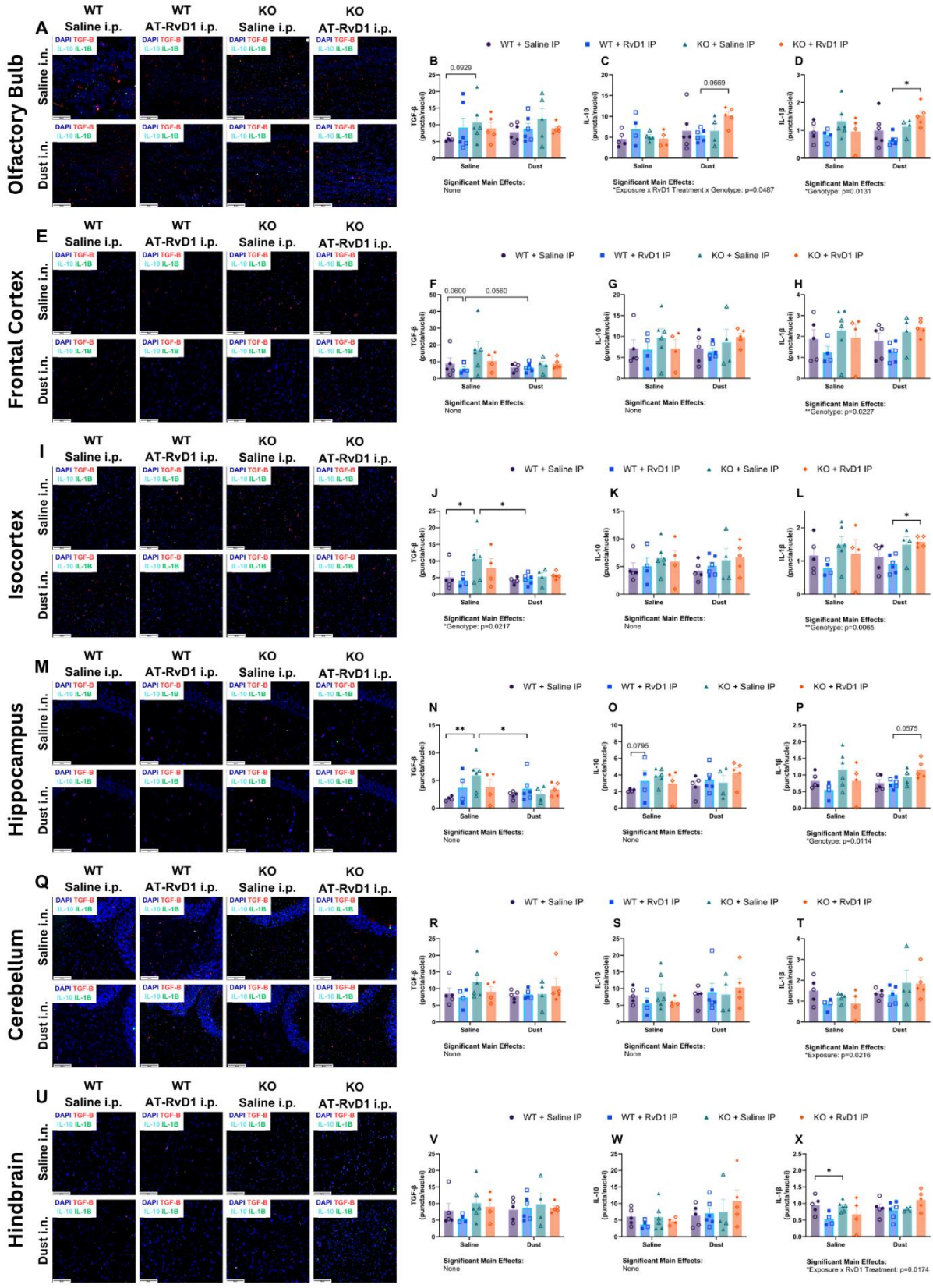

WT Saline i.p.
WT AT-RvD1 i.p.
KO Saline i.p.
KO AT-RvD1 i.p.
Olfactory Bulb
Frontal Cortex
Isocortex
Hippocampus
Cerebellum
Hindbrain
Saline i.n.
Dust i.n.
DAPI TGF-B IL-10 IL-1B
WT + Saline IP
WT + RvD1 IP
KO + Saline IP
KO + RvD1 IP
TGF-β (puncta/nuclei)
IL-10 (puncta/nuclei)
IL-1β (puncta/nuclei)
Saline
Dust
Significant Main Effects:
None
*Exposure x RvD1 Treatment x Genotype: p=0.0487
*Genotype: p=0.0131
**Genotype: p=0.0227
*Genotype: p=0.0217
**Genotype: p=0.0065
*Genotype: p=0.0114
*Exposure: p=0.0216
*Exposure x RvD1 Treatment: p=0.0174

Figure 28. IL-22 knock-out alters brain mRNA transcripts in the presence of AT-RvD1 and DE.
WT and KO animals were instilled i.n. with 12.5% DE 5 days/week for 3 weeks and treated with 250 ng AT-RvD1 i.p. 5 days/week for 3 weeks. (A) representative images of the olfactory bulb at 40X magnification, (B) tgfb expression in the olfactory bulb, (C) il10 expression in the olfactory bulb, (D) il1b expression in the olfactory bulb, (E) representative images of the frontal cortex at 40X magnification, (F) tgfb expression in the frontal cortex, (G) il10 expression in the frontal cortex, (H) il1b expression in the frontal cortex, (I) representative images of the isocortex at 40X magnification, (J) tgfb expression in the isocortex, (K) il10 expression in the isocortex, (L) il1b expression in the isocortex, (M) representative images of the hippocampus at 40X magnification, (N) tgfb expression in the hippocampus, (O) il10 expression in the hippocampus, (P) il1b expression in the hippocampus, (Q) representative images of the cerebellum at 40X magnification, (R) tgfb expression in the cerebellum, (S) il10 expression in the cerebellum, (T) il1b expression in the cerebellum, (U) representative images of the hindbrain at 40X magnification, (V) tgfb expression in the hindbrain, (W) il10 expression in the hindbrain, (X) il1b expression in the hindbrain. Scale bar = 50 μm. 3 way ANOVA with Benjamini, Krieger and Yekutieli post-hoc analysis, error bars = SEM; * = $p \leq 0.05$; ** = $p \leq 0.01$; *** = $p \leq 0.001$; **** = $p \leq 0.0001$. Sample sizes: WT Saline i.n. + Saline i.p (3 female/3 male), WT Saline i.n. + AT-RvD1 i.p (2 female/2 male), WT Dust i.n. + Saline i.p (3 female/3 male), WT Dust i.n. + AT-RvD1 i.p (3 female/3 male), KO Saline i.n. + Saline i.p (3 female/3 male), KO Saline i.n. + AT-RvD1 i.p (2 female/2 male), KO Dust i.n. + Saline i.p (2 female/2 male), KO Dust i.n. + AT-RvD1 i.p. (3 female/3 male).

3.4 Discussion

The pulmonary inflammatory response to ODE has been well established, however the neuroinflammatory effects of this environmental and occupational exposure are not clear [136,160,174]. Other models of environmental exposures examining neuroinflammation have demonstrated that inhalant exposures can be associated with neuroinflammation and can ultimately lead to neurodegenerative disease [27,40,105,215]. In addition, a pulmonary infection model of *Mycobacterium tuberculosis* demonstrated severe pulmonary bacterial infection without microbial dissemination to the brain that produced gliosis, neuroinflammation, and misfolded proteins, pathologies of animals developing neurodegenerative disease [100]. Epidemiological studies have also linked pulmonary inflammation and infection in patients with COPD and *Mycobacterium tuberculosis* to neurological disease and early signs of neurodegenerative disease

including cognitive decline, depression and anxiety, reduced social interaction, and ultimately reduced quality of life [69,108,148]. To assess whether ODE contributes to neurological inflammation, microglia cell numbers were evaluated as an indicator of inflammation [65,100,204]. Glial cells such as microglia are the primary mediators of the neuroinflammatory response and have been evaluated as markers of neuroinflammation in other peripheral inflammation models [100,148]. Proliferation and migration of microglia in different brain regions have been implicated in neurodegenerative disease and impaired neuron functionality. Increases in the number of microglia indicate inflammation or inflammatory processes, while reduction of these cells indicates resolution of inflammation [26,151,171]. AT-RvD1 has shown efficacy in reducing neuroinflammation, suggesting that it may be an effective treatment to restore microglia homeostasis in deficient models, and our data demonstrates that AT-RvD1 may be effective in reducing microglia numbers in a mouse model of ODE (45,46). This could translate into improved disease outcomes in patients by reducing the neuroinflammatory consequences such as memory loss and anxiety/depression. With this treatment we could see improved neurological function in patients exposed to agriculture dust, but more investigation is required.

We found that proliferation of microglia primarily occurred in the rostral brain areas assessed: the olfactory bulb, frontal cortex, and isocortex. This may be attributed to the route of DE exposure, intranasal instillation, and the proximity of these brain regions to the olfactory system. One study found that two intranasal instillations of carbon nanoparticles were disseminated into the olfactory bulbs, which may be a mechanism of the observed gliosis, given the localization of the gliosis [142]. Another possible mechanism is that peripheral inflammation can contribute to gliosis without translocation of the inflammatory substances to the brain, as observed in a study examining gliosis in a guinea pig model of *Mycobacterium tuberculosis*

infection observed gliosis without dissemination of bacteria to the brain [100]. It is also possible that the components of the DE used in this study, such as lipopolysaccharides (LPS) could be transported to the brain through transport proteins and be directly activating microglia via TLR4 pathways [223]. We however did not observe an increase in IL-1β transcripts in brains of mice exposed to DE, so further evaluation of the cytokines profile and signaling is needed. We hypothesize that the inflammatory response observed in the brain of animals exposed to DE is TLR-mediated by microglia, however more information is required to decern the pathways and mechanisms that contribute to neuroinflammation in organic dust exposure. Our study is limited by the intranasal instillation of DE technique that is an effectively sterile, non-live infection model that may not be directly translatable to occupation exposure to ODE, which contains larger particles and live microbes [22,156,174]. In addition, our mice are also only exposed a total of 15 times, which may not provide a sufficient exposure duration to elicit a robust neurological inflammatory response in all brain regions. Our laboratory has previously explored the role of IL-22 in the pulmonary immune response to ODE, but we have not examined the role of this cytokine in a neurological inflammatory model or in a recovery model of repetitive ODE [220]. We previously explored this knock-out model in a 15-intstillation repetitive exposure model, however this study examining tissues 5 hours post-last DE instillation, but we have not yet explored the recovery period in the days following cessation of DE exposure [220]. We have also previously examined the therapeutic actions of AT-RvD1 in a chronic dust exposure model but have not explored its applications in an ODE-induced neuroinflammatory model [48]. We investigated the neuroinflammatory response to agriculture dust, the role of IL-22 in pulmonary and neurological inflammation, and the therapeutic applications of AT-RvD1 in a pulmonary and neurological IL-22 knock-out mouse model repetitively exposed to agriculture dust extract and

treated with AT-RvD1. We found that in many of our parameters, IL-22 KO mice displayed increased disease severity via increased iBALT percentage (Figure 25B), increased microglia numbers in the olfactory bulb and cerebellum of saline-exposed animals (Figures 28B,J), and many of the differences in expression of cytokines and mediators evaluated at the protein (Figures 26D,E) and transcript (Figures 22B,F,16B,D,F,J,L,N,P) levels were genotype-driven. We observed a significant increase in the total cells collected and lymphocyte differential counts in both WT and KO animals following DE exposure and a significant influx of macrophages in KO animals. This is consistent with our previous findings that IL-22 KO is associated with increased total and differential cell counts after DE exposure (Figure 23A) [220]. However, we did find that the differential cell counts differed in our 72-hour recovery model. This is likely due to a shift in the immune response from an innate response characterized by high neutrophil counts to a more adaptive response dominated by lymphocytes (Figures 23A-E) [133,220]. KO animals treated with 250 ng AT-RvD1 once per week displayed decreased total cells and lymphocytes. KO animals also displayed a trend of increased total cell counts and significantly increased lymphocytes compared to WT animals. These data suggest that IL-22 knock-out may modulate cell recruitment to sites of injury and that AT-RvD1 also regulates immune cell recruitment, a well-known action of this SPM [118,189,191,208,220]. In addition, KO animals displayed increased pathology severity including increased iBALT percentage in DE-exposed animals compared to WT DE-exposed animals (Figure 24B). This may also be due to altered lymphocytic recruitment as iBALT is largely composed of organized B and T cells [154,159,201]. One inflammatory mediator, AREG is involved in modulating repair and remodeling in the lung after injury and has previously been evaluated in a repetitive 15-instillation ODE model where mice were allowed to recover for 1, 2, 3, or 4 weeks post-last DE instillation [229]. However, the modulation of AREG

has not been examined in a repetitive ODE model with a shorter, 72-hour recovery period or in an IL-22 knock-out model treated with AT-RvD1 [229]. In our previous study, we observed that AREG concentrations in BALF increased as the recovery timepoints lengthened following cessation of DE exposure [229]. Interestingly, we did not find that AREG was upregulated in WT animals exposed to DE, but we did observe that KO mice exposed to DE and recovered for 72 hours displayed significantly decreased AREG tissue concentrations compared to WT mice exposed to DE. Interestingly, KO mice administered AT-RvD1 also displayed a significant decrease in AREG lung tissue concentrations compared to WT mice exposed to DE and treated with AT-RvD1. This may suggest that IL-22 may play an important role in effective tissue repair and resolution response after DE exposure as other models have found that IL-22 knock-out results in reduced skin wound healing, however the specific mechanisms warrant further investigation [5,140].

We previously explored the use of AT-RvD1 treatment in a chronic 24-week ODE mouse model and observed significantly reduced pathology severity in mice injected with 500 ng AT-RvD1 via intravenous tail injection once weekly for 20 weeks [48]. We found that this dose was effective in reducing lung inflammation and cellular infiltration in this model and aimed to evaluate the efficacy of AT-RvD1 in reducing ODE-induced pulmonary and neurological inflammation in a repetitive 15-instillation exposure model [48]. We evaluated the neurological immune response via microglia counts and mRNA transcript evaluation using RNAscope in several brain regions. We utilized two dosing regimen models to determine which strategy was most effective. We first examined cellular infiltrates and histopathology in animals treated with 250 ng AT-RvD1 once-weekly (Figures 21A,2A-E,3A-D) and found limited efficacy in immune cell influx, and no therapeutic efficacy in lung histopathology (Figures 23A-D). We then

evaluated lung histopathology outcomes in a once-daily AT-RvD1 injection schedule and found that animals treated with 250 ng AT-RvD1 daily displayed significant inflammation resolution in histopathology evaluation (Figures 24A-H), therefore, our 5 day/week injection regimen was employed for further analysis of the pulmonary and neurological inflammatory response to DE. Our histopathological analysis of animals administered daily AT-RvD1 injections revealed that iBALT was the primary parameter improved in AT-RvD1-treated animals. iBALT is considered a pathological phenotype of COPD that is correlated with disease severity and its increased formation has been linked to increased severity of patient clinical signs [24,63,76]. We have previously found that mice exposed to DE, whether repetitively or chronically, develop significant iBALT [48,162,220,229]. In this study, we observed that WT and KO mice exposed to DE revealed increased iBALT formation, with significantly increased iBALT percentage in female mice compared to male mice. This may be due to sex hormones contributing to adaptive immunity to varying degrees, however our study is limited by a lack of estrus cycling and sex hormone quantification data that would be needed to make more informed conclusions on the mechanisms of the observed sex-specific pathology [95]. Sex-dependent metabolic differences could alter the bioavailability of AT-RvD1, for example, female mice have decreased expression of CYP enzymes which may increase the plasma concentration of AT-RvD1 [168]. Furthermore, female animals treated with AT-RvD1 displayed significantly less iBALT formation, indicating its effectiveness in reducing immune cell aggregates in these animals, but more investigation into the mechanism of these sex differences is warranted. This pattern of increased lung pathology severity in females has been documented in human patients with COPD, where female patients tend to experience more severe symptoms and have higher mortality rates (40,41). Together, these data demonstrate that attenuation of IL-22 alters the pulmonary immune response to

agriculture dust and increases the severity of lung pathology and that the efficacy of AT-RvD1 attenuation of lung pathology is IL-22- and sex-dependent. Females have also demonstrated higher toll-like receptor production, present with more $CD4^+$ T cells and B cells compared to males and have a more robust antibody response than males [95]. The increased T and B cell numbers may account for the reduced resolution of iBALT in females, but more investigation of the mechanisms of these sex differences in our dust exposure model is warranted.

mRNA transcript evaluation of whole lung tissue sections revealed significant differences in *cxcl10* expression in WT mice exposed to DE with a significant decrease in WT animals exposed to DE and treated with AT-RvD1. CXCL10 participates in monocyte, neutrophil, and lymphocyte recruitment and significantly contributes to the progression of COPD disease state, which may present as a therapeutic target of AT-RvD1 in dust-induced lung disease [37,72,87]. mRNA transcript evaluation of brains revealed limited significant differences between treatment groups, with significantly reduced *il1b* expression in WT animals exposed to DE and treated with AT-RvD1 compared to KO animals exposed to DE and treated with AT-RvD1. The mechanism of this observation is unclear, but another study found that cultured microglia displayed reduced *il1b* expression after treatment with 17(S)-RvD1 [169]. This is not directly comparable to our model of AT-RvD1 (17(R)-RvD1) treatment but may still be informative as we explore the therapeutic targets of AT-RvD1. A major limitation of this study is our restricted panel of mRNA transcripts in both the lung and brain tissues, with only one pro-inflammatory mediator included per tissue type. This has hindered our investigation of the therapeutic applications of AT-RvD1, and we may simply be missing those mediators that are affected by At-RvD1 treatment. Another limitation is our 72-hour post-last instillation timepoint, where the mice are primarily in the resolution phase and may not be producing high quantities of pro-

inflammatory cytokines. Expansion of our investigation of mRNA transcripts to include a broader range of classic inflammatory mediators may assist our assessment of the contribution of ODE to neuroinflammation and the therapeutic actions of AT-RvD1 in our ODE model.

We aimed to determine whether agriculture dust exposure contributes to neurological inflammation in a repetitive ODE mouse model. Our data support the hypothesis that agriculture dust exposure contributes microgliosis in a mouse model of repetitive ODE. We also aimed to assess the regulation of the pulmonary and neurological inflammatory response to ODE in an IL-22 deficient mouse model and the immune-modulating and therapeutic applications of AT-RvD1. Our data show that ODE leads to pulmonary and neurological inflammation, and that IL-22 attenuation increases the severity of the pulmonary and neurological immune response to ODE. This study confirmed our previous findings and expanded upon our prior knowledge by demonstrating that IL-22 KO mice exhibit increased inflammatory markers in the recovery phase following cessation of DE exposure. We also demonstrate that AT-RvD1 treatment once per week was effective in reducing cellular infiltrates in BALF of KO animals, but did not produce a significant decrease in lung pathology outcomes. We observed that a once daily regimen was more effective in increasing lung anti-inflammatory cytokine protein production, reducing lung pathology severity, reducing lung chemokine transcript expression, and decreasing microglia numbers in mice exposed to DE. These data indicate that AT-RvD1 may require more frequent administration to be effective, however more evidence and exploration is needed. We also demonstrated that AT-RvD1 treatment is more effective in IL-22 KO mice, in terms of reducing lung cellular infiltrates and pro-inflammatory cytokine protein concentrations, but that it is also effective in reducing lung pathology and microglia numbers in both WT and KO animals. We hypothesize that this is due to a dysregulation of the repair processes in KO mice, which is

partially restored by AT-RvD1 treatment, but requires further investigation to determine the specific pathways and mechanisms involved in these observations.

Further investigation aims to identify the mechanisms by which ODE contributes to neurological inflammation through evaluation of various routes of escape from the pulmonary to the neurological systems and the specific cellular mechanisms that lead to neuroinflammation in a model of ODE. These data demonstrate that ODE leads to neurological inflammation and that AT-RvD1 may be an effective treatment for attenuating immune-mediated pulmonary and neurological disease caused by ODE, mitigating its severe health effects.

CHAPTER 4: CHARACTERIZATION OF THE LUNG-BRAIN IMMUNE RESPONSE TO AGRICULTURE DUST IN A SUB-CHRONIC MOUSE MODEL

4.1 Introduction

Agriculture dust exposure in occupational settings has been strongly linked to the development of chronic lower respiratory diseases (CLRD), which was a leading cause of death in the United States (US) with 147,367 deaths in 2023, according to the Centers for Disease Control and Prevention (CDC) [33]. CLRDs include chronic obstructive pulmonary disease (COPD), asthma, and allergies [138,176,198]. CLDRs have also been linked to an increased risk of developing dementia and Alzheimer's disease, with those exposed to agricultural dust at the highest risk [100,105,164,243]. The CDC reported 6.7 million people as diagnosed and living with Alzheimer's disease in the US in 2023, and estimates project that number to increase to 14 million people by 2060 [31,33]. Particulate matter (PM) exposure is the leading cause of the development of CLDRs and has been recently linked to the increased risk of developing dementia, and agricultural PM contains particle sizes from sizes from 2.5 μm to 0.25 μm, microbes, and many other immunogenic compounds such as microbial components, endotoxins, and metals that contribute to the pulmonary immune response [22,155].

A recent study linked agricultural organic dust exposure as the highest risk for developing dementia over all other PM exposures assessed [246]. In surveys, COPD patients have reported increased depressive symptoms, confusion, memory loss, and mental functional decline as their disease progresses . A study of comorbidities of 8,094 patients diagnosed with CLRDs including chronic bronchitis, emphysema, and COPD found that 51.4% of patients with one more CLRD also presented with Alzheimer's disease or dementia ($p < 0.001$), with 27.4% diagnosed with depression ($p=0.012$), 7.7% diagnosed with multiple sclerosis, Parkinson's

disease, or epilepsy (p= 0.020), and 11.7% diagnosed with other mental disorders (p=0.007) [232]. The aggregated data revealed that 64.9% of patients with more CLRD experienced at least one mental or behavioral health disorder, and 11.6% experienced at least one nervous system disorder [232]. Agriculture workers have reported experiencing higher levels of mental disorders including anxiety (males: 22% females: 39%, total: 31%) and depression (males: 35%, females: 42%, total: 39%) [131]. Air pollution exposure has also been linked to neurological inflammation in animal models but agricultural organic dust exposure has not be explicitly assessed [27,105,180].

Our laboratory has extensively studied the pulmonary immune effects of agriculture dust exposure in a mouse model, but there has been limited investigation into the neuroinflammatory effects of agriculture dust exposure. We previously established that three weeks of agriculture dust extract (DE) in a mouse model elicited a neuroinflammatory response characterized by the increase of microglia in the brain [216]. We aimed to establish a link between agriculture dust exposure in mice with behavioral outcomes and neuroinflammatory pathology.

4.2 Methods

4.2.1 Dust Extract Preparation

Dust was collected from hog confinement facilities in the Midwest, United States from surfaces at least 1 meter off the ground to represent the respirable fraction. Dust aliquots were stored at -20 °C until use. Dust extracts were prepared as previously described [137,219]. Briefly, whole dust was combined with Hank's balanced saline solution (HBSS) (HyClone Laboratories) at a ratio of 1 g dust to 10 mL HBSS on a magnetic stir plate for 1 hour at room temperature. The resulting mixture was centrifuged at 2500 rpm for 20 minutes at 4 °C. The supernate was collected, while the pellet was discarded. Supernate was transferred to a new tube and

centrifuged again at 2500 rpm for 20 minutes at 4 °C. Supernate was collected and filtered through 0.22 μm syringe filters to produce 100% dust extract (DE) and stored at -20 °C. The resulting extract contains predominantly gram-positive bacterial components, endotoxins, and trace metals [155]. Complete analysis of dust extract can be found at Online Repository Methods at www.jacionline.org [155].

4.2.2 Animal Husbandry and Care

All animal protocols were reviewed and approved by the CSU Institutional Animal Care and Use Committee (Protocol Number 2887). C57BL/6J mice were purchased from Jackson Laboratories at 8 weeks of age and housed in the Colorado State University Painter Facility in a specific pathogen-free environment with free access to standard mouse feed and water. Animals were acclimated for at least 7 days before performing any procedures.

4.2.3 *In Vivo* 8-Week Repetitive DE Exposure Model

Mice were intranasally (i.n.) or oropharyngeally (o.p.) instilled with 50 μl 12.5% DE or sterile saline 5 days/week for 8 weeks under light isoflurane sedation. The concentration of DE was previously determined by a dose-response study, which was found to elicit a strong pulmonary inflammatory response without the risk of mortality [174]. Sedation for instillations was achieved using a SomnoSuite Small Animal Anesthesia System (Kent Scientific Corporation) fitted with a small animal anesthesia box. Animals were placed into the box with a flow rate of 100 mL/minute at 2.0-3.0% anesthesia. Animals were removed for instillations once breathing appeared slowed and even. Animals were held in a supine position and 50 μl of the appropriate exposure was loaded into a pipette tip and deposited at the tip of the animal's nose one drop at a

time to allow natural inhalation. Afterwards, animals were returned to their enclosures in a supine position to encourage recovery and monitored for several minutes to ensure return of normal behaviors. Animals were allowed to recover for 72 hours past-last DE instillation before sacrifice (Figure 29).

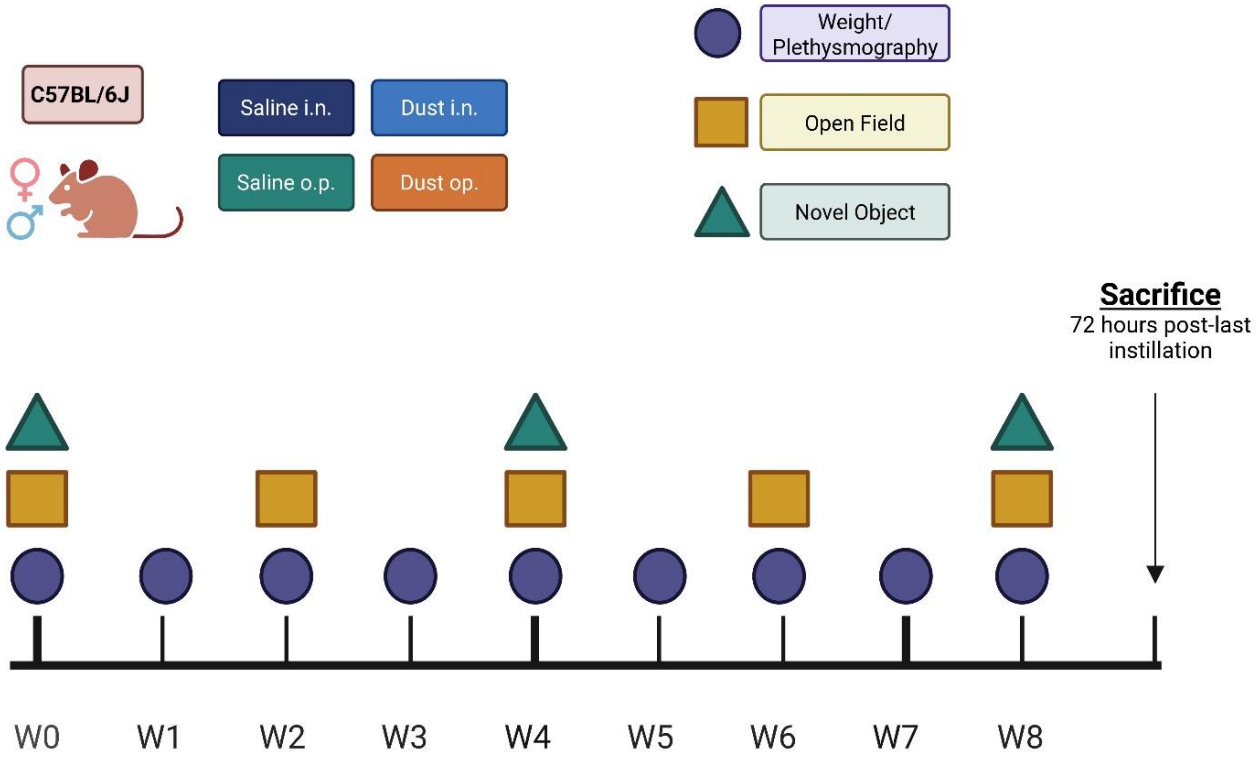


Figure 29. 8-Week Repetitive DE Exposure Model Timeline.
Sample sizes: Saline i.n. (15 Female/15 Male); Dust i.n. (15 Female/15 Male); Saline o.p. (15 Female/15 Male); Dust o.p. (15 Female/15 Male).

4.2.2 Behavioral Assays

Open field (OF) and novel object recognition (NOR) behavioral assays were performed on all animals. OF testing was performed every two weeks following the first saline or dust instillation and NOR testing was performed every 4 weeks following the first saline or dust instillation. Testing for both tests occurred in the same room under the same lighting conditions between 9am and 5pm. Since animals were transferred to an alternate testing room, animals were

transferred to the room and acclimated one hour prior to the start of testing. The order each animal was tested was randomized each time and the order was tracked to limit variability.

4.2.3 Open Field Test

For OF testing, each animal was habituated to a circular container approximately 25 cm in diameter for 5 minutes 24 hours prior to the test, then placed in the same container on the day of the test for 5 minutes and video was recorded of the animals using a 4K digital camera. The videos were analyzed using ANYMaze Software version 7. Time spent immobile was used to determine animal anxiety [100].

4.2.4 Novel Object Recognition Test

Novel object recognition testing was performed in three phases each separated by 24 hours. Phase one consisted of habituating the animals to a circular container approximately 25 cm in diameter for 5 minutes. The second phase habituated the animals to the container for 5 minutes before the addition of two identical objects which the animals were left to explore for 10 minutes. The third phase was the testing phase, each animal was habituated to the contained for 5 minutes before being presented with one of the objects from the previous day (familiar object) and one novel object they had not seen before (novel object) and were recorded for 10 minutes while they explored both objects. The videos were analyzed by laboratory personnel by manually tracking the amount of time each animal spent directly interacting with each object such as sniffing, climbing, or biting. The times were recorded, and the discrimination index was

calculated by subtracting from the time spent with the novel object from the time spent with the familiar object, divided by the time spent with both objects

4.2.5 Animal Sacrifice and Sample Collection

Animals were euthanized in accordance with the American Veterinary Medical Association guidelines by isoflurane overdose immediately followed by cervical dislocation, 72 hours following the final DE instillation and AT-RvD1 injection. The right lung lobes were extracted along with the heart and tracheal tissue, then inflated with 10% neutral-buffered formalin (NBF) (Cancer Diagnostics Inc.) before hanging under 20 cm of pressure and submerged in 10% NBF overnight. They were then transferred to cassettes and stored in 10% NBF for at least 48 hours before further processing. Brains were extracted *en bloc* and immediately fixed whole in tissue cassettes in 10% NBF for at least 48 hours before further processing. All tissues were submitted to the Colorado State University Veterinary Diagnostic Laboratory Experimental Pathology Facility (EPF) for paraffin embedding and sectioning at 5 µm.

4.2.4 Lung Histopathology

Whole right lung coronal sections, collected as previously described above, were stained with hematoxylin and eosin (H&E) following deparaffinization and rehydration with xylene and graded EtOH solutions (xylene, 100% EtOH, 95% EtOH, 80% EtOH, 50% EtOH, and finally 1X PBS). Slides were scanned at 40X on a Vectra Polaris scanning microscope. Images of lungs from animals administered weekly AT-RvD1 injections were blinded and manually scored using a well-established semiquantitative scoring method [48,137,220,221,229]. Images from animals

administered daily AT-RvD1 injections were imported into VisioPharm version 2023.09.3.15043 x64 and processed through an artificial intelligence (AI) workflow for quantitative assessment of alveolar space, alveolar septa thickness, peribronchiolar inflammation, perivascular inflammation, total alveolar septa nuclei, and percentage of inducible bronchus-associated lymphoid tissue (iBALT) formations relative to tissue area. AI quantification was performed on the whole lung tissue with output measurements including area, percentages of parameters to total tissue area or total parameter counts. VisioPharm is one of the leading AI histopathology analysis software available. Our workflow and applications were designed, annotated, trained, and verified by a board-certified veterinary anatomic pathologist to identify our desired readouts and ensure accurate results. The workflow is then trained through a large set of sample images by a board-certified veterinary anatomic pathologist where structures are identified by the software and confirmed by the pathologist, allowing the software to "learn" how structures are organized and are identified in the experimental images. Briefly, the workflow consisted of multiple stepwise applications of increasing specificity, starting with identification of the lung tissue, followed by identification of airways and vessels, then inflammation and iBALT, and finally identification of airways epithelial cells and alveolar nuclei. During each step of the workflow, the results are confirmed manually to ensure accurate detection of structures. All parameters are normalized to tissue area to mitigate size and artifact skewing.

4.2.5 Immunofluorescence

Whole brain sagittal paraffin-embedded tissue sections, as previously described above, were deparaffinized by baking slides at 60 °C for 20 minutes, followed by rehydration through an EtOH gradient (xylene, 50% xylene/50% EtOH, 100% EtOH, 95% EtOH, 70% EtOH), and

then incubated in 1.0 M Tris buffered saline (TBS). Antigen retrieval was achieved using 1 nM EDTA buffer with 0.05% Tween20, pH 8.0 at 95 °C for 20 minutes in a Biocare Medical Decloaking Chamber™ NxGen (Biocare Medical). Tissues were washed three times for 10 minutes each with 0.05M TBS and blocked using 2% donkey serum in 0.2% Triton-X in 1.0 M TBS for 1 hour at room temperature. Microglia were identified using rabbit anti-ionized calcium binding adaptor molecule 1 (Iba1) (1:1000; Abcam, Cat #: ab178846) diluted in 1.0 M TBS and incubated overnight at 4 °C. Astrocytes were identified utilizing a chicken anti-mouse -glial fibrillary acidic protein (GFAP) (1:1000 Aves Labs, Cat #: GFAP), a rabbit anti-mouse -S100 calcium-binding protein β (S100β) (1:200, Abcam ab52642), and a rat anti-mouse C3 (1:200, Abcam ab11862) antibody diluted in 1.0 M TBS and incubated overnight at 4 °C. Tissues were then washed four times for 10 minutes each with 0.05 M TBS. A goat anti-rabbit Alexa Fluor 647 secondary antibody (Invitrogen, Cat#: A21244) diluted 1:500 in 2% donkey serum in 1.0 M TBS, was applied and incubated for 1 hour at room temperature for microglia. For astrocytes, a goat anti-chicken Alexa Fluor 488 (Invitrogen, Cat #: A-11039), donkey anti-rabbit Alexa Fluor 555 (Invitrogen, Cat #: A-31572), and goat anti-rat Alexa Fluor 647 (Invitrogen, Cat #: A-21247) were diluted 1:500 in 2% donkey serum in 1.0 M TBS, applied and incubated for 1 hour at room temperature. Sections were washed three times for 10 minutes each with 0.05 M TBS. Nuclear staining was achieved by incubation with Hoechst 33342, diluted 1:2000 in PBS (Invitrogen, Cat #: H3570), for three minutes, then washed three times for 10 minutes each with 0.05 M M TBS. ProLong Diamond Antifade Mountant (Fisher Scientific, Cat #: P36970) was then applied before mounting with glass coverslips. Slides were kept at room temperature, protected from light, for 24 – 48 hours to cure mounting medium, then stored at 4 °C in the dark prior to imaging. Stained sections were scanned at 40X using a Vectra Polaris microscope, and the number of microglia

per area of each brain region of interest were quantified using QuPath Version 0.5.1. All sections were imaged on the same day with the same exposure settings for each channel.

4.2.6 Statistical Analysis

All statistical and graphical analyses were performed using GraphPad Prism Version 10. Outliers were tested for and removed from the datasets using ROUT analysis with Q=1%. Statistical significance was determined by performing 3-way ANOVA analyses with Benjamini, Krieger and Yekutieli post-hoc analysis for pairwise comparisons to reduce false discovery rate. A p-value of less than or equal to 0.05 was used to determine significance and a p-value of less than or equal to 0.1 was considered a trend. Individual animals are represented by a single symbol on figures, with filled shapes representing male animals and unfilled shapes representing female animals. On figures, significance is denoted by, * = $p \leq 0.05$; ** = $p \leq 0.01$; *** = $p \leq 0.001$; **** = $p \leq 0.0001$.

4.3 Results

4.3.1 Dust exposure does not alter novel object recognition behavioral outcomes

Our behavioral testing revealed no significant differences between animals exposed to dust compared to animals exposed to saline, regardless of the route of administration (i.n. vs.

o.p.), however we did find several significant differences between female and male animals in our open field testing (Figure 30).

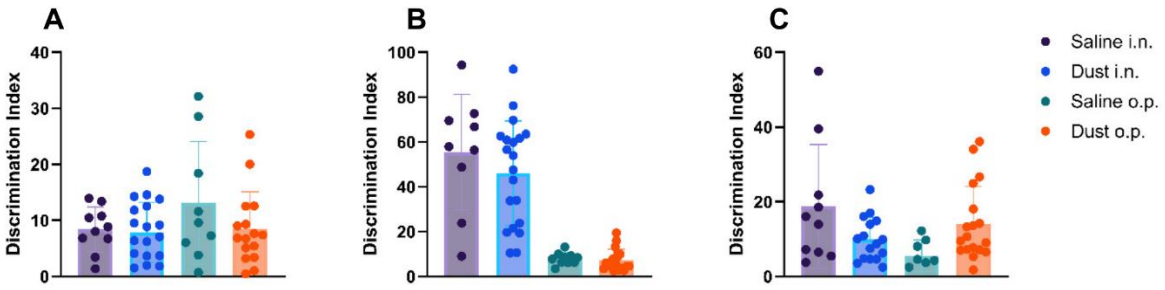


Figure 30. Dust exposure does not alter novel object recognition testing
(A) Baseline; (B) 4 weeks post-exposure; (C) 8 weeks post-exposure. Non-parametric one-way ANOVA with Benjamini, Krieger and Yekutieli post-hoc analysis, error bars = SEM, Sample sizes: Saline i.n. (15 Female/15 Male); Dust i.n. (15 Female/15 Male); Saline o.p. (15 Female/15 Male); Dust o.p. (15 Female/15 Male).

Open field testing revealed several sex differences in average speed, time spent mobile, and time spent immobile. At baseline, males exposed to saline i.n. were observed to have a trend of reduced speed compared to females exposed saline i.n. and males exposed to dust i.n. ($p=0.0116$) were shown to have reduced speed compared to females exposed to dust i.n. ($p=0.0030$). Dust o.p. females were also shown to have increased speed compared to dust o.p. males at 2 weeks ($p=0.0179$) and 4 weeks post-exposure ($p=0.0058$), and observed a trend between these data sets at 6 weeks post-exposure ($p=0.0928$). At 8 weeks post-exposure we again observed males exposed to saline i.n. exhibited reduced speed compared to females

exposed saline i.n. (p=0.0762) and males exposed to dust i.n. were shown to have reduced speed compared to females exposed to dust i.n. (p=0.0046) (Figure 31).

4.3.2 Dust exposure alters open field behavioral outcomes in in a sex-specific manner

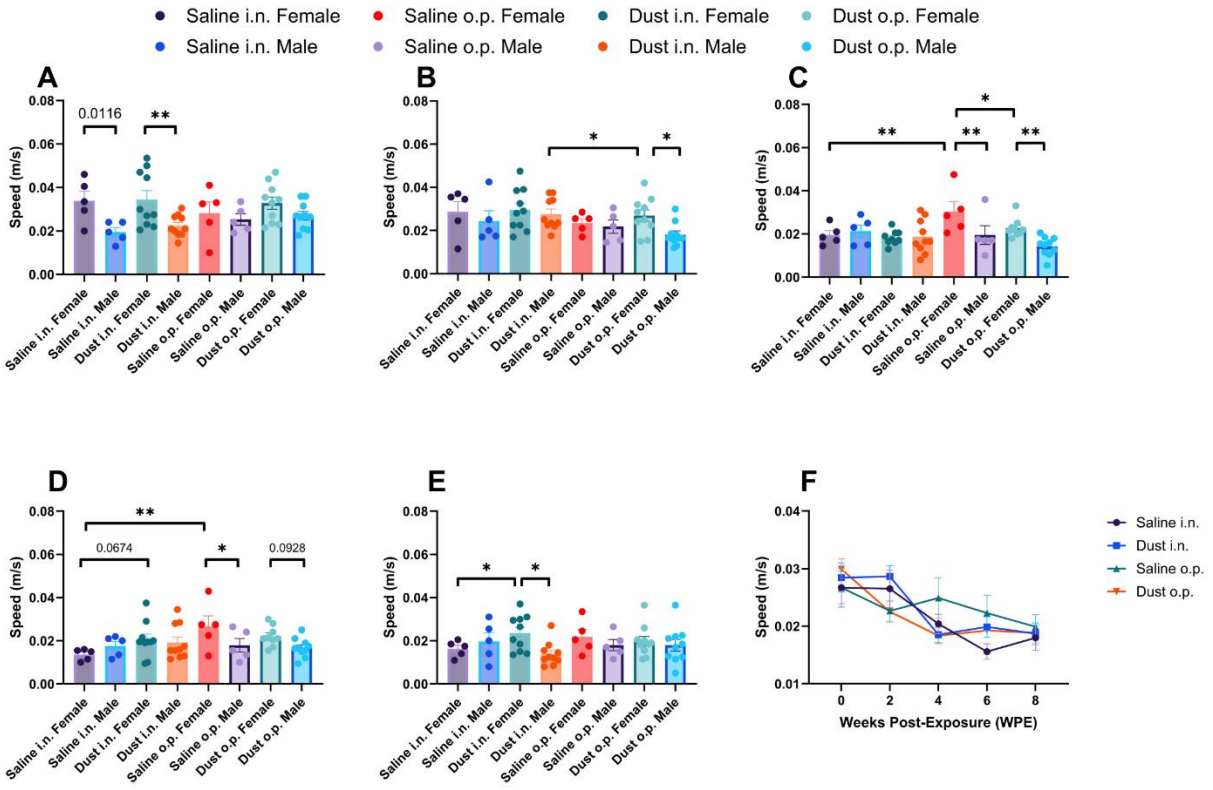


Figure 31. Animals exposed to DE have mild changes in average speed during open field testing.
(A) Baseline, prior to exposure; (B) 2 weeks post-exposure; (C) 4 weeks post-exposure; (D) 6 weeks post-exposure; (E) 8 weeks post-exposure; (F) average speed over time. Non-parametric one-way ANOVA with Benjamini, Krieger and Yekutieli post-hoc analysis, error bars = SEM; * = $p \leq 0.05$; ** = $p \leq 0.01$; *** = $p \leq 0.001$; **** = $p \leq 0.0001$. Sample sizes: Saline i.n. (15 Female/15 Male); Dust i.n. (15 Female/15 Male); Saline o.p. (15 Female/15 Male); Dust o.p. (15 Female/15 Male).

Time spent mobile also displayed similar sex differences, with a trend of reduced speed in males exposed to saline i.n. compared to females exposed to saline i.n. (p=0.0634) and

reduced time spent mobile in males exposed to dust i.n. compared to females exposed to dust i.n. (p=0.0107) at baseline. At 2 weeks post-exposure we observed increased time spent mobile in males exposed to dust i.n. compared to males exposed to saline i.n. (p=0.0139). At 4 weeks post-exposure, we also observed that males exposed to dust i.n. had increased time spent mobile compared to males exposed to saline i.n. (p=0.0252) (Figure 32).

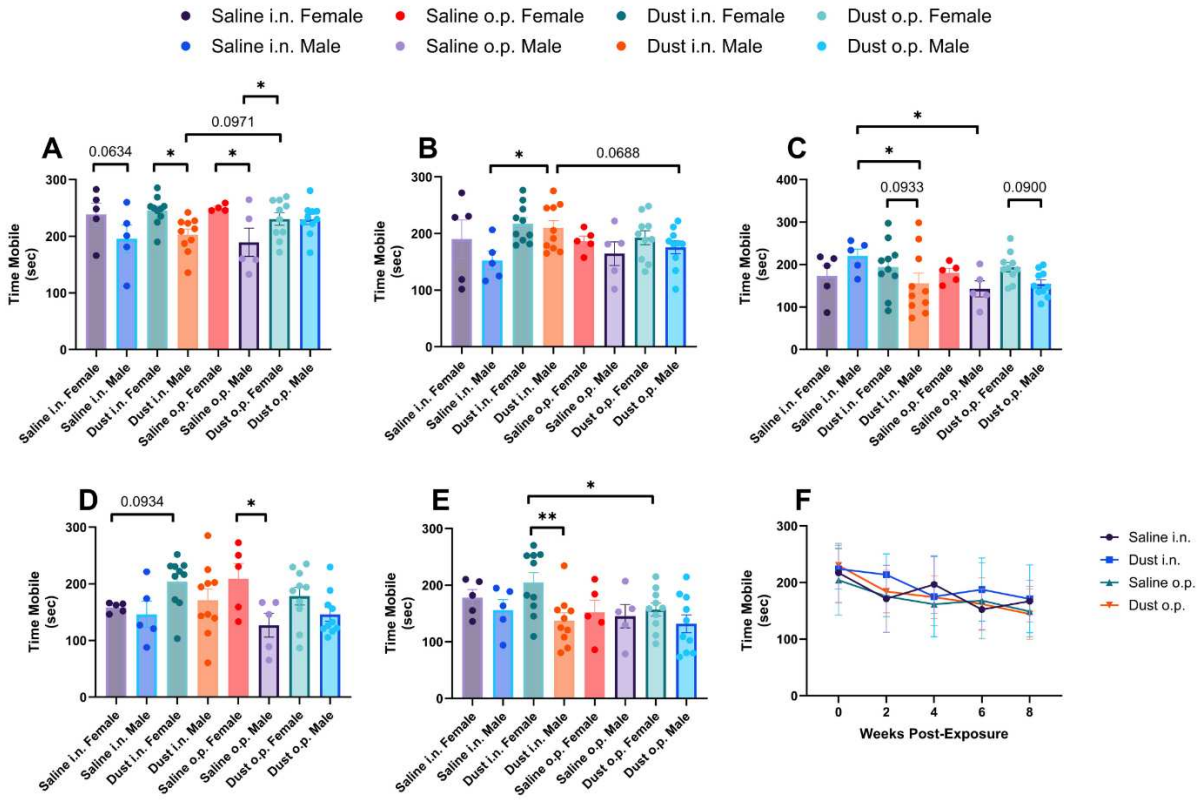


Figure 32. Animals exposed to DE have limited changes in time spent mobile during open field testing.
(A) Baseline, prior to exposure; (B) 2 weeks post-exposure; (C) 4 weeks post-exposure; (D) 6 weeks post-exposure; (E) 8 weeks post-exposure; (F) average speed over time. Non-parametric one-way ANOVA with Benjamini, Krieger and Yekutieli post-hoc analysis, error bars = SEM; * = $p \leq 0.05$; ** = $p \leq 0.01$; *** = $p \leq 0.001$; **** = $p \leq 0.0001$. Sample sizes: Saline i.n. (15 Female/15 Male); Dust i.n. (15 Female/15 Male); Saline o.p. (15 Female/15 Male); Dust o.p. (15 Female/15 Male).

Testing for time spent immobile also revealed similar sex differences as the parameters for average speed and time spent mobile. At baseline, we observed that males exposed to saline

i.n. or dust i.n. displayed increased time spent immobile compared to females exposed to saline i.n. or dust i.n., respectively (p=0.0030), (p=0.0041). At 2 weeks post-exposure, we observed that males exposed to dust i.n. displayed decreased time immobile compared to males exposed to saline i.n. (p=0.0178). This observation was again seen at 4 weeks post-exposure (p=0.0140) (Figure 33).

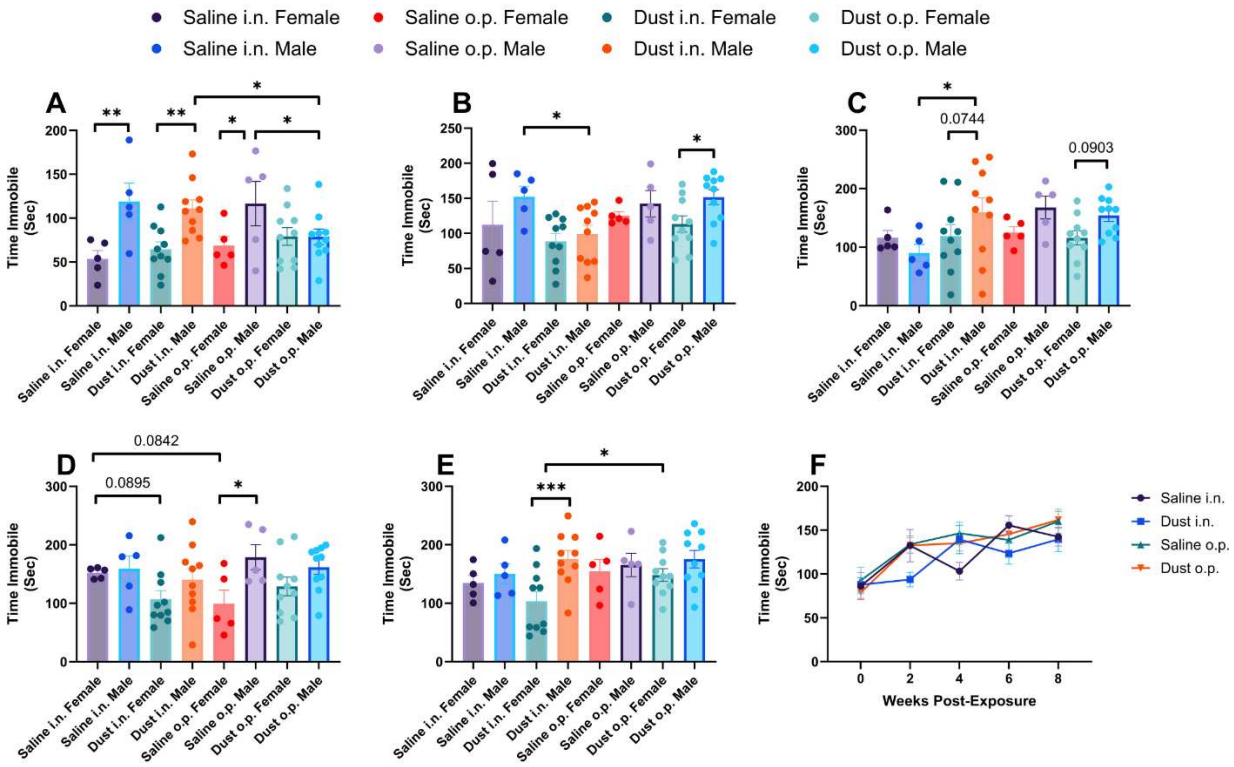


Figure 33. Animals exposed to DE exhibit limited changes in time spent immobile during open field testing.
(A) Baseline, prior to exposure; (B) 2 weeks post-exposure; (C) 4 weeks post-exposure; (D) 6 weeks post-exposure; (E) 8 weeks post-exposure; (F) average speed over time. Non-parametric one-way ANOVA with Benjamini, Krieger and Yekutieli post-hoc analysis, error bars = SEM; * = $p \leq 0.05$; ** = $p \leq 0.01$; *** = $p \leq 0.001$; **** = $p \leq 0.0001$. Sample sizes: Saline i.n. (15

Female/15 Male); Dust i.n. (15 Female/15 Male); Saline o.p. (15 Female/15 Male); Dust o.p. (15 Female/15 Male).

4.3.3 Sub-chronic dust exposure leads to limited lung pathology

Following 8 weeks of dust exposure, we observed an increase in inducible bronchus-associated lymphoid tissue (iBALT) in animals exposed to dust o.p. compared to animals exposed to saline o.p. ($p=0.0116$) and animals exposed to saline i.n. ($p=0.0154$). We also observed an increased in peribronchiolar/perivascular inflammation in animals exposed to dust i.n. only ($p=0.0230$). We observed a small trend of decreased alveolar space ($p=0.0635$) and alveolar septa ($p=0.0271$) in animals exposed to dust o.p. compared to animals exposed to dust i.n.. We also discovered that total alveolar nuclei counts were elevated in animals exposed to dust o.p. compared to animals exposed to saline o.p. ($p=0.0495$) but not between animals exposed to saline or dust i.n.. We also observed an increase in the bronchiolar epithelial cells to total bronchiolar epithelial area in animals exposed to dust o.p. compared to animals exposed to dust i.n. ($p=0.0014$). Analysis of fibrosis revealed a nonsignificant increasing trend in alveolar fibrosis in animals exposed to dust o.p. compared animals exposed to saline o.p. ($p=0.0949$), and

reduced airway fibrosis in animals exposed to dust o.p. compared to animals exposed to saline o.p. (p=0.0439), dust i.n. (p=0.0031), and saline i.n. (p=0.0168) (Figure 34).

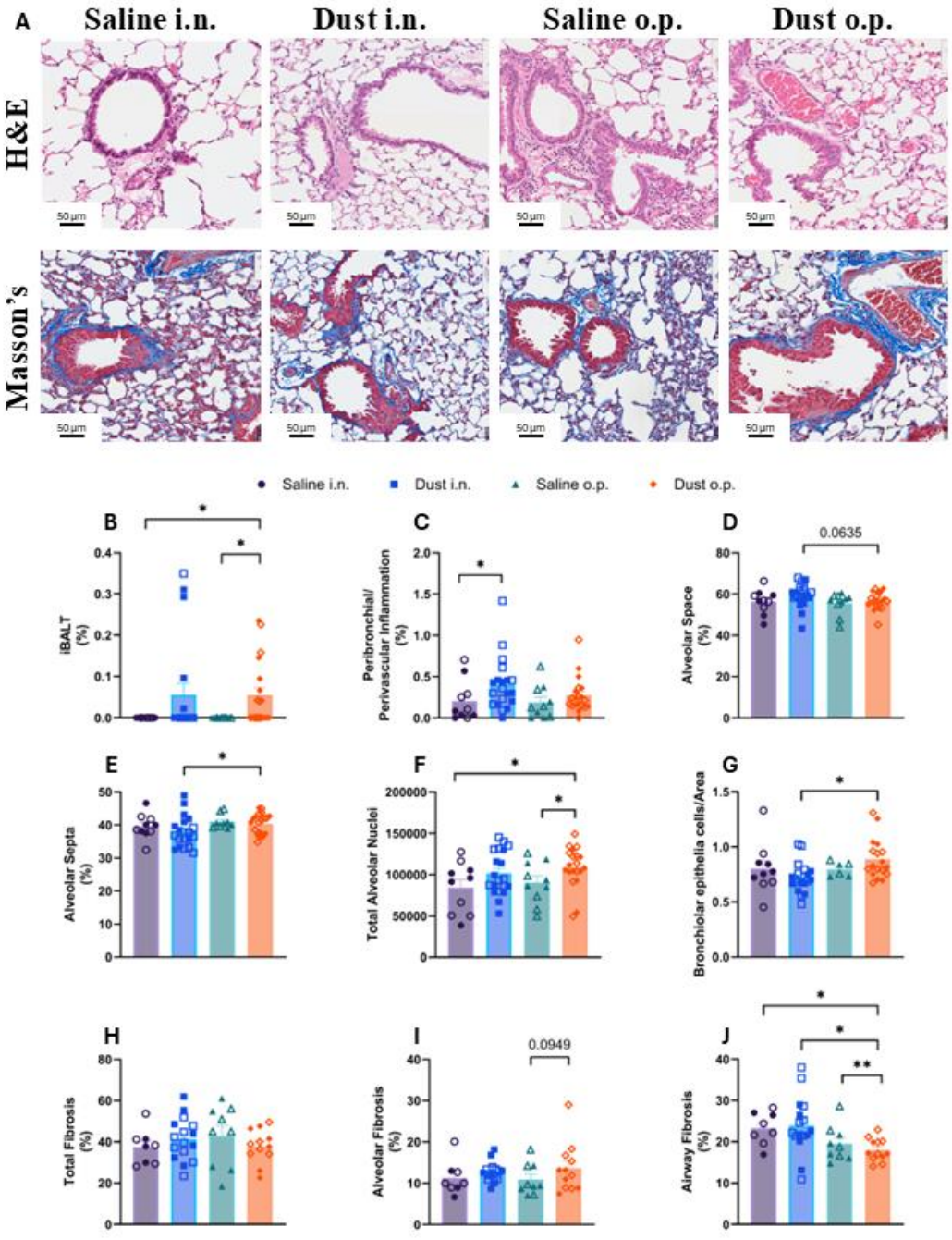


Figure 34. Sub-chronic dust exposure is associated with limited lung pathology. (A) Representative images of H&E and Masson's staining at 40X magnification; (B) iBALT percentage; (C) combined peribronchiolar and perivascular inflammation percentage; (D) alveolar space percentage; (E) alveolar septa percentage; (F) total alveolar nuclei; (G)

bronchiolar epithelium area; (H) total fibrosis percentage in whole lung; (I) fibrosis percentage in alveolar area; (J) fibrosis percentage in airways. Scale bar = 50 μm. 3 way ANOVA with Benjamini, Krieger and Yekutieli post-hoc analysis, error bars = SEM; * = $p \leq 0.05$; ** = $p \leq 0.01$; *** = $p \leq 0.001$; **** = $p \leq 0.0001$. Sample sizes: Saline i.n. (15 Female/15 Male); Dust i.n. (15 Female/15 Male); Saline o.p. (15 Female/15 Male); Dust o.p. (15 Female/15 Male).

4.3.4 Sub-chronic dust exposure is associated with gliosis in animals exposed to DE i.n.

Following 8 weeks of DE exposure, we observed increased microglia counts in the olfactory bulb, frontal cortex, and isocortex, as well as increased astrocyte counts in these regions in mice given DE i.n. only. Microglia counts followed a similar trend of increased counts in animals exposed to DE i.n. compared to animals exposed to saline i.n. in the olfactory bulb ($p=0.0109$), frontal cortex ($p=0.0082$), and isocortex ($p=0.0025$), but not in the hippocampus. We only saw increased astrocyte counts in animals exposed to DE i.n. compared to animals exposed to saline i.n. in the isocortex ($p=0.0367$) and hippocampus ($p=0.0294$). Overall, we did not see any increased cellular counts in animals exposed to DE o.p. compared to animals exposed to saline o.p. in any of the selected brain regions (Figure 35).

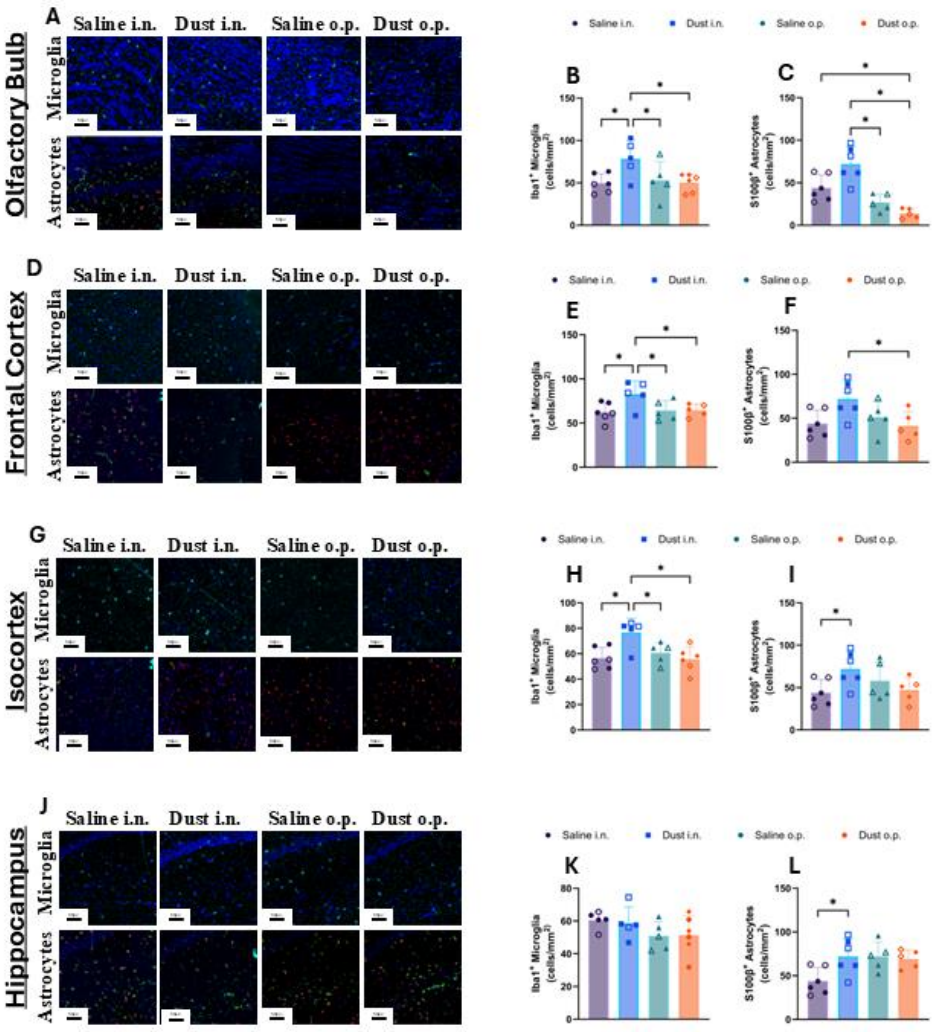


Figure 35. Sub-chronic dust exposure is associated with gliosis.
(A) Representative images of olfactory bulb at 40X magnification; (B) microglia counts in olfactory bulb; (C) astrocyte counts in olfactory bulb; (D) Representative images of frontal cortex at 40X magnification; (E) microglia counts in frontal cortex; (F) astrocyte counts in frontal cortex; (G) Representative images of isocortex at 40X magnification; (H) microglia counts in isocortex; (I) astrocyte counts in isocortex; (J) Representative images of hippocampus at 40X magnification; (K) microglia counts in hippocampus; (L) astrocyte counts in hippocampus. Scale bar = 50 µm. 3 way ANOVA with Benjamini, Krieger and Yekutieli post-hoc analysis, error bars = SEM; * = $p \leq 0.05$; ** = $p \leq 0.01$; *** = $p \leq 0.001$; **** = $p \leq 0.0001$.

Sample sizes: Saline i.n. (3 Female/3 Male); Dust i.n. (3 Female/3 Male); Saline o.p. (3 Female/3 Male); Dust o.p. (3 Female/3 Male).

4.4 Discussion

The pulmonary inflammatory response to ODE has been well characterized, however the neuroinflammatory response of this toxicant has not been well investigated [136,160,174]. We previously established that 3 weeks of DE exposure in mice elicited an increase in microglia counts, which is classically associated with neuroinflammation [216]. Other models of inflammatory lung disease such as infection with *Mycobacterium tuberculosis* was associated with gliosis including increase microglia and astrocyte counts, neuroinflammation, and misfolded proteins, all associated with the development of neurodegenerative disease [100]. Agriculture dust exposure in workers is associated with increased incidence of chronic obstructive pulmonary disease (COPD) which has also been epidemiologically linked to increased incidence of dementia which symptoms include memory loss, depression, anxiety, and reduced quality of life [109,136,211,246].

We assessed an increased exposure period from our previous work as well as additional behavioral testing to determine if the increased exposure elicited significant changes in behavioral outcomes in mice. Additionally, we tested two separate routes of exposure, our traditional intranasal (i.n.) exposure route we have used for this model previously, and a oropharyngeal route (o.p.) as there is evidence in other models that nasal exposure to organic dusts leads to more severe pathology in the frontal brain regions due to tracking of the dust along

the olfactory nerve. We also assessed pulmonary and neurological pathological outcomes to determine how this exposure length affected pulmonary and neurological tissues.

We chose to employ the novel object recognition test to determine if the mice exposed to DE either i.n. or o.p. would have impaired memory, as this has been epidemiologically linked in patients with COPD and with patients working or living near agricultural operations. We found no significant differences in the discrimination index of animals exposed to DE in either route of administration (Figures 30A-C), which may lead us to conclude that the 8-week exposure timeline may still not be long enough to contribute to enough neuroinflammation to elicit changes in memory. Our open field data also did not reveal many changes in the average speed, time spent mobile, and time spent immobile in animals exposed to DE, except for a few timepoints and only in the male animals (Figures 31A-F, Figures 32A-F, Figures 33A-F). A reduction in time spent mobile is an indicator of increased animal anxiety. We also found the reverse to be true in these groups: males exposed to DE i.n. had decreased time spent immobile compared to males exposed to saline i.n., an indicator of anxiety.

The pulmonary pathological response to DE is well established and is typically associated with increased iBALT and peribronchiolar and perivascular inflammation [136,160,174]. In our previous 3-week exposure model we saw increases in both parameters in mice expose to DE [216]. However, in our 8-week exposure model we found that only the mice administered DE o.p. compared to those administered saline o.p. had increased iBALT percentage that reached significance (Figure 34A). We also saw an increase in perivascular inflammation in mice exposed to DE i.n. compared to mice exposed to saline i.n., but not in mice exposed to DE o.p

(Figure 34B). One possibility for these data are that the mice exposed for 8 weeks experience desensitization and acclimation to the exposure.

Even though we observed reduced lung pathology, we again saw gliosis in animals exposed to DE. In animals exposed the i.n. route but not the o.p. route, we observed increased microglia in the rostral regions of the brain including the olfactory bulb, frontal cortex, and isocortex (Figure 35 A-I). We attribute this pattern to dust being transported across the olfactory nerve into the olfactory bulb and other frontal structures as has been previously investigated in a model of ultrafine particle inhalation [142].

In this model we established that prolonged exposure to DE in a mouse model elicits a neuroinflammatory response but does not alter behavioral outcomes. More investigation is warranted to determine if a longer exposure period would elicit changes in memory and to further characterize the neuroinflammatory response to organic dust.

CHAPTER 5: DISCUSSION AND FUTURE DIRECTIONS

5.1 Discussion

These studies aimed to explore the pharmacological applications of AT-RvD1 in the context of agricultural dust-induced chronic inflammation in both *in vitro* alveolar macrophage and microglia culture models and *in vivo* repetitive dust exposure murine models.

It was predicted that treatment with AT-RvD1 in alveolar macrophages *in vitro*, would reduce the inflammatory response by decreasing production of pro-inflammatory cytokines IL-6 and TNF-α and increasing production of anti-inflammatory, pro-resolution cytokines IL-10 and IL-22. In investigating how AT-RvD1 alters the inflammatory response to organic dust exposure the data demonstrated a modest effect of AT-RvD1 in reducing IL-6 and TNF-α production and increasing IL-22 production. Alveolar macrophages exposed to DE with or without AT-RvD1 had a robust inflammatory response by producing high levels of IL-6 and TNF-α. This is consistent with previous data that show organic dust initiates an inflammatory response in resident immune cell populations[62,179]. In cells exposed to DE without AT-RvD1, secreted IL-10 and IL-22 concentrations were significantly higher than their medium-only controls. This was not hypothesized but would be consistent with alveolar macrophages being basally polarized to an anti-inflammatory state to assist in protecting the tissues from immune-mediated injury[55]. Cells exposed to DE and treated with AT-RvD1 displayed decreased IL-6 and TNF-α production 6 hours post co-exposure compared to their DE-only control. IL-10 concentrations were significantly elevated in DE-exposed cells treated with 100 nM AT-RvD1 compared to their DE only controls, indicating higher doses of AT-RvD1 influence increased production of this anti-inflammatory/pro-resolution cytokine. IL-22 concentrations in cells exposed to DE and treated

with AT-RvD1 were significantly increased at 1 and 2 hours, with the peak occurring at 2 hours post co-exposure, compared to their DE-only controls. The temporal relationships between the peak of IL-22 production at 2 hours and the peak of IL-6 and TNF-α production at 6 hours may indicate IL-22 influences the inflammatory response to protect the tissues, and these parameters provide supporting evidence for this hypothesis. IL-22 secreted concentrations then stayed low in the subsequent timepoints investigated. Combined with previous data demonstrating IL-22 is Golgi-localized in macrophages following DE exposure, the data indicate it may participate in intracellular signaling or may be receptor bound by the macrophages for downstream signaling[220]. There appears to be variable outcomes between the 10 nM and 100 nM AT-RvD1 doses, suggesting there may be an optimal dose between 10 nM and 100 nM to alter pro-inflammatory cytokine concentrations, improve clearance of organic dust, and enhance the repair process. *In vitro* evidence suggests AT-RvD1 has a modest effect on the production of pro-inflammatory cytokines in response to organic dust. Contrary to accepted evidence, alveolar macrophages were determined as a source of IL-22 production[51].

In our *in vitro* cultured microglia models, we predicted that agriculture dust would produce a strong inflammatory response via increased TNF-α production and that AT-RvD1 treatment in cultured microglia would reduce TNF-α production as seen previously in our macrophage cultures. Our data revealed that exposure to DE elicited a strong immune response in the form of TNF- α production which was reduced with 10 nM of AT-RvD1 with the onset of DE exposure. These data demonstrated that there is a cellular response to DE and AT-RvD1 in microglia which may have contributed to the reduction of their numbers in our *in vivo* mouse

models of repetitive dust exposure. This established that agriculture dust exposure has an inflammatory effect on microglia, which had not yet been investigated.

We hypothesized that *in vivo* exposure to agriculture dust would produce pulmonary inflammation in the form of increased alveolar cellular infiltration, pro-inflammatory cytokine production in BALF and lung tissue, formation of iBALT, and increased peribronchiolar/perivascular inflammation, as previously seen in this model [48,174,216]. Evaluation of our DE exposure and AT-RvD1 treatment model, we observed strong genotype differences in most of the parameters investigated. We observed increased cellular infiltration, increased BALF and lung tissue cytokines, and increased pulmonary and neurological inflammatory markers in our KO animals compared to their WT controls. This is consistent with our previous work investigating IL-22 KO in DE exposure, as well as other literature describing increased disease severity in IL-22 KO models. In our KO animals, we observed increased IL-10 production in animals exposed to DE and treated with saline and KO animals exposed to DE treated with At-RvD1 compared to their WT controls, respectively. This trend may be due to compensation by IL-10 for the lack of IL-22, but further investigation is needed to evaluate this hypothesis. As seen in the *in vitro* model, IL-10 is upregulated in response to agriculture dust. It is likely to be produced early to assist in the transition to resolution and repair. AT-RvD1 is known to increase immune activity and clearance by macrophages and neutrophils, accelerating the inflammatory response and allowing the transition to resolution sooner, which may account for the increased IL-10 concentrations as well[43].

Total immune cell infiltrate counts in BALF from animals exposed to DE were increased compared to their saline controls, but AT-RvD1 treatment did not have a significant impact on immune cell infiltration. Previous data would suggest AT-RvD1-treated animals should have

decreased immune cell infiltration, which would contribute to the reduction of the total cell infiltrate counts[206]. Neutrophil counts in animals exposed to DE and treated with AT-RvD1 were not significant compared to animals exposed to DE and treated with saline, contrary to previous evidence[43,48]. This is most likely due to the neutrophilic response being activated early and dissipating during the 3-day recovery [160,166,174,175]. Lymphocyte counts in BALF demonstrated no statistical significance in WT animals, but in KO animals, counts were significantly decreased in animals exposed to DE and treated with AT-RvD1 compared to animals exposed to DE and treated with saline with a recovery of 3 days. This is consistent with lymphocytes primarily being recruited later in the inflammatory response and would be expected to be increased in later timepoints[134]. They are also known to secrete IL-22 and be polarized to a Th17 state in response to organic dust so understandably would be highly involved in the repair process[19,51]. Treatment with AT-RvD1 is known to influence immune cell recruitment, and its role in lymphocyte recruitment would reduce the chronic inflammation typically seen in organic dust induced pathology[48,220]. Our lack of statistically significant findings in our pilot study may be due to the low sample size, and more animals are needed to reach statistical significance.

In our larger study exploring DE exposure with AT-RvD1 treatment, we observed increased pulmonary pathological markers including iBALT formation and peribronchiolar/perivascular inflammation as previously seen in this model [136,160,174]. We also observed increased microglia counts in animals exposed to DE, a novel parameter for this agriculture dust exposed model [136,160,174,216]. Increased microglia counts have also been observed in other models of pulmonary and peripheral inflammation [100]. We concluded from these data that agriculture dust exposure produced neurological inflammation, an important step to understanding how this toxicant produces the clinical signs observed in other studies [109,232,246].

We also observed increased pulmonary and neurological pathology in KO animals compared to WT controls, which is consistent with previous literature, further contributing to the hypothesis that IL-22 is an important player in the immune response to agriculture dust [19,46,207,216,220]. In our DE-exposed and AT-RvD1 treated mice, we found that iBALT was significantly reduced compared to their dust-exposed saline-treated controls, confirming our hypothesis that AT-RvD1 reduced pulmonary inflammation in response to agriculture dust exposure. We also observed a significant decrease in microglia counts in DE-exposed, AT-RvD1 treated animals compared to their DE-exposed, saline-treated controls. This is a key finding that indicates that AT-RvD1 may be an effective therapeutic for the neuroinflammation associated with agriculture dust exposure. More investigation is needed to understand the mechanisms by which IL-22 regulates inflammatory disease, but this study is an important step to establish the connections between agriculture dust exposure, IL-22, and neurological inflammation.

Following our establishment of the connection between agriculture dust exposure and neurological inflammation, we aimed to understand the effects of prolonged dust exposure on behavioral outcomes, lung pathology, and neurological inflammation. We employed a longer 8-week, sub-chronic agriculture dust exposure mouse model coupled with intermittent behavioral testing and end-point evaluation of pulmonary and neurological inflammation. We hypothesized that a longer exposure period would produce significant behavioral changes in the form of reduced memory and increased anxiety via novel object recognition and open field testing, as previously seen in other pulmonary inflammatory models [100]. We observed limited behavioral changes in this model and hypothesized that 8 weeks of dust exposure may not be long enough to induce the required neurological damage to elicit behavioral changes. Interestingly, we also observed limited pulmonary inflammation, which was contrary to our previous observations in

this model, but may be due to acclimation by the mice at this timepoint, however further investigation is needed to confirm this hypothesis [104]. Even though our observed pathological markers in our 3-week study were primarily absent in our 8-week study, we still observed increased microglia counts in animals exposed to DE, consistent with our previous findings [216]. We also observed increased astrocyte counts in animals exposed to DE i.n., a novel target for our model.

We concluded that agriculture dust exposure is associated with pulmonary and neurological inflammation and that AT-RvD1 may be an effective novel therapeutic for the treatment of inflammation associated with agriculture dust exposure.

5.2 Limitations

In vitro data sets display high variability and error, which could be corrected by normalizing treatment groups as fold change compared to the media controls. Culture plates incubated for 18 and 24 hours after treatment may have experienced slight media evaporation, resulting in the possibility of increased cytokine concentration due to water loss. In addition, cytokine levels at the 24-hour timepoint may be elevated due to cell proliferation or cytokine accumulation in the medium. *In vitro* studies were performed as a co-exposure, which may alter the kinetics of the cytokines produced compared to pre- or post-treatment investigations. Our microglia culture model had limited sample sizes and could benefit from increased replicates to confirm statistical significance.

Our *in vivo* studies investigated two endpoint timelines, both with a 3-day recovery. This recovery period may be limiting our ability to evaluate the inflammatory response and the addition of a 5-hour recovery as previously explored may assist in understanding the acute

neurological inflammatory response to agricultural dust [47,48,174,220,221]. Additionally, we only evaluated behavioral outcomes in our 8-week exposure model and observed limited results. This may be due to the exposure not being prolonged enough. We could increase our exposure period to 12 or 24 weeks and evaluate behavioral outcomes to see if a longer exposure period could elicit behavioral changes [48].

Additionally, we did not have clearly tested baselines for various dosages of AT-RvD1 in our cellular and mouse models. It would have been beneficial to test multiple dosages of AT-RvD1 in these models first to determine baseline activity before moving into our knockout model. We also used a different mouse stain than previous studies have utilized, which may lead to inconsistencies in our data compared to other datasets. We would need to perform previous studies on our specific strain of mice to better understand the pharmacokinetics of AT-RvD1 in our mouse models.

We also did not test whether the therapeutic actions of AT-RvD1 in the brain was due to the direct transport of AT-RvD1 across the blood brain barrier (BBB) or due to a peripheral response. Other studies have utilized fluorescently tagged RvD1 and shown that it was transported across the BBB, so its plausible that AT-RvD1 could be transported as well but we would need to conduct our own studies in our mouse specific strain.

5.3 Future Directions

Macrophages express the IL-22 receptor which may contribute to the increases in lysate concentrations of IL-22 *in vitro*. There is also previous evidence that IL-22 is localized to the Golgi apparatus[220]. To evaluate the localization of IL-22 in this model, immunocytochemistry staining could be performed at the various timepoints. The timepoints could also be expanded.

Adding a 12 hour post exposure point to evaluate a broader range of the immune response, while expanding the incubation to 48 and 72 hours would assist in characterizing the repair process after dust exposure. Co-culture with mouse alveolar epithelial cells would be beneficial to determine how the production of cytokines influences epithelial barrier integrity. Supernate could also be evaluated for amphiregulin, an epithelial repair marker to determine how AT-RvD1 and IL-22 influence epithelial repair after dust exposure[16,140]. These models could be adjusted to include a post-DE exposure AT-RvD1 treatment to evaluate how AT-RvD1 as a pharmaceutical alters the immune response. Droplet digital polymerase chain reaction (ddPCR) could also be performed on lysed cells to assess the cytokine transcript alterations compared to their protein concentrations.

Our *in vivo* model provided an important first step in understanding the connection between agriculture dust exposure and neurological inflammation, however more investigation is needed to fully understand the mechanisms by which the observed neurological inflammation is initiated. Previous studies investigating PM exposure and neurological inflammation provide a few hypotheses. First, that PM can travel along nerves in the nasal passages via the olfactory nerve to directly infiltrate the brain [141]; second, that PM in the lungs can utilize the vagus nerve to translocate to the brain [92,228]; and finally, that peripheral inflammation releases inflammatory markers into circulation that damage the blood brain barrier and activate microglia and astrocytes, producing neuroinflammation [92]. Given this, we could evaluate tissues including the lung, nasal epithelium, vagus nerve, blood, and brain for particulates to track the trafficking of the instilled DE to determine if the observed neuroinflammation is due to direct translocation or indirect peripheral inflammatory markers. Additionally, we could evaluate peripheral

inflammatory markers such as serum IL-6 and c-reactive protein, as well as complete blood counts to determine the presence of a systemic inflammatory response [21,42,53,68,88,89,174].

5.4 Conclusions

The evidence obtained between both *in vitro* and *in vivo* studies suggest that AT-RvD1 influences the production of IL-6, TNF-α, IL-10, and IL-22. It suggests that IL-22 may influence the immune response to organic dust exposure. The data support alveolar macrophages as a source of IL-22 in the pulmonary immune response to DE and that AT-RvD1 influences its production during inflammation.

Our investigation of agriculture dust exposure in *in vivo* murine models revealed that agriculture dust exposure is associated with increased microglia and astrocyte counts, markers of neuroinflammation, confirming our hypothesis that agriculture dust exposure contributes to neuroinflammation. We also observed that IL-22 knock-out produced increased disease severity compared to our wildtype controls, also confirming our hypothesis that IL-22 is important in immune regulation in this exposure model. Additionally, we also demonstrated that AT-RvD1 reduces both pulmonary and neurological inflammation and may be a viable therapeutic for individuals exposed to agriculture dust.

The implications of this work are a greater understanding of the neurological effects of agriculture dust in the context of IL-22 knock-out and the possibility of the usage of AT-RvD1 as a novel therapeutic for patients with COPD and neurological disorders perpetuated by agriculture dust exposure. Agriculture dust is an interesting toxicant with many negative implications for public health as those who are exposed are not necessarily exclusively agricultural workers. Due to the nature of this exposure, it would be wise to increase public awareness of the risks of

exposure in other circumstances, such as residing near agricultural facilities. We should also consider and further investigate the neuroinflammatory implications of agriculture dust to better understand its risk to public health and to be proactive with developing therapeutics for individuals who may be exposed.

REFERENCES

1. Aghasafari P, George U, Pidaparti R. A review of inflammatory mechanism in airway diseases. Inflammation Research. 2019;68(1):59-74. doi:10.1007/s00011-018-1191-2
2. Ahlfors H, Morrison PJ, Duarte JH, et al. IL-22 Fate Reporter Reveals Origin and Control of IL-22 Production in Homeostasis and Infection. The Journal of Immunology. 2014;193(9):4602-4613. doi:10.4049/jimmunol.1401244
3. Alcorn JF. IL-22 Plays a Critical Role in Maintaining Epithelial Integrity During Pulmonary Infection. Front Immunol. 2020;11. doi:10.3389/fimmu.2020.01160
4. Alveoli: Anatomy, function and clinical points | Kenhub. Accessed January 25, 2023. https://www.kenhub.com/en/library/anatomy/alveoli
5. Arshad T, Mansur F, Palek R, Manzoor S, Liska V. A Double Edged Sword Role of Interleukin-22 in Wound Healing and Tissue Regeneration. Front Immunol. 2020;11:2148. doi:10.3389/FIMMU.2020.02148/BIBTEX
6. Asthma | CDC. Accessed January 20, 2023. https://www.cdc.gov/asthma/default.htm
7. Bailey K, Meza J, Smith L, Von Essen S, Romberger D. Agricultural Exposures in Patients with COPD in Health Systems Serving Rural Areas. https://doi.org/101080/10599240801887918. 2008;12(3):71-76. doi:10.1080/10599240801887918
8. Bannenberg G, Serhan CN. Specialized pro-resolving lipid mediators in the inflammatory response: An update. Biochim Biophys Acta Mol Cell Biol Lipids. 2010;1801(12):1260-1273. doi:10.1016/j.bbalip.2010.08.002
9. Bannenberg GL, Chiang N, Ariel A, et al. Molecular circuits of resolution: formation and actions of resolvins and protectins. J Immunol. 2005;174(7):4345-4355. doi:10.4049/JIMMUNOL.174.7.4345
10. Bar-Dayan Y, Bar-Dayan Y, Shemer J. Food-borne and air-borne streptococcal pharyngitis--a clinical comparison. Infection. 1997;25(1):12-15. doi:10.1007/BF02113500
11. Barkauskas CE, Chung MI, Fioret B, Gao X, Katsura H, Hogan BLM. Lung organoids: current uses and future promise. Development. 2017;144(6):986. doi:10.1242/DEV.140103
12. Barnes PJ. Inflammatory endotypes in COPD. Allergy. 2019;74(7):1249-1256. doi:10.1111/ALL.13760
13. Barnig C, Cernadas M, Dutile S, et al. Lipoxin A4 regulates natural killer cell and type 2 innate lymphoid cell activation in asthma. Sci Transl Med. 2013;5(174). doi:10.1126/SCITRANSLMED.3004812
14. Basics About COPD | CDC. Accessed January 20, 2023. https://www.cdc.gov/copd/basics-about.html
15. Basil MC, Levy BD. Specialized pro-resolving mediators: Endogenous regulators of infection and inflammation. Nat Rev Immunol. 2016;16(1):51-67. doi:10.1038/nri.2015.4
16. Berasain C, Avila MA. Amphiregulin. Semin Cell Dev Biol. 2014;28:31-41. doi:10.1016/j.semcdb.2014.01.005
17. Berman JS, Beer DJ, Theodore AC, Kornfeld H, Bernardo J, Center DM. Lymphocyte recruitment to the lung. Am Rev Respir Dis. 1990;142(1):238-257. doi:10.1164/AJRCCM/142.1.238

18. Berry CE, Wise RA. Mortality in COPD: Causes, Risk Factors, and Prevention. COPD. 2010;7(5):375. doi:10.3109/15412555.2010.510160
19. Besnard AG, Sabat R, Dumoutier L, et al. Dual Role of IL-22 in allergic airway inflammation and its cross-talk with IL-17A. Am J Respir Crit Care Med. 2011;183(9):1153-1163. doi:10.1164/RCCM.201008-1383OC
20. Beyaert R, Fiers W. Molecular mechanisms of tumor necrosis factor-induced cytotoxicity. FEBS Lett. 1994;340(1-2):9-16. doi:10.1016/0014-5793(94)80163-0
21. Bhattarai G, Shrestha SK, Sim HJ, Lee JC, Kook SH. Effects of fine particulate matter on bone marrow-conserved hematopoietic and mesenchymal stem cells: a systematic review. Exp Mol Med. 2024;56(1):118-128. doi:10.1038/s12276-023-01149-z
22. Boissy RJ, Romberger DJ, Roughead WA, Weissenburger-Moser L, Poole JA, LeVan TD. Shotgun Pyrosequencing Metagenomic Analyses of Dusts from Swine Confinement and Grain Facilities. PLoS One. 2014;9(4):95578. doi:10.1371/JOURNAL.PONE.0095578
23. Bousquet J, Demoly P, Michel FB. Specific immunotherapy in rhinitis and asthma. Annals of Allergy, Asthma and Immunology. 2001;87(1 SUPPL.):38-42. doi:10.1016/S1081-1206(10)62193-X
24. Briend E, Ferguson GJ, Mori M, et al. IL-18 associated with lung lymphoid aggregates drives IFNγ production in severe COPD. Respir Res. 2017;18(1). doi:10.1186/s12931-017-0641-7
25. Broquet A, Jacqueline C, Davieau M, et al. Interleukin-22 level is negatively correlated with neutrophil recruitment in the lungs in a Pseudomonas aeruginosa pneumonia model. Sci Rep. 2017;7(1). doi:10.1038/S41598-017-11518-0
26. Caetano-Silva ME, Rund L, Hutchinson NT, Woods JA, Steelman AJ, Johnson RW. Inhibition of inflammatory microglia by dietary fiber and short-chain fatty acids. Sci Rep. 2023;13(1). doi:10.1038/s41598-022-27086-x
27. Calderón-Garcidueñas L, Reed W, Maronpot RR, et al. Brain inflammation and Alzheimer's-like pathology in individuals exposed to severe air pollution. Toxicol Pathol. 2004;32(6):650-658. doi:10.1080/01926230490520232
28. Castanheira FVS, Kubes P. Neutrophils and NETs in modulating acute and chronic inflammation. Blood. 2019;133(20):2178-2185. doi:10.1182/BLOOD-2018-11-844530
29. CDC. National Trends - Chronic Obstructive Pulmonary Disease (COPD). Centers for Disease Control and Prevention. Published online 2020. Accessed November 28, 2024. https://www.cdc.gov/copd/php/case-reporting/national-trends-in-copd.html
30. CDC WONDER. Accessed January 20, 2023. https://wonder.cdc.gov/
31. Centers for Disease Control and Prevention. About Alzheimer's Disease. https://www.cdc.gov/aging/alzheimers-disease-dementia/about-alzheimers.html. April 12, 2023.

Accessed September 3, 2024. https://www.cdc.gov/aging/alzheimers-disease-dementia/about-alzheimers.html
32. Centers for Disease Control and Prevention. Control Asthma | 6|18 Initiative | CDC. Accessed January 20, 2023. https://www.cdc.gov/sixeighteen/asthma/index.htm
33. Centers for Disease Control and Prevention. Mortality in the United States. National Center for Health Statistics. 2021. Accessed January 20, 2023. https://www.cdc.gov/nchs/fastats/leading-causes-of-death.htm
34. Chen W, Wang J, Yang H, et al. Interleukin 22 and its association with neurodegenerative disease activity. Front Pharmacol. 2022;13. doi:10.3389/fphar.2022.958022
35. Chiang N, Fredman G, Bäckhed F, et al. Infection Regulates Pro-Resolving Mediators that Lower Antibiotic Requirements. Nature. 2012;484(7395):524. doi:10.1038/NATURE11042
36. Chiang N, Rosa X de la, Libreros S, Serhan CN. Novel Resolvin D2 receptor axis in infectious inflammation. J Immunol. 2017;198(2):842. doi:10.4049/JIMMUNOL.1601650
37. Chung KF, Adcock IM. Multifaceted mechanisms in COPD: Inflammation, immunity, and tissue repair and destruction. European Respiratory Journal. 2008;31(6):1334-1356. doi:10.1183/09031936.00018908
38. Chusid MJ. Eosinophils: Friends or Foes? J Allergy Clin Immunol Pract. 2018;6(5):1439-1444. doi:10.1016/J.JAIP.2018.04.031
39. COPD Costs. CDC. 2014. Accessed January 20, 2023. https://www.cdc.gov/copd/infographics/copd-costs.html
40. Costa LG, Cole TB, Coburn J, Chang YC, Dao K, Roqué PJ. Neurotoxicity of traffic-related air pollution. Neurotoxicology. 2017;59:133-139. doi:10.1016/j.neuro.2015.11.008
41. Croasdell A, Thatcher TH, Kottmann RM, et al. Resolvins attenuate inflammation and promote resolution in cigarette smoke-exposed human macrophages. Am J Physiol Lung Cell Mol Physiol. 2015;309(8):L888-L901. doi:10.1152/AJPLUNG.00125.2015
42. Dahl M, Vestbo J, Lange P, Bojesen SE, Tybjærg-Hansen A, Nordestgaard BG. C-reactive protein as a predictor of prognosis in chronic obstructive pulmonary disease. Am J Respir Crit Care Med. 2007;175(3):250-255. doi:10.1164/rccm.200605-713OC
43. Dalli J, Serhan CN. Specific lipid mediator signatures of human phagocytes: microparticles stimulate macrophage efferocytosis and pro-resolving mediators. Blood. 2012;120(15). doi:10.1182/BLOOD-2012-04-423525
44. Dalli J, Winkler JW, Colas RA, et al. Resolvin D3 and aspirin-triggered resolvin D3 are potent immunoresolvents. Chem Biol. 2013;20(2):188-201. doi:10.1016/J.CHEMBIOL.2012.11.010
45. Davies LC, Jenkins SJ, Allen JE, Taylor PR. Tissue-resident macrophages. Nat Immunol. 2013;14(10):986-995. doi:10.1038/ni.2705
46. Dean LS, Threatt AN, Jones K, et al. I don't know about you, but I'm feeling IL-22. Cytokine Growth Factor Rev. Published online November 2024. doi:10.1016/j.cytogfr.2024.11.001
47. Dominguez EC, Heires AJ, Pavlik J, et al. A high docosahexaenoic acid diet alters the lung inflammatory response to acute dust exposure. Nutrients. 2020;12(8):1-19. doi:10.3390/nu12082334
48. Dominguez EC, Phandthong R, Nguyen M, et al. Aspirin-Triggered Resolvin D1 Reduces Chronic Dust-Induced Lung Pathology without Altering Susceptibility to Dust-Enhanced Carcinogenesis. Cancers (Basel). 2022;14(8):1900. doi:10.3390/cancers14081900

49. Dosman JA, Senthilselvan A, Kirychuk SP, et al. Positive human health effects of wearing a respirator in a swine barn. Chest. 2000;118(3):852-860. doi:10.1378/CHEST.118.3.852
50. Dravid AA, M. Dhanabalan K, Agarwal S, Agarwal R. Resolvin D1-loaded nanoliposomes promote M2 macrophage polarization and are effective in the treatment of osteoarthritis. Bioeng Transl Med. 2022;7(2). doi:10.1002/btm2.10281
51. Dudakov JA, Hanash AM, Van Den Brink MRM. Interleukin-22: immunobiology and pathology. Annu Rev Immunol. 2015;33:747. doi:10.1146/ANNUREV-IMMUNOL-032414-112123
52. Van Eeden SF, Hogg JC. Immune-Modulation in Chronic Obstructive Pulmonary Disease: Current Concepts and Future Strategies. Respiration. 2020;99(7):550-565. doi:10.1159/000502261
53. Van Eeden SF, Hogg JC. Systemic inflammatory response induced by particulate matter air pollution: The importance of bone-marrow stimulation. J Toxicol Environ Health A. 2002;65(20):1597-1613. doi:10.1080/00984100290071685
54. Eickmeier O, Seki H, Haworth O, et al. Aspirin-triggered resolvin D1 reduces mucosal inflammation and promotes resolution in a murine model of acute lung injury. Mucosal Immunol. 2013;6(2):256-266. doi:10.1038/mi.2012.66
55. Engler AE, Ysasi AB, Pihl RMF, et al. Airway-Associated Macrophages in Homeostasis and Repair. Cell Rep. 2020;33(13). doi:10.1016/j.celrep.2020.108553
56. Environmental Protection Agency. Report on the Environment Chronic Obstructive Pulmonary Disease.; 2022. https://wonder.cdc.gov/mortSQL.html
57. Eriksson Ström J, Pourazar J, Linder R, et al. Cytotoxic lymphocytes in COPD airways: Increased NK cells associated with disease, iNKT and NKT-like cells with current smoking. Respir Res. 2018;19(1):1-10. doi:10.1186/S12931-018-0940-7/FIGURES/3
58. Von Essen SG, Robbins RA, Thompson AB, Ertl RF, Linder J, Rennard S. Mechanisms of Neutrophil Recruitment to the Lung by Grain Dust Exposure. https://doi.org/101164/ajrccm/1384921. 2012;138(4):921-927. doi:10.1164/AJRCCM/138.4.921
59. Essen VS, Von Essen SG, Andersen CI, Smith LM. Organic Dust Toxic Syndrome: A Noninfectious Febrile Illness after Exposure to the Hog Barn Environment. Vol 13.; 2005. http://www.aasv.org/shap.html.
60. Farm and Ranch eXtension in Safety and Health (FReSH) Community of Practice. Respiratory illnesses associated with agriculture. 2012. Accessed February 19, 2023. https://ag-safety.extension.org/tag/organic-dust-toxicity-syndrome/
61. Feehan KT, Gilroy DW. Is Resolution the End of Inflammation? Trends Mol Med. 2019;25(3):198-214. doi:10.1016/J.MOLMED.2019.01.006
62. Fiers W. Tumor necrosis factor Characterization at the molecular, cellular and in vivo level. FEBS Lett. 1991;285(2):199-212. doi:10.1016/0014-5793(91)80803-B
63. Foo SY, Phipps S. Regulation of inducible BALT formation and contribution to immunity and pathology. Mucosal Immunol. 2010;3(6):537-544. doi:10.1038/mi.2010.52
64. Gans MD, Gavrilova T. Understanding the immunology of asthma: Pathophysiology, biomarkers, and treatments for asthma endotypes. Paediatr Respir Rev. 2020;36:118-127. doi:10.1016/J.PRRV.2019.08.002
65. Gao C, Jiang J, Tan Y, Chen S. Microglia in neurodegenerative diseases: mechanism and potential therapeutic targets. Signal Transduct Target Ther. 2023;8(1). doi:10.1038/s41392-023-01588-0

66. Giovannoni F, Quintana FJ. The Role of Astrocytes in CNS Inflammation. Trends Immunol. 2020;41(9):805-819. doi:10.1016/j.it.2020.07.007
67. Global Initiative for Asthma. 2022 GINA Main Report - Global Initiative for Asthma - GINA. 2022. Accessed February 20, 2023. https://ginasthma.org/gina-reports/
68. Goto Y, Ishii H, Hogg JC, et al. Particulate matter air pollution stimulates monocyte release from the bone marrow. Am J Respir Crit Care Med. 2004;170(8):891-897. doi:10.1164/rccm.200402-235OC
69. Greenlund KJ, Liu Y, Deokar AJ, Wheaton AG, Croft JB. Association of chronic obstructive pulmonary disease with increased confusion or memory loss and functional limitations among adults in 21 states, 2011 behavioral risk factor surveillance system. Prev Chronic Dis. 2016;13(1). doi:10.5888/pcd13.150428
70. Gurkan OU, He C, Zielinski R, et al. Interleukin-6 mediates pulmonary vascular permeability in a two-hit model of ventilator-associated lung injury. Exp Lung Res. 2011;37(10):575. doi:10.3109/01902148.2011.620680
71. Hall JCE, Priestley J V., Perry VH, Michael-Titus AT. Docosahexaenoic acid, but not eicosapentaenoic acid, reduces the early inflammatory response following compression spinal cord injury in the rat. J Neurochem. 2012;121(5):738-750. doi:10.1111/J.1471-4159.2012.07726.X
72. Hardaker EL, Bacon AM, Carlson K, et al. Regulation of TNF-alpha- and IFN-gamma-induced CXCL10 expression: participation of the airway smooth muscle in the pulmonary inflammatory response in chronic obstructive pulmonary disease. The FASEB journal : official publication of the Federation of American Societies for Experimental Biology. 2004;18(1):191-193. doi:10.1096/fj.03-0170fje
73. Henkle E, Winthrop KL. Nontuberculous mycobacteria infections in immunosuppressed hosts. Clin Chest Med. 2015;36(1):91-99. doi:10.1016/J.CCM.2014.11.002
74. Hirano S, Zhou Q, Furuyama A, Kanno S. Differential Regulation of IL-1β and IL-6 Release in Murine Macrophages. Inflammation. 2017;40(6):1933-1943. doi:10.1007/S10753-017-0634-1
75. Hirano T, Taga T, Nakano N, et al. Purification to homogeneity and characterization of human B-cell differentiation factor (BCDF or BSFp-2). Proceedings of the National Academy of Sciences. 1985;82(16):5490-5494. doi:10.1073/PNAS.82.16.5490
76. Hogg JC, Chu F, Utokaparch S, et al. The Nature of Small-Airway Obstruction in Chronic Obstructive Pulmonary Disease. Vol 26.; 2004. www.nejm.org
77. Hsiao HM, Sapinoro RE, Thatcher TH, et al. A Novel Anti-Inflammatory and Pro-Resolving Role for Resolvin D1 in Acute Cigarette Smoke-Induced Lung Inflammation. PLoS One. 2013;8(3). doi:10.1371/journal.pone.0058258
78. Hu X, Shen H, Wang Y, Zhang L, Zhao M. Aspirin-triggered resolvin D1 alleviates paraquat-induced acute lung injury in mice. Life Sci. 2019;218:38-46. doi:10.1016/j.lfs.2018.12.028
79. Van Hulst G, Batugedara HM, Jorssen J, Louis R, Bureau F, Desmet CJ. Eosinophil diversity in asthma. Biochem Pharmacol. 2020;179. doi:10.1016/J.BCP.2020.113963
80. Idriss HT, Naismith JH. TNF and the TNF Receptor Superfamily: Structure-Function Relationship(s). Microsc Res Tech. 2000;50:184-195. doi:10.1002/1097-0029
81. Innes JK, Calder PC. Omega-6 fatty acids and inflammation. Prostaglandins Leukot Essent Fatty Acids. 2018;132:41-48. doi:10.1016/J.PLEFA.2018.03.004

82. Institute for Occupational Safety N. Respiratory Disease in Agricultural Workers: Mortality and Morbidity Statistics.; 2007.
83. Ishihara T, Yoshida M, Arita M. Omega-3 fatty acid-derived mediators that control inflammation and tissue homeostasis. Int Immunol. 2019;31(9):559-567. doi:10.1093/INTIMM/DXZ001
84. Ito T, Hirose K, Nakajima H. Bidirectional roles of IL-22 in the pathogenesis of allergic airway inflammation. Allergology International. 2019;68(1):4-8. doi:10.1016/J.ALIT.2018.10.002
85. Ji H. Lysis of cultured cells for immunoprecipitation. Cold Spring Harb Protoc. 2010;5(8). doi:10.1101/pdb.prot5466
86. Jiang S, Shan F, Zhang Y, Jiang L, Cheng Z. Increased serum IL-17 and decreased serum IL-10 and IL-35 levels correlate with the progression of COPD. Int J Chron Obstruct Pulmon Dis. 2018;13:2483. doi:10.2147/COPD.S167192
87. Jing H, Liu L, Zhou J, Yao H. Inhibition of C-X-C motif chemokine 10 (CXCL10) protects mice from cigarette smoke-induced chronic obstructive pulmonary disease. Medical Science Monitor. 2018;24:5748-5753. doi:10.12659/MSM.909864
88. Kaplanski G, Marin V, Montero-Julian F, Mantovani A, Farnarier C. IL-6: A regulator of the transition from neutrophil to monocyte recruitment during inflammation. Trends Immunol. 2003;24(1):25-29. doi:10.1016/S1471-4906(02)00013-3
89. Kaur S, Bansal Y, Kumar R, Bansal G. A panoramic review of IL-6: Structure, pathophysiological roles and inhibitors. Bioorg Med Chem. 2020;28(5):115327. doi:10.1016/J.BMC.2020.115327
90. Kearney GD, Xu X, Balanay JAG, Allen DL, Rafferty AP. Assessment of Personal Protective Equipment Use Among Farmers in Eastern North Carolina: A Cross-sectional Study. https://doi.org/101080/1059924X2014976730. 2015;20(1):43-54. doi:10.1080/1059924X.2014.976730
91. Keddache S, Laheurte C, Boullerot L, et al. Inflammatory and immunological profile in COPD secondary to organic dust exposure. Clinical Immunology. 2021;229:108798. doi:10.1016/J.CLIM.2021.108798
92. Kempuraj D, Thangavel R, Selvakumar GP, et al. Brain and peripheral atypical inflammatory mediators potentiate neuroinflammation and neurodegeneration. Front Cell Neurosci. 2017;11. doi:10.3389/fncel.2017.00216
93. Kim N, Ramon S, Thatcher TH, Woeller CF, Sime PJ, Phipps RP. Specialized pro-resolving mediators (SPMs) inhibit human B-cell IgE production. Eur J Immunol. 2016;46(1):81. doi:10.1002/EJI.201545673
94. Kishimoto T. The Biology of Interleukin-6. Blood. 1989;74(1):1-10. doi:10.1182/BLOOD.V74.1.1.1
95. Klein SL, Flanagan KL. Sex differences in immune responses. Nat Rev Immunol. 2016;16(10):626-638. doi:10.1038/nri.2016.90
96. Krishnamoorthy N, Burkett PR, Dalli J, et al. Cutting edge: maresin-1 engages regulatory T cells to limit type 2 innate lymphoid cell activation and promote resolution of lung inflammation. J Immunol. 2015;194(3):863-867. doi:10.4049/JIMMUNOL.1402534
97. Kuchuk AA, Basanets A V., Louhelainen K. Bronchopulmonary pathology in workers exposed to organic fodder dust. Ann Agric Environ Med. 2000;7(1):17-23. Accessed February 19, 2023. https://pubmed.ncbi.nlm.nih.gov/10865240/

98. Kumar H, Kawai T, Akira S. Pathogen Recognition by the Innate Immune System. https://doi.org/103109/088301852010529976. 2011;30(1):16-34. doi:10.3109/08830185.2010.529976
99. Kumar V. Pulmonary Innate Immune Response Determines the Outcome of Inflammation During Pneumonia and Sepsis-Associated Acute Lung Injury. Front Immunol. 2020;11:1722. doi:10.3389/FIMMU.2020.01722
100. Latham AS, Geer CE, Ackart DF, et al. Gliosis, misfolded protein aggregation, and neuronal loss in a guinea pig model of pulmonary tuberculosis. Front Neurosci. 2023;17. doi:10.3389/FNINS.2023.1157652/FULL
101. Lee D, Jo H, Go C, et al. The Roles of IL-22 and Its Receptor in the Regulation of Inflammatory Responses in the Brain. Int J Mol Sci. 2022;23(2). doi:10.3390/ijms23020757
102. Levy BD, Clish CB, Schmidt B, Gronert K, Serhan CN. Lipid mediator class switching during acute inflammation: signals in resolution. Nat Immunol. 2001;2(7):612-619. doi:10.1038/89759
103. Li D, Li Y, Li G, Zhang Y, Li J, Chen H. Fluorescent reconstitution on deposition of PM 2.5 in lung and extrapulmonary organs. Proc Natl Acad Sci U S A. 2019;116(7):2488-2493. doi:10.1073/pnas.1818134116
104. Li J, Yao Y, Shang B, et al. Ambient air pollution, low-grade inflammation, and lung function: Evidences from the UK Biobank. Ecotoxicol Environ Saf. 2024;284:116998. doi:10.1016/j.ecoenv.2024.116998
105. Li W, Lin G, Xiao Z, et al. A review of respirable fine particulate matter (PM2.5)-induced brain damage. Front Mol Neurosci. 2022;15. doi:10.3389/fnmol.2022.967174
106. Liddelow SA, Guttenplan KA, Clarke LE, et al. Neurotoxic reactive astrocytes are induced by activated microglia. Nature. 2017;541(7638):481-487. doi:10.1038/nature21029
107. Liu F, Peng W, Chen J, et al. Exosomes Derived From Alveolar Epithelial Cells Promote Alveolar Macrophage Activation Mediated by miR-92a-3p in Sepsis-Induced Acute Lung Injury. Front Cell Infect Microbiol. 2021;11:646546. doi:10.3389/FCIMB.2021.646546/FULL
108. Liu Y, Croft JB, Anderson LA, Wheaton AG, Presley-Cantrell LR, Ford ES. The association of chronic obstructive pulmonary disease, disability, engagement in social activities, and mortality among US adults aged 70 years or older, 1994-2006. International Journal of COPD. 2014;9:75-83. doi:10.2147/COPD.S53676
109. Liu Y, Croft JB, Anderson LA, Wheaton AG, Presley-Cantrell LR, Ford ES. The association of chronic obstructive pulmonary disease, disability, engagement in social activities, and mortality among US adults aged 70 years or older, 1994-2006. International Journal of COPD. 2014;9:75-83. doi:10.2147/COPD.S53676
110. Lommatzsch M. Immune Modulation in Asthma: Current Concepts and Future Strategies. Respiration. 2020;99(7):566-576. doi:10.1159/000506651
111. Loymans RJB, Gemperli A, Cohen J, et al. Comparative effectiveness of long term drug treatment strategies to prevent asthma exacerbations: Network meta-analysis. BMJ (Online). 2014;348. doi:10.1136/bmj.g3009
112. Malawista SE, Chevance ADB, Van Damme J, Serhan CN. Tonic inhibition of chemotaxis in human plasma. Proc Natl Acad Sci U S A. 2008;105(46):17949. doi:10.1073/PNAS.0802572105
113. Malmsten CL. Prostaglandins, thromboxanes, and leukotrienes in inflammation. Am J Med. 1986;80(4 SUPPL. 2):11-17. doi:10.1016/0002-9343(86)90073-2

114. Manti S, Salpietro C, Cuppari C. Antihistamines: Recommended Dosage – Divergence between Clinical Practice and Guideline Recommendations. Int Arch Allergy Immunol. 2019;178(1):93-96. doi:10.1159/000492636
115. Martin WT, Zhang Y, Willson P, Archer TP, Kinahan C, Barber EM. Bacterial and fungal flora of dust deposits in a pig building. Occup Environ Med. 1996;53(7):484-487. doi:10.1136/OEM.53.7.484
116. Matsuoka T, Shamji MH, Durham SR. Allergen immunotherapy and tolerance. Allergol Int. 2013;62(4):403-413. doi:10.2332/ALLERGOLINT.13-RAI-0650
117. Mattapallil MJ, Kielczewski JL, Zárate-Bladés CR, et al. Interleukin 22 ameliorates neuropathology and protects from central nervous system autoimmunity. J Autoimmun. 2019;102:65-76. doi:10.1016/j.jaut.2019.04.017
118. Mcaleer JP, Kolls JK. Directing traffic: IL-17 and IL-22 coordinate pulmonary immune defense. Immunol Rev. 2014;260(1):129-144. doi:10.1111/imr.12183
119. McCaskill ML, Romberger DJ, DeVasure J, et al. Alcohol exposure alters mouse lung inflammation in response to inhaled dust. Nutrients. 2012;4(7):695-710. doi:10.3390/NU4070695
120. McCaskill ML, Romberger DJ, DeVasure J, et al. Alcohol exposure alters mouse lung inflammation in response to inhaled dust. Nutrients. 2012;4(7):695-710. doi:10.3390/NU4070695
121. McMahon AW, Levenson MS, McEvoy BW, Mosholder AD, Murphy D. Age and Risks of FDA-Approved Long-Acting β2-Adrenergic Receptor Agonists. Pediatrics. 2011;128(5):e1147-e1154. doi:10.1542/PEDS.2010-1720
122. Mendivil CO. Dietary Fish, Fish Nutrients, and Immune Function: A Review. Front Nutr. 2021;7:373. doi:10.3389/FNUT.2020.617652/BIBTEX
123. Mendy A, Forno E, Niyonsenga T, Gasana J. Blood Biomarkers as Predictors of Long-Term Mortality in COPD. Clin Respir J. 2018;12(5):1891. doi:10.1111/CRJ.12752
124. Mesnil C, Raulier S, Paulissen G, et al. Lung-resident eosinophils represent a distinct regulatory eosinophil subset. J Clin Invest. 2016;126(9):3279. doi:10.1172/JCI85664
125. Mitsi E, Kamng'ona R, Rylance J, et al. Human alveolar macrophages predominately express combined classical M1 and M2 surface markers in steady state. Respir Res. 2018;19(1). doi:10.1186/S12931-018-0777-0
126. Miyata R, van Eeden SF. The innate and adaptive immune response induced by alveolar macrophages exposed to ambient particulate matter. Toxicol Appl Pharmacol. 2011;257(2):209-226. doi:10.1016/J.TAAP.2011.09.007
127. Montrose L, Schuller A, D'Evelyn SM, Migliaccio C. Wildfire Smoke Toxicology and Health. In: ; 2023:217-231. doi:10.1002/9781119757030.ch11
128. Moore KW, De Waal Malefyt R, Coffman RL, O'Garra A. Interleukin-10 and the interleukin-10 receptor. Annu Rev Immunol. 2001;19:683-765. doi:10.1146/ANNUREV.IMMUNOL.19.1.683
129. Most Recent National Asthma Data | CDC. Accessed January 20, 2023. https://www.cdc.gov/asthma/most_recent_national_asthma_data.htm
130. Naclerio R. Clinical manifestations of the release of histamine and other inflammatory mediators. Journal of Allergy and Clinical Immunology. 1999;103(3 SUPPL.):S382-S385. doi:10.1016/S0091-6749(99)70216-2
131. National Center for Farmworker Health. Agricultural Workers and Mental Health. Published online April 2021. https://www.ncfh.org/mental-health-fact-

sheet.html#:~:text=Elevated%20levels%20of%20anxiety%20and,females)%20had%20elevated%20depressive%20symptoms.
132. National Centre for Farmer Health. Farmer's fever – Organic Toxic Dust Syndrome (ODTS) | National Centre for Farmer Health. 2022. Accessed February 19, 2023. https://farmerhealth.org.au/2014/03/20/farmers-fever
133. Netea MG, Schlitzer A, Placek K, Joosten LAB, Schultze JL. Innate and Adaptive Immune Memory: an Evolutionary Continuum in the Host's Response to Pathogens. Cell Host Microbe. 2019;25(1):13-26. doi:10.1016/j.chom.2018.12.006
134. Newson J, Stables M, Karra E, et al. Resolution of acute inflammation bridges the gap between innate and adaptive immunity. Blood. 2014;124(11):1748-1764. doi:10.1182/BLOOD-2014-03-562710
135. Nguyen HMH, Torres JA, Agrawal S, Agrawal A. Nicotine Impairs the Response of Lung Epithelial Cells to IL-22. Mediators Inflamm. 2020;2020. doi:10.1155/2020/6705428
136. Nordgren TM, Bailey KL. Pulmonary health effects of agriculture. Curr Opin Pulm Med. 2016;22(2):144-149. doi:10.1097/MCP.0000000000000247
137. Nordgren TM, Bauer CD, Heires AJ, et al. Maresin-1 reduces airway inflammation associated with acute and repetitive exposures to organic dust. Translational Research. 2015;166(1):57-69. doi:10.1016/j.trsl.2015.01.001
138. Nordgren TM, Charavaryamath C. Agriculture Occupational Exposures and Factors Affecting Health Effects. Curr Allergy Asthma Rep. 2018;18(12):65. doi:10.1007/S11882-018-0820-8
139. Nordgren TM, Friemel TD, Heires AJ, Poole JA, Wyatt TA, Romberger DJ. The omega-3 fatty acid docosahexaenoic acid attenuates organic dust-induced airway inflammation. Nutrients. 2014;6(12):5434-5452. doi:10.3390/nu6125434
140. Nordgren TM, Heires AJ, Bailey KL, et al. Docosahexaenoic acid enhances amphiregulin-mediated bronchial epithelial cell repair processes following organic dust exposure. Am J Physiol Lung Cell Mol Physiol. 2018;314:421-431. doi:10.1152/ajplung.00273.2017.-Injurious
141. Oberdörster G, Sharp Z, Atudorei V, et al. Translocation of Inhaled Ultrafine Particles to the Brain. Inhal Toxicol. 2004;16(6-7):437-445. doi:10.1080/08958370490439597
142. Oberdörster G, Sharp Z, Atudorei V, et al. Translocation of inhaled ultrafine particles to the brain. In: Inhalation Toxicology. Vol 16. ; 2004:437-445. doi:10.1080/08958370490439597
143. Ortega H, Llanos JP, Lafeuille MH, et al. Burden of disease associated with a COPD eosinophilic phenotype. Int J Chron Obstruct Pulmon Dis. 2018;13:2425. doi:10.2147/COPD.S170995
144. Ouyang W, Rutz S, Crellin NK, Valdez PA, Hymowitz SG. Regulation and Functions of the IL-10 Family of Cytokines in Inflammation and Disease. https://doi.org/101146/annurev-immunol-031210-101312. 2011;29:71-109. doi:10.1146/ANNUREV-IMMUNOL-031210-101312
145. Özgül Özdemir RB, Soysal Gündüz Ö, Özdemir AT, Akgül Ö. Low levels of pro-resolving lipid mediators lipoxin-A4, resolvin-D1 and resolvin-E1 in patients with rheumatoid arthritis. Immunol Lett. 2020;227:34-40. doi:10.1016/J.IMLET.2020.08.006
146. Palmberg L, Larsson BM, Sundblad BM, Larsson K. Partial protection by respirators on airways responses following exposure in a swine house. Am J Ind Med. 2004;46(4):363-370. doi:10.1002/AJIM.20079

147. Pekny M, Pekna M, Messing A, et al. Astrocytes: a central element in neurological diseases. Acta Neuropathol. 2016;131(3):323-345. doi:10.1007/s00401-015-1513-1
148. Peng YH, Chen CY, Su CH, et al. Increased Risk of Dementia Among Patients With Pulmonary Tuberculosis. American Journal of Alzheimer's Disease & Other Dementiasr. 2015;30(6):629-634. doi:10.1177/1533317515577186
149. Perna E, Aguilera-Lizarraga J, Florens M V., et al. Effect of resolvins on sensitisation of TRPV1 and visceral hypersensitivity in IBS. Gut. 2021;70(7):1275-1286. doi:10.1136/GUTJNL-2020-321530
150. Peters A, Veronesi B, Calderón-Garcidueñas L, et al. Translocation and potential neurological effects of fine and ultrafine particles a critical update. Part Fibre Toxicol. 2006;3. doi:10.1186/1743-8977-3-13
151. Piano I, Votta A, Colucci P, et al. Anti-inflammatory reprogramming of microglia cells by metabolic modulators to counteract neurodegeneration; a new role for Ranolazine. Sci Rep. 2023;13(1). doi:10.1038/s41598-023-47540-8
152. Pociask DA, Scheller E v., Mandalapu S, et al. IL-22 Is Essential for Lung Epithelial Repair following Influenza Infection. Am J Pathol. 2013;182(4):1286-1296. doi:10.1016/J.AJPATH.2012.12.007
153. Pociask DA, Scheller E V., Mandalapu S, et al. IL-22 is essential for lung epithelial repair following influenza infection. American Journal of Pathology. 2013;182(4):1286-1296. doi:10.1016/j.ajpath.2012.12.007
154. Polverino F, Seys LJM, Bracke KR, Owen CA. B cells in chronic obstructive pulmonary disease: moving to center stage. American Journal of Physiology-Lung Cellular and Molecular Physiology. 2016;311(4):L687-L695. doi:10.1152/ajplung.00304.2016
155. Poole JA, Alexis NE, Parks C, et al. Repetitive organic dust exposure in vitro impairs macrophage differentiation and function. Journal of Allergy and Clinical Immunology. 2008;122(2). doi:10.1016/j.jaci.2008.05.023
156. Poole JA, Alexis NE, Parks C, et al. Repetitive organic dust exposure in vitro impairs macrophage differentiation and function. J Allergy Clin Immunol. 2008;122(2):375-382. doi:10.1016/J.JACI.2008.05.023
157. Poole JA, Gleason A, Romberger DJ, Kielian T. Repetitive Intranasal Inhalation Of Organic Dust Induces A Predominant Th17-Polarized Airway Inflammatory Response. American Thoracic Society International Conference Meetings Abstracts American Thoracic Society International Conference Meetings Abstracts. Published online May 2011:A4802-A4802. doi:10.1164/AJRCCM-CONFERENCE.2011.183.1_MEETINGABSTRACTS.A4802
158. Poole JA, Gleason AM, Bauer C, et al. αβ T Cells and a Mixed Th1/Th17 Response are Important in Organic Dust-Induced Airway Disease. Ann Allergy Asthma Immunol. 2012;109(4):266. doi:10.1016/J.ANAI.2012.06.015
159. Poole JA, Mikuls TR, Duryee MJ, et al. A role for B cells in organic dust induced lung inflammation. Respir Res. 2017;18(1). doi:10.1186/s12931-017-0703-x
160. Poole JA, Romberger DJ. Immunological and inflammatory responses to organic dust in agriculture. Curr Opin Allergy Clin Immunol. 2012;12(2):126-132. doi:10.1097/ACI.0B013E3283511D0E
161. Poole JA, Wyatt TA, Oldenburg PJ, et al. Intranasal organic dust exposure-induced airway adaptation response marked by persistent lung inflammation and pathology in mice.

American Journal of Physiology-Lung Cellular and Molecular Physiology. 2009;296(6):L1085-L1095. doi:10.1152/ajplung.90622.2008
162. Poole JA, Wyatt TA, Oldenburg PJ, et al. Intranasal organic dust exposure-induced airway adaptation response marked by persistent lung inflammation and pathology in mice. Am J Physiol Lung Cell Mol Physiol. 2009;296(6):1085-1095. doi:10.1152/AJPLUNG.90622.2008/ASSET/IMAGES/LARGE/ZH50070954610008.JPEG
163. Poole JA, Zamora-Sifuentes JL, De las Vecillas L, Quirce S. Respiratory Diseases Associated With Organic Dust Exposure. Journal of Allergy and Clinical Immunology: In Practice. Published online 2024. doi:10.1016/j.jaip.2024.02.022
164. Pryor JT, Cowley LO, Simonds SE. The Physiological Effects of Air Pollution: Particulate Matter, Physiology and Disease. Front Public Health. 2022;10. doi:10.3389/fpubh.2022.882569
165. Rask-Andersen A. 1633c Determinants for asthma in farmers with special reference to odts (organic dust toxic syndrome). Occup Environ Med. 2018;75(Suppl 2):A472-A472. doi:10.1136/OEMED-2018-ICOHABSTRACTS.1343
166. Ray A, Kolls JK. Neutrophilic Inflammation in Asthma and Association with Disease Severity. Trends Immunol. 2017;38(12):942. doi:10.1016/J.IT.2017.07.003
167. Razzaghi H, Wang Y, Lu H, et al. Estimated County-Level Prevalence of Selected Underlying Medical Conditions Associated with Increased Risk for Severe COVID-19 Illness — United States, 2018. MMWR Morb Mortal Wkly Rep. 2020;69(29):945-950. doi:10.15585/MMWR.MM6929A1
168. Renaud HJ, Cui JY, Khan M, Klaassen CD. Tissue distribution and gender-divergent expression of 78 cytochrome p450 mRNAs in mice. Toxicological Sciences. 2011;124(2):261-277. doi:10.1093/toxsci/kfr240
169. Rey C, Nadjar A, Buaud B, et al. Resolvin D1 and E1 promote resolution of inflammation in microglial cells in vitro. Brain Behav Immun. 2016;55:249-259. doi:10.1016/j.bbi.2015.12.013
170. Reynolds SJ, Donham KJ, Whitten P, Merchant JA, Burmeister LF, Popendorf WJ. Longitudinal evaluation of dose-response relationships for environmental exposures and pulmonary function in swine production workers. Am J Ind Med. 1996;29(1):33-40. doi:10.1002/(sici)1097-0274(199601)29:1<33::aid-ajim5>3.0.co;2-#
171. Risen SJ, Boland SW, Sharma S, et al. Targeting Neuroinflammation by Pharmacologic Downregulation of Inflammatory Pathways Is Neuroprotective in Protein Misfolding Disorders. ACS Chem Neurosci. 2024;15(7):1533-1547. doi:10.1021/acschemneuro.3c00846
172. Rivoire B, Attucci S, Anthonioz P, Carré P, Lemarié E, Hazouard E. Occupational acute lung injury due to Alternaria alternata: early stage of organic dust toxic syndrome requires no corticosteroids. Intensive Care Med. 2001;27(7):1236-1237. doi:10.1007/S001340100983
173. Romberger DJ, Bodlak V, von Essen SG, Mathisen T, Wyatt TA. Hog barn dust extract stimulates IL-8 and IL-6 release in human bronchial epithelial cells via PKC activation. J Appl Physiol (1985). 2002;93(1):289-296. doi:10.1152/JAPPLPHYSIOL.00815.2001
174. Romberger DJ, Bodlak V, Von Essen SG, Mathisen T, Wyatt TA. Hog barn dust extract stimulates IL-8 and IL-6 release in human bronchial epithelial cells via PKC activation. J Appl

Physiol. 2002;93(1):289-296. doi:10.1152/JAPPLPHYSIOL.00815.2001/ASSET/IMAGES/LARGE/DG0721698005.JPEG
175. Rosales C, Lowell CA, Schnoor M, Uribe-Querol E. Neutrophils: Their Role in Innate and Adaptive Immunity 2017. J Immunol Res. 2017;2017. doi:10.1155/2017/9748345
176. S. Von Essen, D. Romberger. The Respiratory Inflammatory Response to the Swine Confinement Building Environment: The Adaptation to Respiratory Exposures in the Chronically Exposed Worker. J Agric Saf Health. 2003;9(3):185-196. doi:10.13031/2013.13684
177. Saraiva M, O'Garra A. The regulation of IL-10 production by immune cells. Nature Reviews Immunology 2010 10:3. 2010;10(3):170-181. doi:10.1038/nri2711
178. Saranz RJ. Innate immunity and asthma risk in amish and hutterite farm children. Arch Argent Pediatr. 2017;115(1):e49-e50. doi:10.1056/nejmoa1508749
179. Scheller J, Chalaris A, Schmidt-Arras D, Rose-John S. The pro- and anti-inflammatory properties of the cytokine interleukin-6. Biochim Biophys Acta Mol Cell Res. 2011;1813(5):878-888. doi:10.1016/J.BBAMCR.2011.01.034
180. Schuller A, Montrose L. Influence of Woodsmoke Exposure on Molecular Mechanisms Underlying Alzheimer's Disease: Existing Literature and Gaps in Our Understanding. Epigenet Insights. 2020;13:251686572095487. doi:10.1177/2516865720954873
181. Schwab JM, Serhan CN. Lipoxins and new lipid mediators in the resolution of inflammation. Curr Opin Pharmacol. 2006;6(4):414-420. doi:10.1016/J.COPH.2006.02.006
182. Seidel J, Magzamen S, Wang YH, Neujahr V, Schaeffer JW. Lessons from Dairy Farmers for Occupational Allergy and Respiratory Disease. Curr Allergy Asthma Rep. 2023;23(6):325-339. doi:10.1007/s11882-023-01081-2
183. Serhan CN. Novel Pro-Resolving Lipid Mediators in Inflammation Are Leads for Resolution Physiology. Nature. 2014;510(7503):92. doi:10.1038/NATURE13479
184. Serhan CN, Arita M, Hong S, Gotlinger K. Resolvins, docosatrienes, and neuroprotectins, novel omega-3-derived mediators, and their endogenous aspirin-triggered epimers. Lipids. 2004;39(11):1125-1132. doi:10.1007/S11745-004-1339-7/METRICS
185. Serhan CN, Chiang N. Resolution phase lipid mediators of inflammation: agonists of resolution. Curr Opin Pharmacol. 2013;13(4):632-640. doi:10.1016/J.COPH.2013.05.012
186. Serhan CN, Chiang N, Dalli J, Levy BD. Lipid mediators in the resolution of inflammation. Cold Spring Harb Perspect Biol. 2015;7(2). doi:10.1101/cshperspect.a016311
187. Serhan CN, Krishnamoorthy S, Recchiuti A, Chiang N. Novel Anti-Inflammatory -- Pro-Resolving Mediators and Their Receptors. Curr Top Med Chem. 2011;11(6):629. doi:10.2174/1568026611109060629
188. Serhan CN, Levy BD. Resolvins in inflammation: emergence of the pro-resolving superfamily of mediators. J Clin Invest. 2018;128(7):2657-2669. doi:10.1172/JCI97943
189. Serhan CN, Levy BD. Resolvins in inflammation: Emergence of the pro-resolving superfamily of mediators. Journal of Clinical Investigation. 2018;128(7):2657-2669. doi:10.1172/JCI97943
190. Serhan CN, Levy BD. Resolvins in inflammation: emergence of the pro-resolving superfamily of mediators. J Clin Invest. 2018;128(7):2657. doi:10.1172/JCI97943
191. Serhan CN, Petasis NA. Resolvins and Protectins in Inflammation-Resolution. Chem Rev. 2011;111(10):5922-5943. doi:10.1021/CR100396C
192. Serhan CN, Yacoubian S, Yang R. Anti-Inflammatory and Pro-Resolving Lipid Mediators. Annu Rev Pathol. 2008;3:279. doi:10.1146/ANNUREV.PATHMECHDIS.3.121806.151409

193. Shamji MH, Boyle RJ. Immune modulation and the role of innate immune cells in allergy and asthma. Clin Exp Allergy. 2022;52(4):474-475. doi:10.1111/CEA.14132
194. Shamji MH, Sharif H, Layhadi JA, Zhu R, Kishore U, Renz H. Diverse immune mechanisms of allergen immunotherapy for allergic rhinitis with and without asthma. Journal of Allergy and Clinical Immunology. 2022;149(3):791-801. doi:10.1016/J.JACI.2022.01.016
195. Shi JH, Sun SC. Tumor Necrosis Factor Receptor-Associated Factor Regulation of Nuclear Factor κB and Mitogen-Activated Protein Kinase Pathways. Front Immunol. 2018;9(AUG). doi:10.3389/FIMMU.2018.01849
196. Siewe L, Bollati-Fogolin M, Wickenhauser C, Krieg T, Müller W, Roers A. Interleukin-10 derived from macrophages and/or neutrophils regulates the inflammatory response to LPS but not the response to CpG DNA. Eur J Immunol. 2006;36(12):3248-3255. doi:10.1002/EJI.200636012
197. Sigsgaard T, Basinas I, Doekes G, et al. Respiratory diseases and allergy in farmers working with livestock: a EAACI position paper. Clin Transl Allergy. 2020;10(1). doi:10.1186/S13601-020-00334-X
198. Sigsgaard T, Basinas I, Doekes G, et al. Respiratory diseases and allergy in farmers working with livestock: a EAACI position paper. Clin Transl Allergy. 2020;10(1):29. doi:10.1186/s13601-020-00334-x
199. Silva BSA, Lira FS, Ramos D, et al. Severity of COPD and its relationship with IL-10. Cytokine. 2018;106:95-100. doi:10.1016/J.CYTO.2017.10.018
200. Silva JR, Burger B, Kühl CMC, Candreva T, dos Anjos MBP, Rodrigues HG. Wound Healing and Omega-6 Fatty Acids: From Inflammation to Repair. Mediators Inflamm. 2018;2018. doi:10.1155/2018/2503950
201. Silva-Sanchez A, Randall TD. Role of iBALT in Respiratory Immunity. In: Current Topics in Microbiology and Immunology. Vol 426. Springer Science and Business Media Deutschland GmbH; 2020:21-43. doi:10.1007/82_2019_191
202. Simon D. Recent Advances in Clinical Allergy and Immunology 2019. Int Arch Allergy Immunol. 2019;180(4):291-305. doi:10.1159/000504364
203. Singh D, Agusti A, Anzueto A, et al. Global Strategy for the Diagnosis, Management, and Prevention of Chronic Obstructive Lung Disease: the GOLD science committee report 2019. European Respiratory Journal. 2019;53(5). doi:10.1183/13993003.00164-2019
204. Skaper SD, Facci L, Zusso M, Giusti P. An inflammation-centric view of neurological disease: Beyond the neuron. Front Cell Neurosci. 2018;12. doi:10.3389/fncel.2018.00072
205. Söderquist B, Sundqvist KG, Vikerfors T. Adhesion molecules (E-selectin, intercellular adhesion molecule-1 (ICAM-1) and vascular cell adhesion molecule-1 (VCAM-1)) in sera from patients with Staphylococcus aureus bacteraemia with or without endocarditis. Clin Exp Immunol. 1999;118(3):408-411. doi:10.1046/J.1365-2249.1999.01081.X
206. Sperling RI. The effects of dietary n-3 polyunsaturated fatty acids on neutrophils. Proc Nutr Soc. 1998;57(4):527-534. doi:10.1079/PNS19980077
207. Starkey MR, Plank MW, Casolari P, et al. IL-22 and its receptors are increased in human and experimental COPD and contribute to pathogenesis. European Respiratory Journal. 2019;54(1):1800174. doi:10.1183/13993003.00174-2018
208. Sun YP, Oh SF, Uddin J, et al. Resolvin D1 and its aspirin-triggered 17R epimer: Stereochemical assignments, anti-inflammatory properties, and enzymatic inactivation. Journal of Biological Chemistry. 2007;282(13):9323-9334. doi:10.1074/jbc.M609212200

209. Sveiven SN, Anesko K, Morgan J, Nair MG, Nordgren TM. Lipid-Sensing Receptor FFAR4 Modulates Pulmonary Epithelial Homeostasis following Immunogenic Exposures Independently of the FFAR4 Ligand Docosahexaenoic Acid (DHA). Int J Mol Sci. 2023;24(8). doi:10.3390/ijms24087072
210. Syamlal G, Doney B, Mazurek JM. Chronic Obstructive Pulmonary Disease Prevalence Among Adults Who Have Never Smoked, by Industry and Occupation — United States, 2013–2017. MMWR Morb Mortal Wkly Rep. 2019;68(13):303-307. doi:10.15585/MMWR.MM6813A2
211. Syamlal G, Kurth LM, Dodd KE, et al. Morbidity and Mortality Weekly Report Chronic Obstructive Pulmonary Disease Mortality by Industry and Occupation-United States, 2020.; 2020. https://www.cdc.gov/nchs/data/dvs/Industry-and-Occupation-
212. Takatsuki F, Okano A, Suzuki C, et al. Human recombinant IL-6/B cell stimulatory factor 2 augments murine antigen-specific antibody responses in vitro and in vivo. The Journal of Immunology. 1988;141(9):3072-3077. doi:10.4049/JIMMUNOL.141.9.3072
213. Tanaka T, Narazaki M, Kishimoto T. IL-6 in inflammation, immunity, and disease. Cold Spring Harb Perspect Biol. 2014;6(10). doi:10.1101/CSHPERSPECT.A016295
214. Taylor JA, Karas JL, Ram MK, Green OM, Seidel-Dugan C. Activation of the high-affinity immunoglobulin E receptor Fc epsilon RI in RBL-2H3 cells is inhibited by Syk SH2 domains. Mol Cell Biol. 1995;15(8):4149-4157. doi:10.1128/MCB.15.8.4149
215. Terzano C, Di Stefano F, Conti V, Graziani E, Petroianni A. Air pollution ultrafine particles: toxicity beyond the lung. Eur Rev Med Pharmacol Sci. 2010;14(10):809-821. http://www.ncbi.nlm.nih.gov/pubmed/21222367
216. Threatt AN, White J, Klepper N, et al. Aspirin-triggered resolvin D1 modulates pulmonary and neurological inflammation in an IL-22 knock-out organic dust exposure mouse model. Front Immunol. 2024;15. doi:10.3389/fimmu.2024.1495581
217. Tiberi M, Chiurchiù V. Specialized Pro-resolving Lipid Mediators and Glial Cells: Emerging Candidates for Brain Homeostasis and Repair. Front Cell Neurosci. 2021;15. doi:10.3389/fncel.2021.673549
218. Tsai MJ, Chang WA, Tsai PH, et al. Montelukast Induces Apoptosis-Inducing Factor-Mediated Cell Death of Lung Cancer Cells. Int J Mol Sci. 2017;18(7). doi:10.3390/IJMS18071353
219. Ulu A, Burr A, Heires AJ, et al. A high docosahexaenoic acid diet alters lung inflammation and recovery following repetitive exposure to aqueous organic dust extracts. J Nutr Biochem. 2021;97. doi:10.1016/j.jnutbio.2021.108797
220. Ulu A, Sveiven S, Bilg A, et al. IL-22 regulates inflammatory responses to agricultural dust-induced airway inflammation. Toxicol Appl Pharmacol. 2022;446:116044. doi:10.1016/j.taap.2022.116044
221. Ulu A, Velazquez J V., Burr A, et al. Sex-Specific Differences in Resolution of Airway Inflammation in Fat-1 Transgenic Mice Following Repetitive Agricultural Dust Exposure. Front Pharmacol. 2022;12. doi:10.3389/fphar.2021.785193
222. USDA ERS - Ag and Food Sectors and the Economy. Accessed January 20, 2023. https://www.ers.usda.gov/data-products/ag-and-food-statistics-charting-the-essentials/ag-and-food-sectors-and-the-economy/

223. Vargas-Caraveo A, Sayd A, Maus SR, et al. Lipopolysaccharide enters the rat brain by a lipoprotein-mediated transport mechanism in physiological conditions. Sci Rep. 2017;7(1). doi:10.1038/s41598-017-13302-6
224. Vitenberga Z, Pilmane M, Babjoniševa A. The evaluation of inflammatory, anti-inflammatory and regulatory factors contributing to the pathogenesis of COPD in airways. Pathol Res Pract. 2019;215(1):97-105. doi:10.1016/J.PRP.2018.10.029
225. Wang B, Wu L, Chen J, et al. Metabolism pathways of arachidonic acids: mechanisms and potential therapeutic targets. Signal Transduct Target Ther. 2021;6(1). doi:10.1038/S41392-020-00443-W
226. Wang J. Neutrophils in tissue injury and repair. Cell Tissue Res. 2018;371(3):531. doi:10.1007/S00441-017-2785-7
227. Wang L, Wang X, Tong L, et al. Recovery from acute lung injury can be regulated via modulation of regulatory T cells and Th17 cells. Scand J Immunol. 2018;88(5):e12715. doi:10.1111/SJI.12715
228. Wang X, Cui X, Wu J, Bao L, Tan Z, Chen C. Peripheral Nerves Directly Mediate the Transneuronal Translocation of Silver Nanomaterials from the Gut to Central Nervous System.; 2023. https://www.science.org
229. Warren KJ, Wyatt TA, Romberger DJ, et al. Post-injury and resolution response to repetitive inhalation exposure to agricultural organic dust in mice. Safety (Basel). 2017;3(1). doi:10.3390/SAFETY3010010
230. Wechsler ME, Munitz A, Ackerman SJ, et al. Eosinophils in Health and Disease: A State-of-the-Art Review. Mayo Clin Proc. 2021;96(10):2694-2707. doi:10.1016/j.mayocp.2021.04.025
231. Wei H, Li B, Sun A, Guo F. Interleukin-10 family cytokines immunobiology and structure. Adv Exp Med Biol. 2019;1172:79-96. doi:10.1007/978-981-13-9367-9_4/FIGURES/6
232. Wheaton AG, Ford ES, Cunningham TJ, Croft JB. Chronic obstructive pulmonary disease, hospital visits, and comorbidities: National Survey of Residential Care Facilities, 2010. J Aging Health. 2015;27(3):480-499. doi:10.1177/0898264314552419
233. Wilkinson TMA. Immune checkpoints in chronic obstructive pulmonary disease. European Respiratory Review. 2017;26(144). doi:10.1183/16000617.0045-2017
234. Wintermeyer SF, Kuschner WG, Wong H, D'Alessandro A, Blanc PD. Pulmonary responses after wood chip mulch exposure. J Occup Environ Med. 1997;39(4):308-314. doi:10.1097/00043764-199704000-00007
235. Work-Related Asthma — 38 States and District of Columbia, 2006–2009. Accessed January 20, 2023. https://www.cdc.gov/mmwr/preview/mmwrhtml/mm6120a4.htm
236. Wunschel J, Poole JA. Occupational agriculture organic dust exposure and its relationship to asthma and airway inflammation in adults. Journal of Asthma. 2016;53(5):471-477. doi:10.3109/02770903.2015.1116089
237. Wyatt TA, Canady K, Heires AJ, et al. Alcohol Inhibits Organic Dust-induced ICAM-1 Expression on Bronchial Epithelial Cells. Safety (Basel). 2017;3(1). doi:10.3390/SAFETY3010005
238. Wyatt TA, Nemecek M, Chandra D, et al. Organic dust-induced lung injury and repair: Bi-directional regulation by TNFα and IL-10. https://doi.org/101080/1547691X20201776428. 2020;17(1):153-162. doi:10.1080/1547691X.2020.1776428
239. Yamasaki K, Van Eeden SF. Lung Macrophage Phenotypes and Functional Responses: Role in the Pathogenesis of COPD. Int J Mol Sci. 2018;19(2). doi:10.3390/IJMS19020582

240. Yellepeddi VK, Baker OJ. Predictive modeling of aspirin-triggered resolvin D1 pharmacokinetics for the study of Sjögren's syndrome. Clin Exp Dent Res. 2020;6(2):225-235. doi:10.1002/cre2.260
241. Yellepeddi VK, Parashar K, Dean SM, Watt KM, Constance JE, Baker OJ. Predicting Resolvin D1 Pharmacokinetics in Humans with Physiologically-Based Pharmacokinetic Modeling. Clin Transl Sci. 2021;14(2):683-691. doi:10.1111/cts.12930
242. You DJ, Lee HY, Taylor-Just AJ, Bonner JC. Synergistic induction of IL-6 production in human bronchial epithelial cells in vitro by nickel nanoparticles and lipopolysaccharide is mediated by STAT3 and C/EBPβ. Toxicol In Vitro. 2022;83. doi:10.1016/J.TIV.2022.105394
243. You R, Ho YS, Chang RCC. The pathogenic effects of particulate matter on neurodegeneration: a review. J Biomed Sci. 2022;29(1):15. doi:10.1186/s12929-022-00799-x
244. Zenewicz LA. IL-22: There Is a Gap in Our Knowledge. Immunohorizons. 2018;2(6):198-207. doi:10.4049/immunohorizons.1800006
245. Zhang B, Weuve J, Langa KM, et al. Comparison of Particulate Air Pollution From Different Emission Sources and Incident Dementia in the US. JAMA Intern Med. Published online August 14, 2023. doi:10.1001/jamainternmed.2023.3300
246. Zhang B, Weuve J, Langa KM, et al. Comparison of Particulate Air Pollution from Different Emission Sources and Incident Dementia in the US. JAMA Intern Med. 2023;183(10):1080-1089. doi:10.1001/jamainternmed.2023.3300
247. Zhang L, Cheng Z, Liu W, Wu K. Expression of Interleukin (IL)-10, IL-17A and IL-22 in Serum and Sputum of Stable Chronic Obstructive Pulmonary Disease Patients. COPD: Journal of Chronic Obstructive Pulmonary Disease. 2013;10(4):459-465. doi:10.3109/15412555.2013.770456
248. Zhang Q, Raoof M, Chen Y, et al. Circulating mitochondrial DAMPs cause inflammatory responses to injury. Nature. 2010;464(7285):104-107. doi:10.1038/NATURE08780
249. Zhang Y, Ye B, Zheng H, et al. Association between organic dust exposure and adult-asthma: A systematic review and meta-analysis of case-control studies. Allergy Asthma Immunol Res. 2019;11(6):818-829. doi:10.4168/aair.2019.11.6.818
250. Zuberbier T, Aberer W, Asero R, et al. The EAACI/GA2LEN/EDF/WAO guideline for the definition, classification, diagnosis and management of urticaria. Allergy. 2018;73(7):1393-1414. doi:10.1111/ALL.13397